

JOURNAL OF MATHEMATICAL SCIENCES AND MODELLING

ISSN: 2636-8692

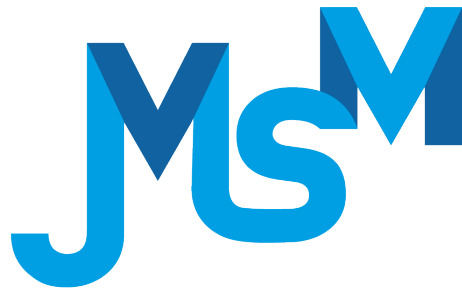
VOLUME II
ISSUE III

JMS^M

VOLUME II ISSUE III
ISSN 2636-8692

December 2019
<http://dergipark.gov.tr/jmsm>

**JOURNAL OF
MATHEMATICAL SCIENCES
AND MODELLING**



Editors

Editor in Chief

Murat Kirişçi
Department of Mathematics,
Faculty of Science and Arts, İstanbul University,
İstanbul-TÜRKİYE
murat.kirisci@istanbul.edu.tr

Editor in Chief

Mahmut Akyiğit
Department of Mathematics,
Faculty of Science and Arts, Sakarya University,
Sakarya-TÜRKİYE
makyigit@sakarya.edu.tr

Managing Editor

Merve İlkan
Department of Mathematics,
Faculty of Science and Arts, Düzce University,
Düzce-TÜRKİYE
merveilkhan@duzce.edu.tr

Editorial Board of Journal of Mathematical Sciences and Modelling

Murat Tosun
Sakarya University,
TÜRKİYE

Hari Mohan Srivastava
University of Victoria,
CANADA

George D. Magoulas
University of London,
UNITED KINGDOM

James F. Peters
University of Manitoba,
CANADA

Florentin Smarandache
University of New Mexico,
USA

Mujahid Abbas
University of Pretoria,
SOUTH AFRICA

Syed Abdul Mohiuddine
King Abdulaziz University,
SAUDI ARABIA

Emrah Evren Kara
Düzce University,
TÜRKİYE

Wei Gao
School of Information Science and Technology,
P. R. CHINA

Gülşah Aktüre,
Düzce University
TÜRKİYE

F. G. Lupianez
Complutense University of Madrid,
SPAIN

Khrisnan Balasubramanian
Arizona State University,
USA

Ismat Beg
Lahor School of Economics,
PAKISTAN

Fuat Usta
Düzce University,
TÜRKİYE

Hidayet Hüda kosal
Sakarya University,
TÜRKİYE

Contents

1	Mathematical Model: Thermal Effects of Two Wheeler Rider's Speed in His/Her Eye <i>Gokul KC, Dil Bahadur Gurung</i>	143-154
2	SITEM for the Conformable Space-Time fractional (2+1)-Dimensional Asymmetric Nizhnik-Novikov-Veselov Equations <i>Handan Çerdik Yaslan, Ayşe Girgin</i>	155-162
3	Some Exact Bianchi Types Cosmological Models in $f(R, T)$ Theory of Gravity <i>Abdulvahid Harunbhai Hasmani, Ahmed Mohammed Al-Haysah</i>	163-175
4	Analysis of the Convergence and Periodicity of a Rational Difference Equation <i>Mohammed B. Almatrafi, Marwa M. Alzubaidi</i>	176-182
5	Bayesian Analysis of the Discrete Two-Parameter Bathtub Hazard Distribution <i>Ammar M. Sarhan</i>	183-192
6	2-Absorbing Semiprimary Fuzzy Ideal of Commutative Rings <i>Deniz Sönmez, Gürsel Yeşilot, Serkan Onar, Bayram Ali Ersoy</i>	193-197
7	Korovkin Type Approximation Theorem for Functions of Two Variables Through $\alpha\beta$ -Statistical Convergence <i>Selma Altundağ, Bayram Sözbir</i>	198-204

Mathematical Model: Thermal Effects of Two Wheeler Rider's Speed in His/Her Eye

Gokul KC^{1*} and Dil Bahadur Gurung¹

¹Department of Mathematics, School of Science, Kathmandu University, Dhulikhel, Nepal

*Corresponding author E-mail: gokul.kc@ku.edu.np

Article Info

Keywords: Airflow forced convection, Bio-heat transfer, Eyelid blinking, Temperature distribution, Two wheeler rider

2010 AMS: 92B05, 80A20

Received: 23 December 2018

Accepted: 31 August 2019

Available online: 26 December 2019

Abstract

High speed airflow into the cornea accelerates evaporation and heat transfer. Eyelid blinking increases with increased airflow speed into the eye. Increased blinking increases corneal temperature when drops below normal level. In cold climatic condition high speed airflow causes rapid temperature drop. Most often, eye injuries caused by cold exposure occur in individuals who try to force their eyes open in high speed wind and cold weather such as two wheeler rider. The purpose of this study is to investigate the temperature changes in two wheeler rider's cornea, considering eyelid blinking, in his/her different speed. Thus, in this paper, bio-heat transfer process is simulated using finite element method at rider's different speed in transient state cases. In still air, blinking increases corneal temperature by 2.74°C at normal ambient temperature 22.5°C than in open eye. At ambient temperature 0°C and rider's speed 60km/hr , corneal temperature drops to 5.45°C in open eye, while blinking increases this temperature by 6.28°C . Similarly at ambient temperature 40°C , blinking reduces corneal temperature by 0.51°C . Corneal temperature approaches steady state quickly at higher rider's speed.

1. Introduction

1.1. Background of the study

Dry eye condition affects millions of people, interfering with their daily living and normal activities. Actual causes associated with dry eye are multifactorial [1]. Certain environmental conditions such as high or low temperatures, low humidity and wind flow are known factors to cause dry eye. Among them, the most striking change of corneal surface temperature is brought about by air movement. High speed air into the eye causes significant decrease in lipid layer and tear stability [2]. This may destroy or make thinner the lipid layer, which increases evaporation. Increased evaporation of tear causes dry eye. The heat transfer between air molecules and cornea increases with air velocity. Since more air molecules would hit the corneal surface, high amount of heat is transferred by evaporation of water from precorneal tear film. Also with airflow, the thermal boundary layer of air between cornea and environment becomes thinner. This decreases the diffusion distance between cornea and environment, causes high heat transfer.

High air velocity causes more evaporation of water from the pre-corneal tear film and increases heat transfer by eliminating the boundary of air adjacent to tear film than in stagnant ambient air. High speed air is associated with forced convection by which significant amount of heat can be transported quickly and effectively [3]. The amount of heat transported by air through forced convection is proportional to the flow speed. The forced convection by hot/cold high speed airflow increases/decreases eye temperature. As the temperature within the eye increases/decreases, the eye will respond with more protective cooling/heating mechanism, such as more frequent blinking [4].

Blinking agitates the pre-corneal tear film secreted at body core temperature. With each blink a warm lacrimal secretion is layered across the cornea giving heat both to environment and to the cornea. The act of blinking expels and sucks alternatively a new layer of air over the surface of the pre-corneal film [5]. The ocular exposure to most of the cornea and lens is strongly affected by the blinking [6]. During blinking, the eyelid closure time is much shorter than opening; however, the convected heat of perfusing blood from vascular conjunctiva

may contribute to anterior corneal temperature[7].

Lagendijk [8] used a finite difference method to calculate the temperature distribution in human and rabbit eyes during hyperthermia treatment. The heat transport from the sclera to the surrounding anatomy is described by a single heat transfer coefficient which includes the impact of blood flow in choroid and sclera. Flyckt et al. [9] studied the impact of choroidal blood flow by using three methods: Lagendijk model, bio-heat model and discrete vasculature model in the eye and the orbit. Scott [10] utilized finite element method to obtain the temperature profile based on heat conduction using various heat transfer coefficients given by Lagendijk. He acknowledged the deficiencies were the lack of including the effects of eyelid closure, eyelid blinking and the environmental wind flow. Shafai and vafai [11] proposed the porous media model along with natural convection to analyze the eye thermal characteristics during exposure to thermal disturbances. Sharon et al. [12] studied the heat exposure and damage to the eye lens, using finite volume and finite element method, when exposed to environmental temperature fluctuations. Ng and Ooi [13] presented a 2D finite element model, simulated ocular surface temperature and compared the results with the model developed by Scott. Ooi and Ng [14] studied the effect of aqueous humor hydrodynamics on heat transfer within human eye. The limitation they conceded was excluding the presence of eyelid on ocular surface and thermal effects of blinking. Scott [4] studied the effects of eyelid shielding by considering normal blinking rate without considering the effect of blood flow in eyelid. Some models ([4], [15]) performed sensitivity analysis by varying the values of convection heat transfer coefficient between cornea and environment. Some authors([8], [9]) studied the convection effects of blood flow in posterior eye. However, most authors neglected the effects of eyelid blinking and forced convection due to air velocity in corneal surface, although it is significant.

1.2. Significance of blinking in forced convection

Blinking is regarded as the continuous interrupted eyelid closure or opening and its thermal effect will compromise between these two. Infants blink at an average rate of one or two times in a minute. The mean eye blink rate in normal individuals varies from 2 – 25 blink per minute. Many factors may affect blink rate, including gender (the rate is higher in women than in men), the time of day (blinking is more frequent in the evening), the degree of concentration on visual tasks and presence of ocular discomfort or disease [16]. During a blink the act of eyelid closure occupies 0.05 seconds, the closure is maintained for 0.15 seconds and is followed by eyelid opening taking 0.2 seconds, thus the whole blink lasts approximately 0.4 seconds with mean inter blink time of 2.8 seconds in male and 4 seconds in female [5]. There are four types of temperature effects of blinking on anterior corneal surface: heating/cooling due to spread of warm tears and lipids across the surface of cornea, heating/cooling caused by the movement of the eyelid, heating/cooling via convection, radiation and tear evaporation and heating/cooling by the formation of new layer of air over the surface of cornea [17].

The use of two wheelers in developing countries has been increasing rapidly. While driving, two wheeler rider wears helmet with visor. Visor prevents driver's eye from dust, smoke, foreign body, and hot/cold wind flow. In several cases, the driver used to open their visor. Some of the cases are:

1. When the environmental temperature is very low than normal, the water vapor due to respiration covers hole area of visor's inner part causes poor vision
2. When raining, the rain water drops hits the visor surface continuously causes blurred vision
3. At night, the refraction of light into the visor by anti-vehicles light or street lights causes poor vision.

In the above cases, the airflow caused by riders speed directly interacts with riders' cornea or eyelid skin surface, cause forced convection heat transfer.

In outdoor condition, the wind accelerates the drop in temperature of the ocular surface below normal level. Most often, eye injuries caused by cold exposure occur in individuals who try to force their eyes open in high wind or cold weather such as in the case of two-wheeler rider. The normal human corneal temperature ranges from 32 – 34°C [5, 7, 18]. However, in cold conditions and high-speed wind flow the temperature of human eyelids and the corneal surface drops well below normal level. If the ocular surface and the eyelid temperature drop below 30°C (a distinctive possibility in cold weather, especially in combination with wind), the chances are that:

1. Meibomian gland would impede its normal delivery of meibum [19]
2. The blood flow rate in eyelid decreases due to vasoconstriction [20]
3. Uniform distribution of lipid layer is broken that causes greater evaporation [21]
4. Tear secretion increases to maintain eye temperature normal that causes excess tearing [5]
5. Blink frequency increases to maintain normal eye temperature where possible [22]
6. Eye pain, blurred vision starts

These events may limit the protective effect of lipid layer, tear layer, eyelid and meibomian gland. Thus long time exposure of eye in cold weather in combination with wind may cause dry eye, refractive errors and severe sensitivity to light. Thus, it is worth investigating the temperature changes and its effects in the eye during eyelid opening, closure and blinking with appropriate forced convection coefficient. In this study eyelid is considered as heating/cooling source of anterior cornea and model as a part of ocular component. The effect of wind flow in temperature distribution specially the temperature drop in two wheeler riders eye surface is modeled using appropriate physical and physiological values at rider's different speed. The purpose of this study are 1) to develop computational approach to predict temperature distribution and 2) to demonstrate the impact of high speed wind flow on temperature, which may be regarded to cause several eye injuries. The potential users of this model would be the visor industries, general public(two wheeler rider) and biological and medical persons.

2. Model formulation

2.1. Discretization

A schematic diagram of two dimensional human eye is presented in figure 2.1. The human eye is considered to have 8 major components: cornea, aqueous humor, lens, vitreous humor, ciliary body, iris, retina, sclera. The diameter of eye along pupillary axis (x-axis) is 25.10mm and along vertical axis is (y-axis) is 23mm.

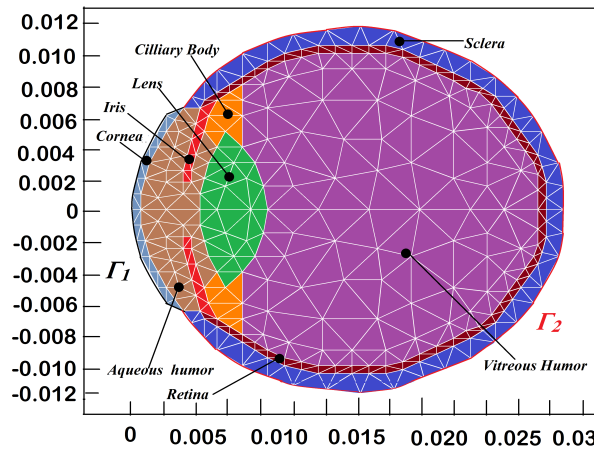


Figure 2.1: Finite element discretization of human eye tissues in two dimension.

The human eye when eyelid is opened is considered to have 11 major components: skin, orbicularis oculi, tarsal plate, cornea, aqueous humor, lens, vitreous humor, ciliary body, iris, retina and sclera. The diameter of eye along pupillary axis(x-axis) is 29.35mm and along vertical axis is (y-axis) is 23mm. Initially, the open eye with eyelid is divided into 635 triangular elements with 350 nodes. The skin, orbicularis oculi, tarsal plate, cornea, aqueous humor, iris, ciliary body, lens, vitreous humor, retina, and sclera are divided into 14, 51, 18, 26, 72, 20, 16, 32, 180, 110 and 96 triangular elements as shown on figure 2.2.

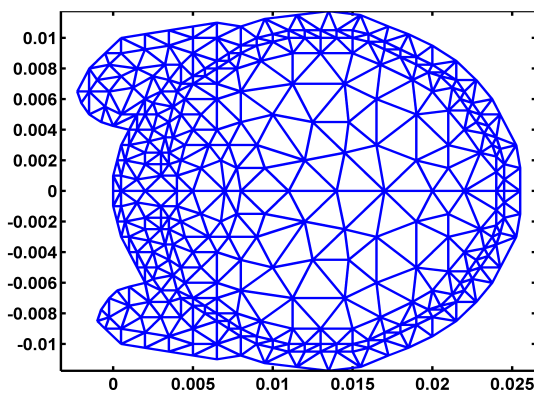


Figure 2.2: Two dimensional eye when eyelid is open

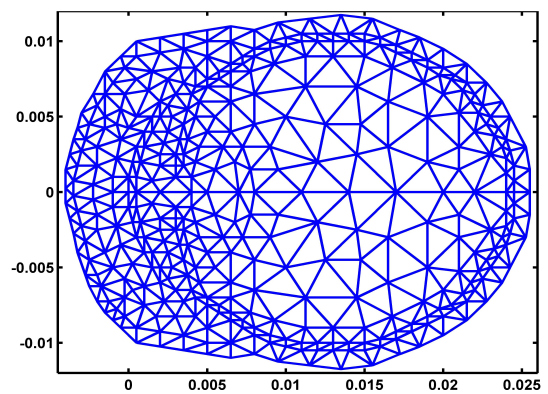


Figure 2.3: Two dimensional eye when eyelid is closed

Similarly, the human eye when eyelid is closed is considered to have 11 major components: skin, orbicularis oculi, tarsal plate, cornea, aqueous humor, lens, vitreous humor, ciliary body, iris, retina and sclera. The diameter of eye along pupillary axis(x-axis) is 29.35mm and along vertical axis is (y-axis) is 23mm. The closed eye is divided into 730 triangular elements with 395 nodes. The skin, orbicularis oculi, tarsal plate, cornea, aqueous humor, iris, ciliary body, lens, vitreous humor, retina, and sclera are divided into 44, 100, 34, 26, 72, 20, 16, 32, 180, 110 and 96 triangular elements as shown on figure 2.3.

2.2. Governing equation and boundary condition

The governing differential equation representing the bio-heat transfer in the human eye can be written by the well known Pennes equation addressing the effect of blood perfusion and metabolism [23] is given by:

$$\rho c \frac{\partial T}{\partial t} = \nabla \cdot (K \nabla T) + \omega \rho_b c_b (T_b - T) + Q_m + Q \tag{2.1}$$

where, ρ_b = blood density (Kgm^{-3}), c_b = blood specific heat ($JKg^{-1}oC^{-1}$), k = tissue thermal conductivity ($Wm^{-1}oC^{-1}$), ω = volumetric blood perfusion rate per unit volume (s^{-1}), T_b = blood temperature (oC), T = tissue temperature (oC), Q_m = heat generation due to metabolism (Wm^{-3}) and Q = heat generation due to external heat source (Wm^{-3}).

Boundary conditions for the system can be defined as follows:

1. On the outer surface of the sclera, the heat flows run into the eye with the complicated network of ophthalmic vessels which are located inside the choroidal layer acting as a heating source to the sclera. This heat exchange between the eye and the surrounding is modeled using the following convection boundary condition:

$$\Gamma_2 : -k_s \frac{\partial T}{\partial \eta} = h_b (T - T_b) \tag{2.2}$$

where η is the normal direction to the surface boundary, k_s is the thermal conductivity of sclera, h_b is the heat transfer coefficient between blood and eye ($Wm^{-2}C^{-1}$), and T_b is blood temperature ($^{\circ}C$).

2. Since outer surface of the eye (cornea or skin) is exposed to the environment, the heat loss caused via convection, radiation, and evaporation. This loss is modeled using the following boundary condition :

$$\Gamma_1 : -k_c \frac{\partial T}{\partial \eta} = h_a(T - T_a) + \sigma \varepsilon (T^4 - T_a^4) + E \quad (2.3)$$

where $h_a = \begin{cases} h_c, & \text{When eyelid is opened} \\ h_s, & \text{When eyelid is closed} \end{cases}$, h_c represents heat transfer coefficient between environment and cornea and h_s represents heat transfer coefficient between skin and environment ($Wm^{-2}C^{-1}$), T_a is the ambient temperature ($^{\circ}C$), σ is the Stefan Boltzmann constant ($5.67 \times 10^{-8} Wm^{-2}C^{-4}$), $\varepsilon = \begin{cases} \varepsilon', & \text{emissivity of cornea} \\ \varepsilon, & \text{emissivity of skin} \end{cases}$, and $E = \begin{cases} E', & \text{When eyelid is opened} \\ E, & \text{When eyelid is closed} \end{cases}$, E' is evaporative heat loss (Wm^{-2}) between cornea and environment and E is evaporative heat loss (Wm^{-2}) between eyelid skin surface and environment.

The inner body core temperature T_c is assumed to be $37^{\circ}C$. Therefore, the initial boundary condition is

$$T_c = 37^{\circ}C \quad (2.4)$$

2.3. Forced convection

Forced convection heat transfer from cornea or eyelid skin surface results from an airstream perturbing the insulating boundary layer of air clinging to the surface. The fundamental non-dimensional quantities describing forced convection are Nusselt number(Nu), Prandtl number(Pr) and Reynolds number(Re). These three dimensionless groups are related together with the following equation [24]

$$Nu = CRe^n Pr^m \quad (2.5)$$

where C, m and n are constants to be determined from experimental data. The three quantities Nu, Re, and Pr further expressed as follows

$$Nu = \frac{h_a d}{k_f} \quad (2.6)$$

$$Pr = \frac{v_f}{\alpha} \quad (2.7)$$

$$Re = \frac{u_a d}{v_f} \quad (2.8)$$

where h_a is convective heat transfer coefficient($wm^{-2}C^{-1}$), k_f is the thermal conductivity of the air($wm^{-1}C^{-1}$), d is the diameter of cornea(m), u_a is ambient air speed(ms^{-1}), v_f is kinematic viscosity(m^2s^{-1}) and α is thermal diffusivity(m^2s^{-1}).

The correlations of the experimental data of Hilpert for gases indicate that the average heat transfer coefficients may be calculated with the following equation

$$Nu = CRe^n Pr^{\frac{1}{3}} \quad (2.9)$$

where the constants C and n are tabulated in table 2 [25]. Properties for use with equation(2.9) are evaluated at the film temperature as

Re	C	n
0.4-4	0.989	0.330
4-40	0.911	0.385
40-4000	0.683	0.466
4000-40000	0.193	0.618
40000-400000	0.0266	0.805

Table 1: Constants C and n for use with equation(2.9)

indicated by the subscript f . The film temperature T_f , defined as the arithmetic mean between the eye surface(cornea or eyelid skin) and ambient air temperature

$$T_f = \frac{T_s + T_a}{2} \quad (2.10)$$

where T_s is the eye surface temperature and T_a air temperature. The parameter values k_f , v_f and Pr_f based on film temperature T_f for air are tabulated in table 3. We assume that all these parameter values are linearly dependent with film temperature T_f . The calculated convective heat transfer coefficient h_a from equation (2.9) is substituted in boundary condition (2.3).

T_f (°C)	v_f (m^2s^{-1})	k_f ($Wm^{-1}°C$)	Pr
27	15.69×10^{-6}	0.02624	0.708
77	20.76×10^{-6}	0.03003	0.697

Table 2: Properties of air[25]

2.4. Methodology

Effects of air flow in temperature distribution, specially, temperature drop in two wheeler riders eye surface is modeled using appropriate physical and physiological values at rider’s different speed. For modeling purpose, we suppose that the effects of airflow in resting cornea is equivalent to the effects of still air in moving cornea. Based on this assumption the riders speed in still air is assumed as airflow speed. The two-wheeler rider’s speed in valleys and hills is assumed 20km/hr as low, 40km/hr as normal and 60km/hr as high. The normal speed 40km/hr is the mean speed which the two-wheeler companies marked as most economy and efficient speed. Hence, to investigate the effects of air speed, the numerical calculations are carried out at speeds 0km/hr, 20km/hr, 40km/hr and 60km/hr.

The governing equation (2.1) with boundary conditions (2.3) and (2.2) are solved using different parameter values. Two dimensional computations are carried out in steady and transient state cases. Transient thermal behavior of human eye is observed using Crank-Nicholson scheme for 1 hour. Eyelids are considered as a heating/cooling source of anterior cornea and model as a part of ocular component. In case of open eyelid, heat loss occurs from cornea and in closed eyelid, heat loss occurs from eyelid skin surface. Different parameter values for this loss are used in the analysis.

Blinking is the interrupted eyelid closure and opening. Beside various functions of eyelid blinking, heating and cooling mechanism play important role in maintaining anterior eye temperature. In transient analysis of blinking, the mesh size and the corresponding parameter values are continuously changed on each time step, this situation is modeled accordingly. At starting time (t = 0), the eyelids are supposed open and temperature values are calculated in open eye with eyelids. When eye blinks, eye mesh with closed lids are used to calculate temperature values. This mesh changing process continues until final time step.

2.5. The control parameters

Normal parameter values: ambient convection coefficient of skin(h_s)= 6.28 $Wm^{-2}°C^{-1}$ [26], ambient convection coefficient of cornea(h_c) = 10 $Wm^{-2}°C^{-1}$ [2], heat transfer coefficient of sclera (h_b) = 65 $Wm^{-2}°C^{-1}$ [27], blood temperature (t_b) = 37°C, evaporation rate of skin E_s = 96 W/m^2 [3], evaporation rate of cornea E_c = 40 W/m^2 [2]. The parameter values for different parts of eye are presented in table ??.

There are various biological and environmental factors that affect blinking rate. Some factors increase, while other decrease blinking

Tissue Type	Thermal Conductivity K ($Wm^{-1}°C^{-1}$)	Blood Perfusion ω (s^{-1})	Metabolic Rate Q_m (Wm^{-3})	Density ρ (Kgm^{-3})	Specific heat C ($JKg^{-1}°C^{-1}$)
Dermis	0.34[9]	0.0087[9]	1620[28]	1070[9]	3662[9]
Orbicularis	0.56[9]	0.0034[9]	480[28]	1050[9]	3639[9]
Tarsal	0.47[28]	0.0082[28]	1600[28]	1250[28]	3600[28]
Cornea	0.58[13]	0[9]	0[28]	1050[13]	4178[13]
Aqueous	0.58[13]	0[9]	0[28]	996[13]	3997[13]
Lens	0.40[13]	0[9]	0[28]	1050[13]	3000[13]
Vitreous	0.603[13]	0[9]	0[28]	1000[13]	4178[13]
Retina	0.565[29]	0.0222[9]	22000[28]	1050[29]	3680[29]
Iris	0.52[28]	0.01[28]	10000[28]	1050[28]	3600[28]
Ciliary	0.498[29]	0.008[29]	6900[29]	1050[29]	3340[29]
Sclera	1.0042[13]	0[29]	0[29]	1100[13]	3180[13]

Table 3: Thermal properties of human eye tissues

rates. In normal condition, the average rate is lowest during high level of mental activity like reading and highest during conversation[30]. Generally, the time interval between two consecutive blink is 2 – 10 seconds, actual rate varies by individual averaging around 10 blinks per minute in a laboratory setting [16]. In this study 10 blinks/min is taken as normal blink rate in still air and at normal ambient temperature. Based on many previous studies[4, 13, 15], 20 – 25°C is assumed as normal air temperature and the temperature below and above this range is cold and hot. In this model, the normal ambient temperature is taken as 22.5°C (mean of the normal range 20 – 25°C). To simulate airflow effects in cold and hot climatic conditions the corneal temperature values are calculated at 0°C, 10°C, 30°C and 40°C respectively.

For modeling purpose, we supposed that the effects of airflow in resting cornea is equivalent to the effects of still air in moving cornea. Based on this assumption the two wheeler riders speed in still air is assumed as airflow speed. Hence, to simulate the effects of wind speed and its effects, the numerical calculations are carried out at airflow speeds 0, 20, 40 and 60 km/hr. The rider’s speed 40 km/hr is the mean speed which the two-wheeler companies marked as most economy and efficient speed, is assumed as normal speed.

Nakamori et al.[22] reported that high air velocity (1.4m/s) is associated with an increase (16.92.9 to 22.84.0) in blinking frequency in normal eyes. Koh et al.[21] reported that blink frequency increased significantly by 59% in dry eye patients after airflow exposure. We supposed that the blink frequency is increased by 50% in every increase of riders speed by 20 km/hr. Thus, the blink frequency of eyelid is taken as 10, 15, 22 and 33 blinks/min with inter-blink time interval of 5.5, 3.6, 2.32 and 1.41 seconds respectively at riders different speed.

The oily layer of the pre-corneal tear film retards evaporation from the eye and if it destroyed, the rate may increase by a factor of four [31]. The increased airflow into the corneal surface increases evaporation. Increased airflow also increases blinking rate. Increased blinking rate reduces eyelid opening time and with each blink a new lipid layer is spread across cornea that prevents evaporation. Hence evaporation is assumed as constant for different airflow speed. The corneal evaporation rate $40Wm^{-2}$ is used as normal rate at normal ambient temperature [13, 15, 11]. Evaporation rate increases/decreases with increase/decrease in ambient temperature. In this study, corneal evaporation rates 0, 15, 40, 100 and $150Wm^{-2}$ are used for ambient temperatures 0, 10, 22.5, 30 and $40^{\circ}C$ respectively. Similarly, skin evaporation rate at normal ambient temperature is $96Wm^{-2}$ [32]. Hence 0, 20, 96, 140 and $192Wm^{-2}$ are used for eyelid evaporation rate for ambient temperatures 0, 10, 22.5, 30 and $40^{\circ}C$ respectively [20].

3. Convergence study

In this section we studied the convergence pattern of temperature values by varying the mesh size in open eye without eyelids. At first, initial triangular mesh of size 552 elements (coarse mesh) are constructed and temperature values are obtained as shown in figure 3.1. Next we subdivide each triangle into four sub-triangles by joining the mid point of each sides of that triangle. The corresponding mesh of size 2208 elements (normal mesh) and its temperature distribution are shown in figure 3.2. The triangular mesh is again further subdivided to get fine and extremely fine mesh of size 8832 and 35328 elements as shown in figures 3.3 and 3.4 respectively. The temperature values of cornea are tabulated in table 4.

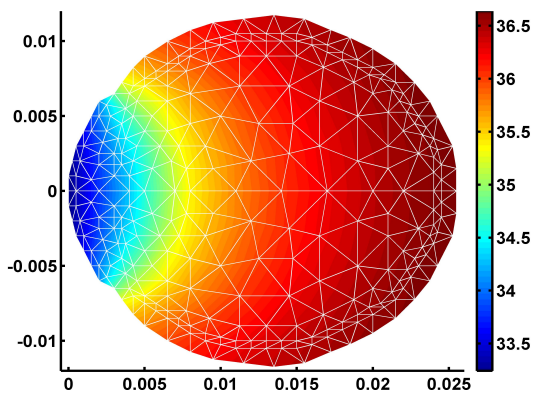


Figure 3.1: Temperature distribution of human eye tissues at triangular mesh of size 552 elements.

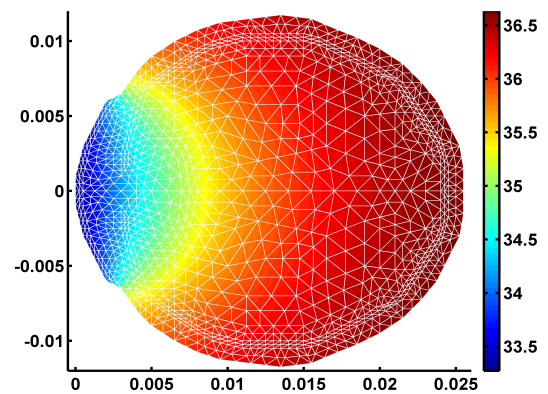


Figure 3.2: Temperature distribution of human eye tissues at triangular mesh of size 2208 elements.

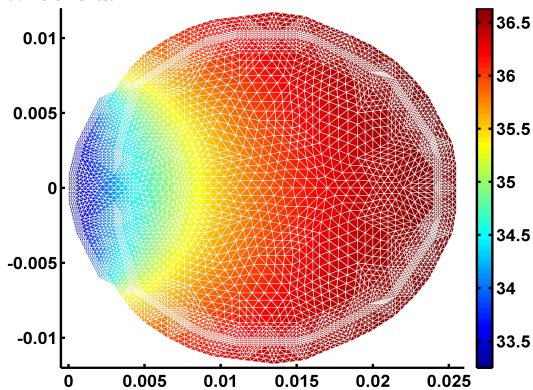


Figure 3.3: Temperature distribution of human eye tissues at triangular mesh of size 8832 elements.

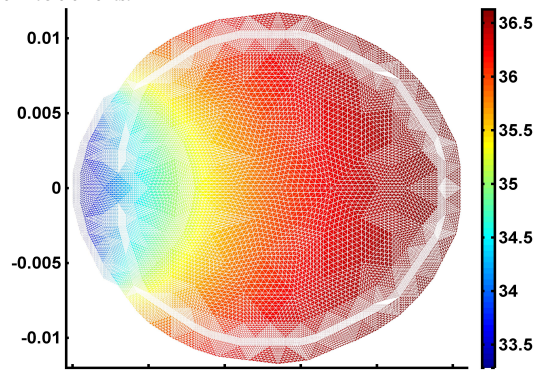


Figure 3.4: Temperature distribution of human eye tissues at triangular mesh of size 35328 elements.

Mesh type	Mesh size	Temperature values
Coarse	552	33.21°C
Normal	2208	33.23°C
Fine	8832	33.25°C
Extremely fine	35328	33.26°C

Table 4: Convergence study in Two dimensional temperature variation of cornea

4. Results

The temperature distribution of human eye in case of eyelid opening and closure at ambient temperature $22.5^{\circ}C$ and at air flow rates $20km/hr$, $40km/hr$ and $60km/hr$ are shown in 4.1.

The transient temperature distributions are calculated at different air temperatures 0, 10, 22.5, 30 and $40^{\circ}C$ and air speeds $0km/hr$, $20km/hr$, $40km/hr$

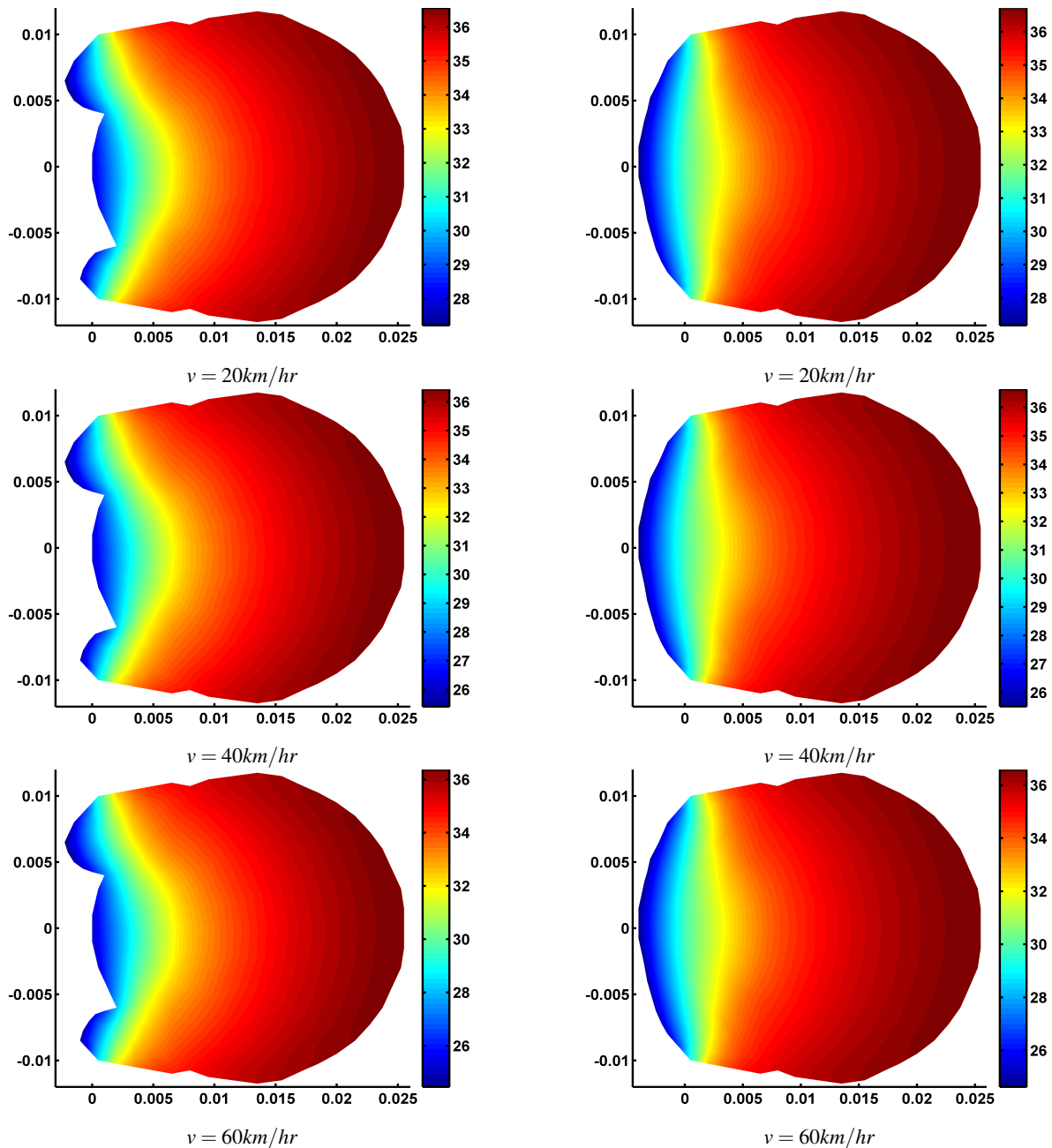


Figure 4.1: Influence of different air speeds and eyelid positions (opened and closed) temperature distribution at ambient temperature $T_a = 22.5^\circ\text{C}$.

and 60 km/hr as discussed above. The transient thermal behavior of human eye is observed for 1 hour using 1–second time step size. The temperature values for eyelid opening, eyelid closure and different blinking rates 10, 15, 22 and 33 blinks/min at ambient temperature 22.5°C and in still air is presented in figure 4.2.

Figure 4.2 shows that the corneal surface temperature values obtained are $30.36, 32.73, 33.10, 33.47, 33.84$ and 35.58°C at eyelid opening, 10 blinks/min, 15 blink/min, 22 blink/min, 33 blink/min and eyelid closure respectively. The steady state corneal temperature is observed in around 41 and 25 minutes during eyelid opening and closure respectively. When blinking rate increases from 10 to 33 the steady state temperature is observed in around 38, 35, 33 and 30 minutes respectively. However, in figure 4.2, the actual blinking pattern is unable to see because blinking time (eyelid closure time) and inter-blink interval is very short. Hence to show the blinking pattern, the further graphs are plotted by showing only one blinking pattern in a minute.

In figure 4.3, we observed the temperature distribution of cornea at different blinking rates and air speeds at 0°C ambient temperature. The corneal temperature is dropped by $11.54, 16.88$ and 17.46°C during closure, blinking and opening respectively.

Figure 4.4 shows the corneal temperature distribution at different airflow speeds and at different blinking rates at ambient temperature 10°C . The corneal temperature observed is $34.95, 29.34, 27.64$ and 26.68°C during eyelid closure, $30.61, 20.90, 19.10$ and 18.52°C during blinking and $26.22, 16.77, 14.84$ and 13.93°C during eyelid opening respectively.

The corneal temperature at 22.5°C temperature and at different blinking rates and air speeds is shown in figure 4.5. The temperature decreases from 30.36°C to 24.50°C , 33.10°C to 26.97°C and 35.58°C to 31.34°C at eyelid opening, blinking and closure respectively.

In figure 4.6, we observed the temperature distribution of cornea at different blinking rates and air speeds at 30°C ambient temperature. The corneal temperature is dropped by $1.84, 2.57$ and 2.02°C during closure, blinking and opening respectively.

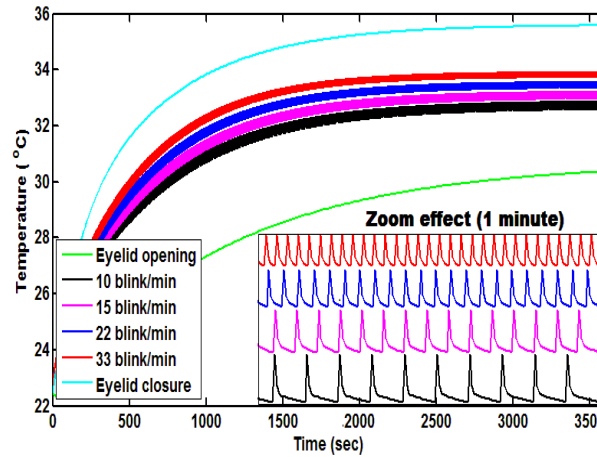


Figure 4.2: Temperature values for different blinking rates

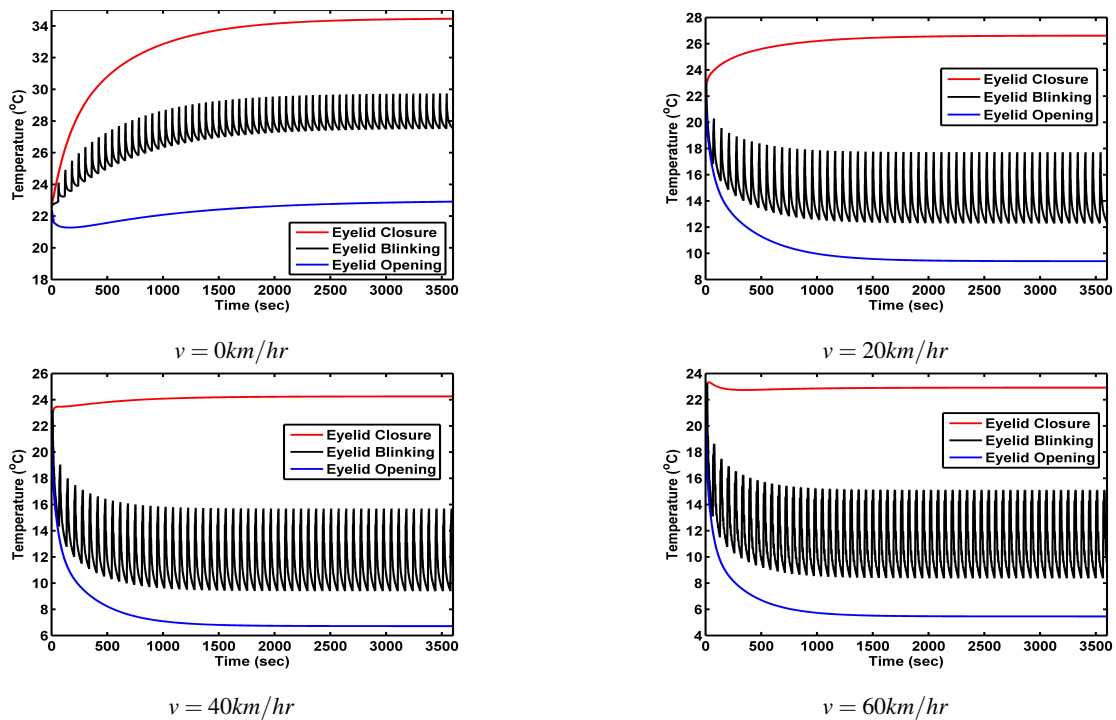


Figure 4.3: Corneal temperatures at ambient temperature 0°C

Figure 4.7 shows the corneal temperature at different air speeds and blinking rates and at 40°C ambient temperature. The corneal temperature is dropped by 0.36, 1.31, 1.4°C and 1.42°C at 0, 20, 40 and 60km/hr air speeds respectively.

5. Discussion

The corneal temperature is highest in eyelid closure, lowest in eyelid opening and in between these two values during blinking when ambient temperature is less than physiological temperature of body(37°C) and vice versa. In eyelid closure heat is conducted/conducted from vascular eyelid to avascular cornea, since the perfused blood flow in eyelid has temperature approaching to body core. If eye surface temperature drops or rises beyond normal level then heat is convected in or out via blood flow through eyelid.

When blinking rate increases 1) eyelid closure time increases 2) secretion and spread of tear layer across cornea increases and 3) uniform distribution and thickness of lipid layer increases. Uniform distribution and thick lipid layer across cornea prevents evaporation of tear from cornea. Closure of eyelid prevents convection, radiation and tear evaporation from cornea. Hence, all these factors increase corneal temperature for ambient temperature less than 37°C and vice versa.

Rapid decrease in corneal temperature is observed at low atmospheric temperatures. The decreasing rate is highest in eyelid opening than blinking and lowest in closure. High amount of heat is lost to environment via convection and radiation in low ambient temperature. In open eye heat conducted from eye core to cornea is insufficient to maintain corneal temperature in normal level. Increased blinking rate may help to increase corneal temperature at low ambient temperature conditions. In our case at ambient temperature 0°C, blinking increases eye temperature by 5.40°C, 5.64°C, 5.82°C and 6.28°C at air speeds 0km/hr, 20km/hr, 40km/hr and 60km/hr respectively. Similarly at ambient temperature 40°C, blinking decreases eye temperature by 0.27°C, 0.42°C, 0.46°C and 0.51°C at air speeds 0km/hr, 20km/hr,

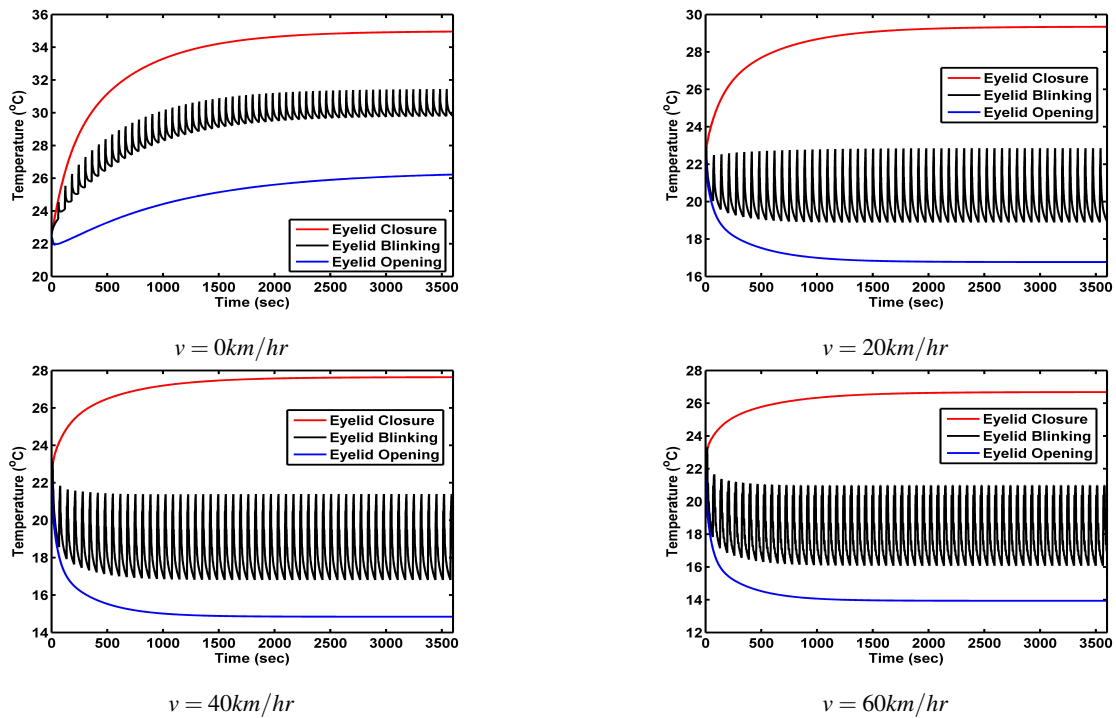


Figure 4.4: Corneal temperatures at ambient temperature 10°C

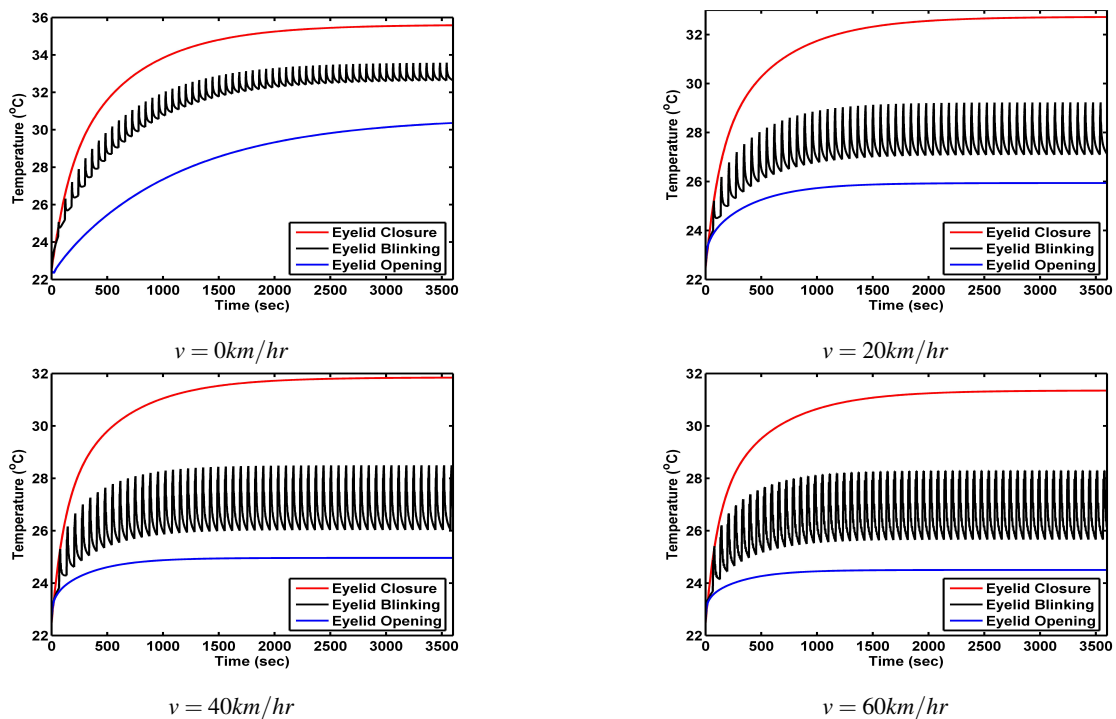


Figure 4.5: Corneal temperatures at ambient temperature 22.5°C

40km/hr and 60km/hr respectively.

Increase in ambient air speed decreases corneal temperature. The rapid decrease of corneal surface temperature is observed at high air speeds. With increase in air speed, more air molecules hit the corneal surface, which may increase the rate of evaporation of water molecules from cornea. In cold temperatures and in still air the difference in temperature between air molecules and corneal surface is very high (22.91°C, 28.61°C and 34.45°C in open, blinking and closed eye respectively at 0°C ambient temperature). This obviously increases heat transfer. However, the cornea is continuously heated by conduction from body core to maintain steady temperature in open eye.

In addition, cornea is heated by warm conjunctiva of eyelid and tearing in eyelid closure. On the other hand, in still air there is a thick thermal boundary layer at the surface of cornea. The increase in air speed plays a role of catalyst in heat transfer, which makes thinner the boundary layer and decreases the diffusion distance. This phenomenon increases heat transfer between ambient air and cornea in eyelid opening and skin surface in eyelid closure. But in hot temperature the difference is very small (3.18°C, 3.45°C and 3.54°C in open, blinking

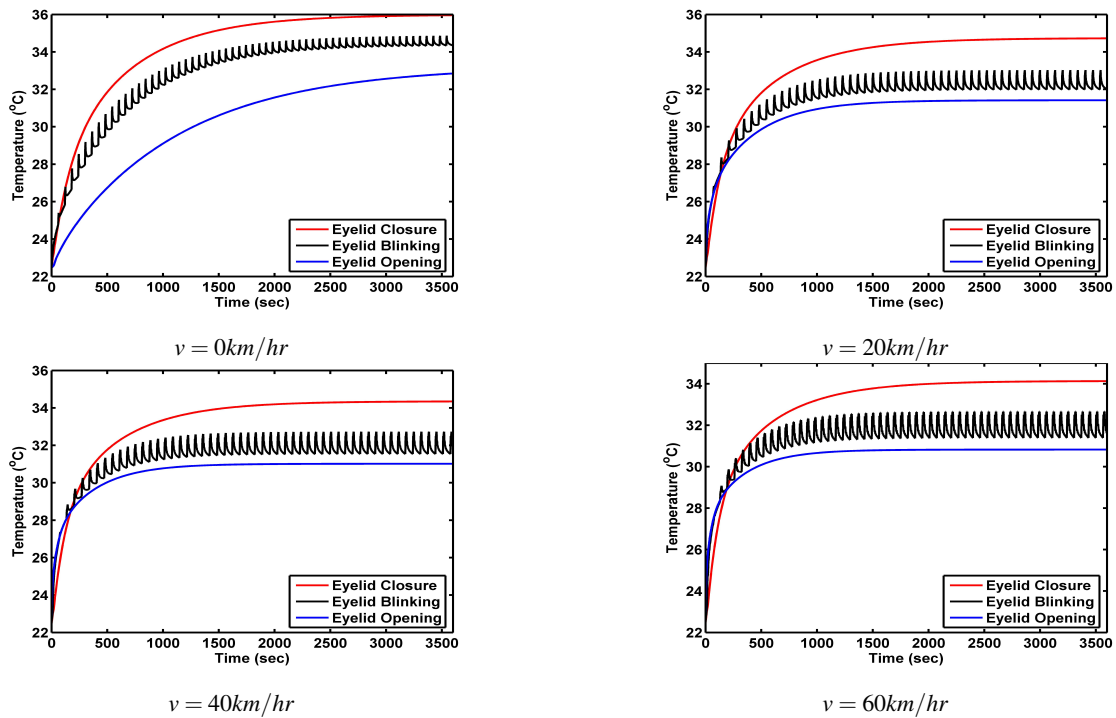


Figure 4.6: Corneal temperatures at ambient temperature 30°C

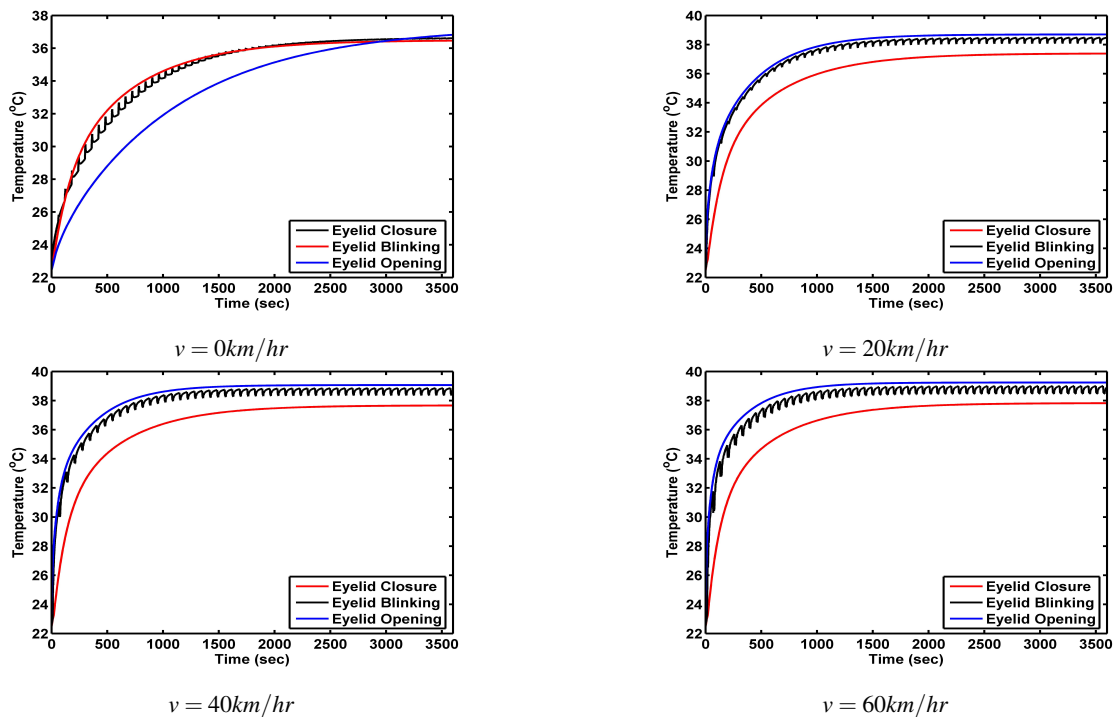


Figure 4.7: Corneal temperatures at ambient temperature 40°C

and closed eye respectively at 40°C air temperature). Although heat transfer increases with increase in air speed the corneal temperature is not significantly affected by air speeds in hot climatic conditions due to this small temperature difference.

The outermost layer of the cornea (meibomian lipid layer) solidifies below 19°C, quasi solid in the range between 20 – 30°C and completely clear liquid in the range between 30 – 45°C [19]. Thus, if the corneal surface temperature drops below 30°C, the meibomian layer may become thicker and solid than usual, this can lead blurred vision. In our case, in still air and at 0°C ambient temperature, corneal temperature is found as 22.91°C, 28.61°C and 34.45°C in eyelid opening, blinking and closure respectively. Similarly at air speed 60km/hr and ambient temperature 0°C the corneal surface temperature drops to 5.45°C, 11.73°C and 22.91°C in eyelid opening, blinking and closure respectively. This may solidify the meibomian lipid layer, which may cause blurred vision. In addition, high air speed affects the distribution of tear film and lipid layer which protects the corneal epithelium against the evaporation of aqueous tears [33]. High air velocity causes greater evaporation of water from the pre-corneal tear film. Exposure of tear film to high air velocity caused significant decrease in lipid layer

stability, tear stability and tear meniscus [21]. If the lipid layer destroyed, the evaporation from the tear film increases approximately 4 times greater than with the lipid layer [31]. This higher rate of evaporation reduces corneal temperature rapidly.

The steady state temperature is achieved earlier in higher air speeds. The corneal temperature reaches in steady state very fast at air speed 60km/hr (approximately 9 minutes, 13 minutes and 20 minutes in open, blinking, and closed eye respectively) than in still air (approximately 25 minutes, 35 minutes and 41 minutes in closed, blinking and open eye respectively). In cold temperatures, the steady state temperature drops very well and plateau of corneal temperature is achieved faster in higher air speeds. In hot climatic conditions the steady state temperature of cornea does not drop significantly but plateau of corneal temperature is achieved faster as in cold climatic conditions.

The flow speed equally affects the thermal boundary layer (reducing the thickness) either in hot or cold conditions. This causes increase in heat transfer approximately at the same manner in both hot and cold climatic conditions. The value of heat transfer coefficient at air speed 60km/hr is found as $122.80\text{Wm}^{-2}\text{C}^{-1}$ and $119.30\text{Wm}^{-2}\text{C}^{-1}$ at ambient temperatures 0°C and 40°C respectively.

6. Validation studies

Gurung and Saxena [20] studied the effects of air flow in human skin temperature. They found a drop in human skin temperature of 7.45°C at 0°C atmospheric temperature and at 4m/s air speed. Our result at atmospheric temperature 0°C and air speed 5m/s shows a higher temperature value 15.03°C on eyelid skin surface. They modeled skin including subcutaneous tissue with increasing blood perfusion from 2mm deep to body core. In our case only 0.6mm of eyelid outer surface having no blood perfusion. Also concentration of blood vessels in eyelid is higher than in normal skin. In such cases our results may valid compare to the results from Gurung and Saxena.

Freeman and Fatt [34] studied the effects of air velocity on human cornea temperature experimentally using thermistor probe and Thermometer Bridge. They observed 13°C temperature drop at 4m/s air velocity and at 0°C ambient temperature. In our case, the corneal surface temperature is obtained to be 9.39°C at 5m/s air speed and at 0°C ambient temperature. This shows that our modeling results are valid with Freeman and Fatt's experimental results.

7. Conclusion

We have presented finite element model of human eye and computed its steady and transient state temperature distribution during eyelid opening, closure and blinking. The airflow forced convection effects on temperature distribution of cornea is simulated. The study focused on the change in temperature of two wheeler rider's cornea in hot and cold climatic conditions at different air speeds. Increased blinking rate is found to increase corneal temperature significantly. In our case anterior corneal temperature is increased by 2.74°C while blinking than in open eye at normal ambient temperature and in still air.

The temperature difference at cornea during eyelid opening, blinking and closure increases as ambient temperature decreases and vice versa. Similarly the difference increases as air speed increases. Corneal temperature plateaus very fast in high air speed than in still air in all climatic conditions. High air speed in cold ambient temperature is hazardous for ocular surface. In this situation, thermal feedback mechanism would require to increase local temperature. Long time exposure of cornea to cold weather and in high air speed may reduce refractive outcomes and increase the risk of dry eye.

References

- [1] K. R. Bhatnagar, A. Sapovadia, D. Gupta, P. Kumar, H. Jasani, *Dry eye syndrome: A rising occupational hazard in tropical countries*, Medical J. Dr. D. Y. Patil Uni., **7** (2014), 13–18.
- [2] K. C. Gokul, D. B. Gurung, P. R. Adhikary, *Transient thermal model of airflow effects in human eye temperature*, Kathmandu Uni. J. Uni. Sci. Eng. Tech., **9** (2013), 47–58.
- [3] K. C. Gokul, D. B. Gurung, P. R. Adhikary, *Modeling airflow effects in human eye temperature with and without eyelids*, Int. J. Appl. Math. Mech., **10** (2014), 82–98.
- [4] J. A. Scott, *The computation of temperature rises in the human eye induced by infrared radiation*, Phys. Med. Biol., **33** (1988), 243–257.
- [5] R. Mapstone, *Determinants of corneal temperature*, British J. Ophthalmology, **52** (1968), 729–741.
- [6] D. H. Sliney, *Physical factors in cataractogenesis: Ambient ultraviolet radiation and temperature*, Investigative Ophthalmology Vis. Sci., **27** (1986), 781–790.
- [7] H. Fujishima, I. Toda, M. Yamada, N. Sato, K. Tsubota, *Corneal temperature in patients with dry eye evaluated by infrared radiation thermometry*, British J. Ophthalmology, **80** (1996), 29–32.
- [8] J. J. Lagendijk, *A mathematical model to calculate temperature distributions in human and rabbit eyes during hyperthermia treatment*, Phys. Med. Biol., **27** (1982), 1301–1311.
- [9] V. M. M. Flycket, B. W. Roaymakers, J. J. W. Lagendijk, *Modeling the impact of blood flow on the temperature distribution in the human eye and the orbit: fixed heat transfer coefficient versus the penne's bioheat model versus discrete blood vessels*, Phys. Med. Biol., **51** (2006), 5007–5021.
- [10] J. A. Scott, *A finite element model of heat transport in the human eye*, **51**(33) (1988), 227–241.
- [11] M. Shafahi, K. Vafai, *Human eye response to thermal disturbances*, J. Heat Transfer, **133** (2011), Article ID 011009.
- [12] N. Sharon, P. Z. B. Yoseph, B. Bormusov, A. Dovrat, *Simulation of heat exposure and damage to the eye lens in a neighborhood bakery*, Experiment. Eye Res., **87** (2008), 49–55.
- [13] E. Y. K. Ng, E. H. Ooi, *Fem simulation of the eye structure with bio-heat analysis*, Comput. Methods Programs Biomedicine, **82** (2006), 268–276.
- [14] E. H. Ooi, E. Y. K. Ng, *Simulation of aqueous humor hydrodynamics in human eye heat transfer*, Computer. Biol. Med., **38** (2007), 252–262.
- [15] K. C. Gokul, D. B. Gurung, P. R. Adhikary, *Effects of blood perfusion and metabolism in temperature distribution in human eye*, Adv. Appl. Math. Biosci., **4** (2013), 13–23.
- [16] S. A. Schellini, A. A. Sampaio, E. Hoyama, A. A. V. Cruz, C. R. Padovani, *Spontaneous eye blink analysis in the normal individual*, Orbit, **24** (2005), 239–242.
- [17] D. B. Gurung, K. C. Gokul, *Mathematical model of thermal effects of blinking in human eye*, Int. J. Biomath., **9** (2016), 1650006.
- [18] L. Kessel, L. Johnson, H. Aridsson, M. Larsen, *The relationship between body and ambient temperature and corneal temperature*, Investigative Ophthalmology Vis. Sci., **51** (2010), 6593–6597.
- [19] I. A. Butovich, J. C. Arciniega, J. C. Wojtowicz, *Meibomian lipid films and the impact of temperature*, Investigative Ophthalmology Vis. Sci., **51** (2010), 5508–5518.
- [20] D. B. Gurung, V. P. Saxena, *Peripheral temperature distribution in human subjects exposed to wind flow*, Int. J. Math. Engrg., **2** (2010), 728–740.
- [21] S. Koh, C. Tung, R. Kottaiyan, J. Zavislam, G. Yoon, J. Aquavella, *Effect of airflow exposure on the tear meniscus*, J. Ophthalmology, (2012), Article ID 983182.
- [22] K. Nakamori, M. Odawara, T. Nakajima, T. Mizutani, K. Tsubota, *Blinking is controlled primarily by ocular surface conditions*, Amer. J. Ophthalmology **124** (1997), 23–30.
- [23] H. H. Pennes, *Analysis of tissue and arterial blood temperatures in the resting human forearm*, J. Appl. Physiology, **85** (1998), 5–34.

- [24] R. J. Dear, E. Arens, Z. Hui, *Convective and radiative heat transfer coefficients for individual human body segments*, Int. J. Biometeorol., **40** (1997), 141–156.
- [25] J. P. Holman, *Heat Transfer*, eighth si metric ed., Mc Graw Hill, India, 2001.
- [26] K. C. Gokul, D. B. Gurung, P. R. Adhikary, *Thermal effects of eyelid in human eye tempearture*, J. Appl. Math. Inform., **32** (2014), 649–663.
- [27] K. C. Gokul, D. B. Gurung, *Mathematical model: Comparative study of thermal effects of laser in corneal refractive surgeries*, Appl. Appl. Math., **10** (2015), 609–619.
- [28] A. Hirata, S. Watanabe, O. Fujiwara, M. Kojima, K. Sasaki, T. Shiozawa, *Temperature elevation in the eye of anatomically based human head models for plane-wave exposures*, Phys. Med. Biol., **52** (2007), 6389–6399.
- [29] M. Cvetkovic, D. Poljak, A. Peratta, *Fetd computation of the temperature distribution induced into a human eye by a pulsed laser*, Prog. Electromagn., **120** (2011), 403–421.
- [30] J. Kaminer, A. S. Powers, K. G. Horn, C. Hui, C. Evinger, *Characterizing the spontaneous blink generator: An animal model*, J. Neurosci., **31** (2011), 11256–11267.
- [31] S. Iwata, M. A. Lemp, F. J. Holly, C. H. Dohlman, *Evaporation rate of water from the precorneal tear film and cornea in the rabbit*, Investigative Ophthalmology Vis. Sci., **8** (1969), 613–619.
- [32] S. Acharya, D. B. Gurung, V. P. Saxena, *Effect of metabolic reactions on thermoregulation in human males and females body*, Appl. Math., **4** (2013), 39–48.
- [33] A. H. Rantamaki, M. Javanainen, I. Vattulainen, J. H. Holopainen, *Do lipids retard the evaporation of the tear fluid?*, Investigative Ophthalmology Vis. Sci., **53** (2012), 6442–6447.
- [34] R. D. Freeman, I. Fatt, *Environmental influences on ocular temperature*, Investigative Ophthalmology Vis. Sci., **12** (1973), 596–602.

SITEM for the Conformable Space-Time fractional (2+1)-Dimensional Asymmetric Nizhnik-Novikov-Veselov Equations

Handan Çerdik Yaslan^{1*} and Ayse Girgin¹

¹Department of Mathematics, Pamukkale University, Denizli, 20070, Turkey

*Corresponding author E-mail: hcerdik@pau.edu.tr

Article Info

Keywords: Conformable derivative, Simplified $\tan\left(\frac{\phi(\xi)}{2}\right)$ -expansion method (SITEM), Space-time fractional (2+1)-dimensional asymmetric Nizhnik-Novikov-Veselov equations

2010 AMS: 35R11, 35C07, 35Qxx

Received: 29 April 2019

Accepted: 25 July 2019

Available online: 26 December 2019

Abstract

In the present paper, new analytical solutions for the space-time fractional (2+1)-dimensional asymmetric Nizhnik-Novikov-Veselov (ANNV) equations are obtained by using the simplified $\tan\left(\frac{\phi(\xi)}{2}\right)$ -expansion method (SITEM).

1. Introduction

Nonlinear model arising from the field of mathematical physics is a popular topic since it is widely applied in many natural science such as chemistry, biology, mathematics, communication and particularly in almost all branches of physics like the fluid dynamics, plasma physics, field theory, nonlinear optics and condensed matter physics. Exact solutions of nonlinear models have extensively been investigated by different methods. For example, solutions of the (1 + 1)-dimensional KdV-type model by means of the modified tanh-function method with three different ansatz has been obtained [1]. Non-linear differential-difference sine-Gordon equation has been solved by using Jacobian elliptic function method [2]. Hierarchies of Peregrine solution and breather solution have been derived in a (2+1)-dimensional variable-coefficient nonlinear Schrodinger equation with partial nonlocality [3]. Extended tanh-function method based on the mapping method has been applied to the (2+1)-dimensional asymmetric Nizhnik-Novikov-Veselov system [4].

Nizhnik-Novikov-Veselov (NNV) equations have an important place in many fields of physics including condense matter physics, optics, fluid mechanics and plasma physics [5]-[7]. Solutions of the NNV equations have been investigated by many researchers. Extended tanh-function method, exp-function method, generalized auxiliary equation method have been applied to (2+1)-dimensional ANNV equations [8]-[10]. Generalized Nizhnik-Novikov-Veselov (GNNV) equations have been solved by using exp-function method, the extended hyperbolic function method, the tanh method, generalized F-expansion method and auxiliary ordinary differential equation method [11]-[15]. Combining the generalized direct method with the classical Lie method, solutions of the GNNV equations have been investigated [16]. The generalized, asymmetric and the modified NNV equations have been studied by using Hirota's bilinear method [17].

Fractional NNV equations have been studied in [18]-[22]. In these works, fractional derivatives are described in modified Riemann-Liouville sense (see, for example, [18]-[20]) and conformable sense (see, for example, [21, 22]). Generalized exp-function method has been applied to the space-time fractional ANNV equations [18]. Solitary-wave ansatz method, the (G'/G) expansion method and sub equation method have been used to obtain exact solutions of the space-time fractional GNNV equations [19, 20]. Exp-function method, (G'/G) expansion method and homotopy analysis method have been applied to the time fractional GNNV [21, 22].

Recently, the improved $\tan\left(\frac{\phi(\xi)}{2}\right)$ -expansion method (ITEM) has been applied by many authors [23]-[25]. In [26], ITEM has been simplified and called simplified ITEM (SITEM). SITEM has been applied to the Kundu-Eckhaus equation and Konopelchenko- Dubrovsky equations

in [26, 27], respectively. In this paper, we obtain new analytical solutions of the space-time fractional (2+1)-dimensional ANNV equations by using SITEM.

2. Description of the conformable fractional derivative and its properties

For a function $f : (0, \infty) \rightarrow R$, the conformable fractional derivative of f of order $0 < \alpha < 1$ is defined as (see, for example, [28])

$$T_t^\alpha f(t) = \lim_{\varepsilon \rightarrow 0} \frac{f(t + \varepsilon t^{1-\alpha}) - f(t)}{\varepsilon}.$$

Some important properties of the the conformable fractional derivative are as given follows:

$$\begin{aligned} T_t^\alpha (af + bg)(t) &= aT_t^\alpha f(t) + bT_t^\alpha g(t), \quad \forall a, b \in R, \\ T_t^\alpha (t^\mu) &= \mu t^{\mu-\alpha}, \\ T_t^\alpha (f(g(t))) &= t^{1-\alpha} g'(t) f'(g(t)). \end{aligned}$$

3. Analytic solutions to the conformable space-time fractional ANNV equations

Conformable space-time fractional ANNV equations are given in the following form [8, 9]

$$T_t^\alpha u - T_x^\beta T_x^\beta T_x^\beta u - 3T_x^\beta (uv) = 0, \quad (3.1)$$

$$T_x^\beta u = T_y^\theta v, \quad 0 < \alpha \leq 1, \quad 0 < \beta \leq 1, \quad 0 < \theta \leq 1. \quad (3.2)$$

Eqs.(3.1)-(3.2) were first derived by Boiti et al. [29] which may be considered as a model for an incompressible fluid.

Let us consider the following transformation

$$u(x, y, t) = U(\xi), \quad v(x, y, t) = V(\xi), \quad \xi = k \frac{t^\alpha}{\alpha} + m \frac{x^\beta}{\beta} + n \frac{y^\theta}{\theta}, \quad (3.3)$$

where k, m, n are constants. Substituting (3.3) into Eqs.(3.1)-(3.2) we obtain the following differential equations

$$kU' - m^3 U''' - 3m(UV)' = 0, \quad (3.4)$$

$$mU' = nV' \quad (3.5)$$

Integrating of Eqs.(3.4)-(3.5) with zero constant of integration and eliminating V , we have

$$kU - m^3 U'' - \frac{3m^2}{n} U^2 = 0. \quad (3.6)$$

Let us suppose that the solution of Eq.(3.6) can be expressed in the form

$$U(\xi) = \sum_{k=0}^N A_k \left[p + \tan \left(\frac{\phi(\xi)}{2} \right) \right]^k + \sum_{k=1}^N B_k \left[p + \tan \left(\frac{\phi(\xi)}{2} \right) \right]^{-k}. \quad (3.7)$$

Here $\phi(\xi)$ satisfies the following ordinary differential equation

$$\phi'(\xi) = a \sin(\phi(\xi)) + b \cos(\phi(\xi)) + c, \quad (3.8)$$

$a, b, c, A_k (0 \leq k \leq N)$ and $B_k (1 \leq k \leq N)$ are constants to be determined. The solution of Eq. (3.8) has been given in [27].

Substituting Eq.(3.7) into Eq.(3.6) for $p = 0$ and then by balancing the highest order derivative term and nonlinear term in result equation, the value of N can be determined as 2. Therefore, Eq.(3.7) reduces to

$$\begin{aligned} U(\xi) &= A_0 + A_1 \left[\tan \left(\frac{\phi(\xi)}{2} \right) \right] + A_2 \left[\tan \left(\frac{\phi(\xi)}{2} \right) \right]^2 + B_1 \left[\tan \left(\frac{\phi(\xi)}{2} \right) \right]^{-1} \\ &+ B_2 \left[\tan \left(\frac{\phi(\xi)}{2} \right) \right]^{-2}. \end{aligned} \quad (3.9)$$

Substituting Eq.(3.9) into Eq.(3.6) and collecting all the terms with the same power of $\tan(\frac{\phi}{2})$, we can obtain a set of algebraic equations for the unknowns $A_0, A_1, A_2, B_1, B_2, k, m, n$:

$$\begin{aligned} -6A_2^2 m^2 - 3nA_2 b^2 m^3 + 6nA_2 b c m^3 - 3nA_2 c^2 m^3 &= 0, \\ -A_1 n b^2 m^3 + 2A_1 n b c m^3 + 10aA_2 n b m^3 - A_1 n c^2 m^3 - 10aA_2 n c m^3 - 12A_1 A_2 m^2 &= 0, \\ -8A_2 n a^2 m^3 + 3naA_1 b m^3 - 3naA_1 c m^3 - 6A_1^2 m^2 + 4A_2 n b^2 m^3 - 4A_2 n c^2 m^3 - 12A_0 A_2 m^2 + 2A_2 k n &= 0, \\ 2A_1 k n - 12A_0 A_1 m^2 - 12A_2 B_1 m^2 - 2a^2 A_1 m^3 n + A_1 b^2 m^3 n - A_1 c^2 m^3 n - 6aA_2 b m^3 n - 6aA_2 c m^3 n &= 0, \\ 2A_0 k n - 6A_0^2 m^2 - 12A_1 B_1 m^2 - 12A_2 B_2 m^2 - A_2 b^2 m^3 n - A_2 c^2 m^3 n - b^2 B_2 m^3 n - B_2 c^2 m^3 n - aA_1 b m^3 n - aA_1 c m^3 n + abB_1 m^3 n - aB_1 c m^3 n &= 0, \\ -2A_2 b c m^3 n + 2bB_2 c m^3 n &= 0, \\ 2B_1 k n - 12A_0 B_1 m^2 - 12A_1 B_2 m^2 - 2a^2 B_1 m^3 n + b^2 B_1 m^3 n - B_1 c^2 m^3 n + 6abB_2 m^3 n - 6aB_2 c m^3 n &= 0, \\ -8B_2 n a^2 m^3 - 3nabB_1 m^3 - 3naB_1 c m^3 + 4B_2 n b^2 m^3 - 6B_1^2 m^2 - 4B_2 n c^2 m^3 - 12A_0 B_2 m^2 + 2B_2 k n &= 0, \\ -B_1 n b^2 m^3 - 2B_1 n b c m^3 - 10aB_2 n b m^3 - B_1 n c^2 m^3 - 10aB_2 n c m^3 - 12B_1 B_2 m^2 &= 0, \\ -3nb^2 B_2 m^3 - 6nbB_2 c m^3 - 6B_2^2 m^2 - 3nB_2 c^2 m^3 &= 0. \end{aligned}$$

Solving the algebraic equations in the Mathematica, we obtain the following set of solutions:

Case 1: $A_0 = \frac{1}{2}(b^2 - c^2)mn, A_1 = 0, A_2 = 0, B_1 = -amn(b+c), B_2 = -\frac{1}{2}(b+c)^2mn, k = \Delta m^3$:

For $b = c$ and $a = 0$, we have

$$U_1(\xi) = -2b^2mn \left[b\xi + c_1 \right]^{-2}.$$

For $b = c$ and $a \neq 0$, we have

$$U_2(\xi) = -amn2b \left[c_1 \exp(a\xi) - \frac{b}{a} \right]^{-1} - 2b^2mn \left[c_1 \exp(a\xi) - \frac{b}{a} \right]^{-2}.$$

For $\Delta > 0$ and $b \neq c$, we obtain

$$\begin{aligned} U_3(\xi) &= \frac{1}{2}(b^2 - c^2)mn \\ &- amn(b+c) \left[\frac{2}{b-c} \frac{c_1 r_1 \exp(r_1 \xi) + c_2 r_2 \exp(r_2 \xi)}{c_1 \exp(r_1 \xi) + c_2 \exp(r_2 \xi)} \right]^{-1} \\ &- \frac{1}{2}(b+c)^2mn \left[\frac{2}{b-c} \frac{c_1 r_1 \exp(r_1 \xi) + c_2 r_2 \exp(r_2 \xi)}{c_1 \exp(r_1 \xi) + c_2 \exp(r_2 \xi)} \right]^{-2}. \end{aligned} \quad (3.10)$$

For $\Delta < 0$ and $b \neq c$, we have

$$\begin{aligned} U_4(\xi) &= \frac{1}{2}(b^2 - c^2)mn \\ &- amn(b+c) \left[\frac{a}{b-c} + \frac{\sqrt{-\Delta}}{b-c} \frac{-c_1 \sin(\frac{\sqrt{-\Delta}}{2}\xi) + c_2 \cos(\frac{\sqrt{-\Delta}}{2}\xi)}{c_1 \cos(\frac{\sqrt{-\Delta}}{2}\xi) + c_2 \sin(\frac{\sqrt{-\Delta}}{2}\xi)} \right]^{-1} \\ &- \frac{1}{2}(b+c)^2mn \left[\frac{a}{b-c} + \frac{\sqrt{-\Delta}}{b-c} \frac{-c_1 \sin(\frac{\sqrt{-\Delta}}{2}\xi) + c_2 \cos(\frac{\sqrt{-\Delta}}{2}\xi)}{c_1 \cos(\frac{\sqrt{-\Delta}}{2}\xi) + c_2 \sin(\frac{\sqrt{-\Delta}}{2}\xi)} \right]^{-2}. \end{aligned}$$

Case 2: $A_0 = \frac{1}{2}(b^2 - c^2)mn, A_1 = a(b-c)mn, A_2 = -\frac{1}{2}(b-c)^2mn, B_1 = 0, B_2 = 0, k = \Delta m^3$:

For $\Delta > 0$ and $b \neq c$, we have

$$\begin{aligned} U_5(\xi) &= \frac{1}{2}(b^2 - c^2)mn + 2amn \left[\frac{c_1 r_1 \exp(r_1 \xi) + c_2 r_2 \exp(r_2 \xi)}{c_1 \exp(r_1 \xi) + c_2 \exp(r_2 \xi)} \right] \\ &- 2mn \left[\frac{c_1 r_1 \exp(r_1 \xi) + c_2 r_2 \exp(r_2 \xi)}{c_1 \exp(r_1 \xi) + c_2 \exp(r_2 \xi)} \right]^2. \end{aligned}$$

For $\Delta < 0$ and $b \neq c$, we have

$$\begin{aligned} U_6(\xi) &= \frac{1}{2}(b^2 - c^2)mn \\ &+ amn \left[a + \sqrt{-\Delta} \frac{-c_1 \sin(\frac{\sqrt{-\Delta}}{2}\xi) + c_2 \cos(\frac{\sqrt{-\Delta}}{2}\xi)}{c_1 \cos(\frac{\sqrt{-\Delta}}{2}\xi) + c_2 \sin(\frac{\sqrt{-\Delta}}{2}\xi)} \right] \\ &- \frac{1}{2}mn \left[a + \sqrt{-\Delta} \frac{-c_1 \sin(\frac{\sqrt{-\Delta}}{2}\xi) + c_2 \cos(\frac{\sqrt{-\Delta}}{2}\xi)}{c_1 \cos(\frac{\sqrt{-\Delta}}{2}\xi) + c_2 \sin(\frac{\sqrt{-\Delta}}{2}\xi)} \right]^2. \end{aligned} \quad (3.11)$$

Case 3: $A_0 = \frac{1}{6}(-2a^2mn + b^2mn - c^2mn), A_1 = 0, A_2 = 0, B_1 = -amn(b+c), B_2 = -\frac{1}{2}(b+c)^2mn, k = -\Delta m^3$:

For $b = c$ and $a = 0$, we obtain

$$U_7(\xi) = -2b^2mn \left[b\xi + c_1 \right]^{-2}.$$

For $b = c$ and $a \neq 0$, we have

$$\begin{aligned} U_8(\xi) &= -\frac{1}{3}(a^2mn) - amn(2b) \left[c_1 \exp(a\xi) - \frac{b}{a} \right]^{-1} \\ &- 2b^2mn \left[c_1 \exp(a\xi) - \frac{b}{a} \right]^{-2}. \end{aligned}$$

For $\Delta > 0$ and $b \neq c$, we have

$$\begin{aligned} U_9(\xi) &= \frac{1}{6}(-2a^2mn + b^2mn - c^2mn) \\ &- amn(b+c) \left[\frac{2}{b-c} \frac{c_1 r_1 \exp(r_1 \xi) + c_2 r_2 \exp(r_2 \xi)}{c_1 \exp(r_1 \xi) + c_2 \exp(r_2 \xi)} \right]^{-1} \\ &- \frac{1}{2}(b+c)^2mn \left[\frac{2}{b-c} \frac{c_1 r_1 \exp(r_1 \xi) + c_2 r_2 \exp(r_2 \xi)}{c_1 \exp(r_1 \xi) + c_2 \exp(r_2 \xi)} \right]^{-2}. \end{aligned}$$

For $\Delta < 0$ and $b \neq c$, we have

$$\begin{aligned}
 U_{10}(\xi) &= \frac{1}{6}(-2a^2mn + b^2mn - c^2mn) \\
 &- amn(b+c) \left[\frac{a}{b-c} + \frac{\sqrt{-\Delta} - c_1 \sin(\frac{\sqrt{-\Delta}}{2}\xi) + c_2 \cos(\frac{\sqrt{-\Delta}}{2}\xi)}{c_1 \cos(\frac{\sqrt{-\Delta}}{2}\xi) + c_2 \sin(\frac{\sqrt{-\Delta}}{2}\xi)} \right]^{-1} \\
 &- \frac{1}{2}(b+c)^2mn \left[\frac{a}{b-c} + \frac{\sqrt{-\Delta} - c_1 \sin(\frac{\sqrt{-\Delta}}{2}\xi) + c_2 \cos(\frac{\sqrt{-\Delta}}{2}\xi)}{c_1 \cos(\frac{\sqrt{-\Delta}}{2}\xi) + c_2 \sin(\frac{\sqrt{-\Delta}}{2}\xi)} \right]^{-2}.
 \end{aligned} \tag{3.12}$$

Case 4: $A_0 = \frac{1}{6}(-2a^2mn + b^2mn - c^2mn)$, $A_1 = a(b-c)mn$, $A_2 = -\frac{1}{2}(b-c)^2mn$, $B_1 = 0$, $B_2 = 0$, $k = -\Delta m^3$:
 For $\Delta > 0$ and $b \neq c$, we have

$$\begin{aligned}
 U_{11}(\xi) &= \frac{1}{6}(-2a^2mn + b^2mn - c^2mn) \\
 &+ 2amn \left[\frac{c_1 r_1 \exp(r_1 \xi) + c_2 r_2 \exp(r_2 \xi)}{c_1 \exp(r_1 \xi) + c_2 \exp(r_2 \xi)} \right] \\
 &- 2mn \left[\frac{c_1 r_1 \exp(r_1 \xi) + c_2 r_2 \exp(r_2 \xi)}{c_1 \exp(r_1 \xi) + c_2 \exp(r_2 \xi)} \right]^2.
 \end{aligned}$$

For $\Delta < 0$ and $b \neq c$, we have

$$\begin{aligned}
 U_{12}(\xi) &= \frac{1}{6}(-2a^2mn + b^2mn - c^2mn) \\
 &+ amn \left[a + \sqrt{-\Delta} \frac{-c_1 \sin(\frac{\sqrt{-\Delta}}{2}\xi) + c_2 \cos(\frac{\sqrt{-\Delta}}{2}\xi)}{c_1 \cos(\frac{\sqrt{-\Delta}}{2}\xi) + c_2 \sin(\frac{\sqrt{-\Delta}}{2}\xi)} \right] \\
 &- \frac{1}{2}mn \left[a + \sqrt{-\Delta} \frac{-c_1 \sin(\frac{\sqrt{-\Delta}}{2}\xi) + c_2 \cos(\frac{\sqrt{-\Delta}}{2}\xi)}{c_1 \cos(\frac{\sqrt{-\Delta}}{2}\xi) + c_2 \sin(\frac{\sqrt{-\Delta}}{2}\xi)} \right]^2,
 \end{aligned}$$

where $\xi = -\Delta m^3 \frac{t^\alpha}{\alpha} + m \frac{x^\beta}{\beta} + n \frac{y^\theta}{\theta}$, $\Delta = a^2 + b^2 - c^2$. From the formula $V(\xi) = \frac{m}{n} U(\xi)$, $v(x, y, t)$ can be computed.

The solutions $u_2(x, y, t)$, $u_5(x, y, t)$, $u_6(x, y, t)$ and $u_{10}(x, y, t)$ of the Eqs.(3.1)-(3.2) are simulated as traveling wave solutions for various values of the physical parameters in Fig.3.1-Fig.3.8. Figs.3.1, 3.2 show kink waves solutions, Figs.3.3 and 3.4 show solitary waves solutions, Figs.3.5, 3.6, 3.7 and 3.8 show periodic waves solutions of Eqs.(3.1)-(3.2). Figs.3.1 and 3.2 are 3D and 2D plots of the traveling wave solution $u_2(x, 1, t)$ and $u_2(x, 1, 1)$ in Eq.(3.10). 3D plot of the obtained solution $u_2(x, 1, t)$ is given for parameters $\alpha = 0.5$, $\beta = 1$, $\theta = 0.75$, $m = 0.25$, $n = -0.5$, $a = 0.5$, $b = 0.25$, $c = 0.25$, $c_1 = 1$, $c_2 = 1$ in Fig.3.1. Fig.3.2 demonstrate the same solution with 2D plot for $-40 \leq x \leq 40$ at $t = 1$. Figs.3.3 and 3.4 are 3D and 2D plots of the traveling wave solution $u_5(x, 1, t)$ and $u_5(x, 1, 1)$ in Eq.(3.11) for $\alpha = 0.5$, $\beta = 1$, $\theta = 0.75$, $m = 1$, $n = -0.5$, $a = 0.02$, $b = 0.2$, $c = 0.01$, $c_1 = 2$, $c_2 = 1$, respectively. Figs.3.5 and 3.6 are 3D and 2D plots of the traveling wave solution $u_6(x, 1, t)$ and $u_6(x, 1, 1)$ in Eq.(3.11) for $\alpha = 0.5$, $\beta = 1$, $\theta = 0.75$, $m = 0.1$, $n = -0.5$, $a = 1$, $b = 2$, $c = 5$, $c_1 = 2$, $c_2 = 2$, respectively. Figs.3.7 and 3.8 show 3D and 2D plots of the traveling wave solution $u_{10}(x, 1, t)$ and $u_{10}(x, 1, 1)$ in Eq.(3.12) for $\alpha = 0.75$, $\beta = 1$, $\theta = 0.5$, $m = 0.25$, $n = 0.05$, $a = 1$, $b = 2$, $c = 3$, $c_1 = 1$, $c_2 = 1$, respectively. Note that the 3D graphs describe the behavior of u in space x and time t at fixed $y = 1$, which represents the change of amplitude and shape for each obtained solitary wave solutions. 2D graphs describe the behavior of u in space x at fixed time $t = 1$ and fixed $y = 1$. All graphics in figures are drawn by the aid of Mathematica 10.

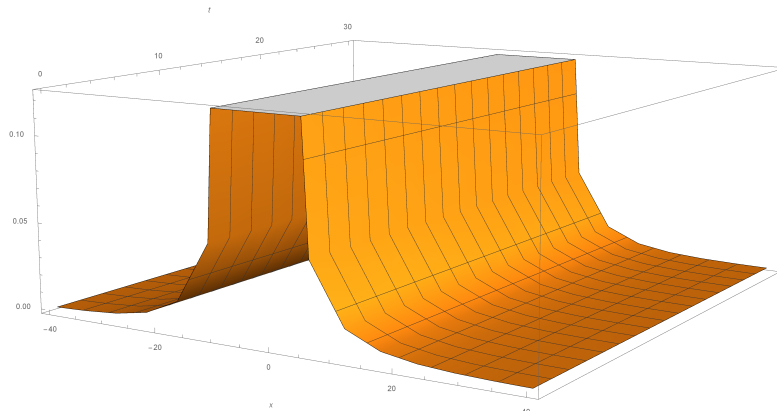


Figure 3.1: King wave solution $u_2(x, 1, t)$ of Eq.(3.10).

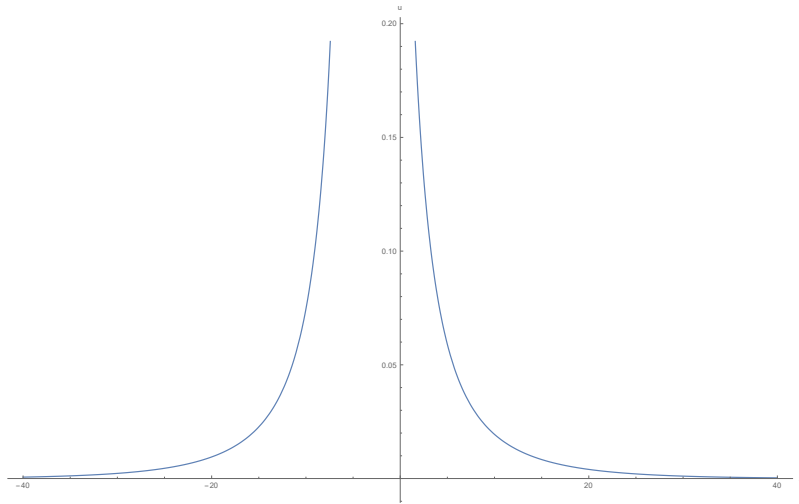


Figure 3.2: King wave solution $u_2(x, 1, 1)$ of Eq.(3.10).

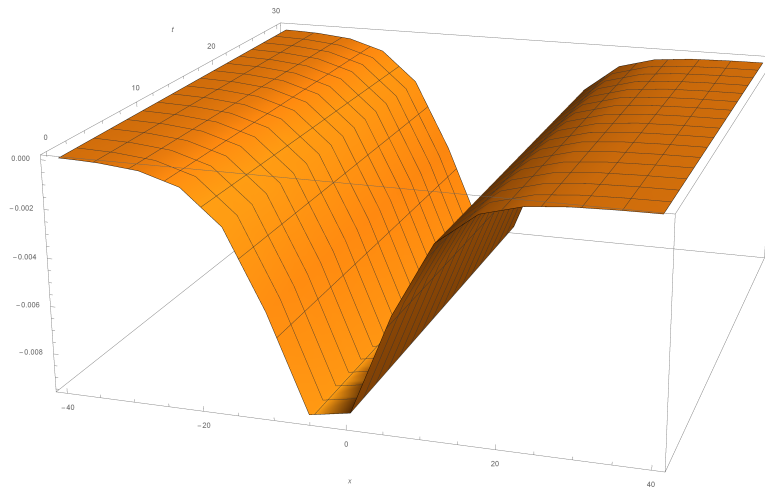


Figure 3.3: Solitary wave solution $u_5(x, 1, t)$ of Eq.(3.11).

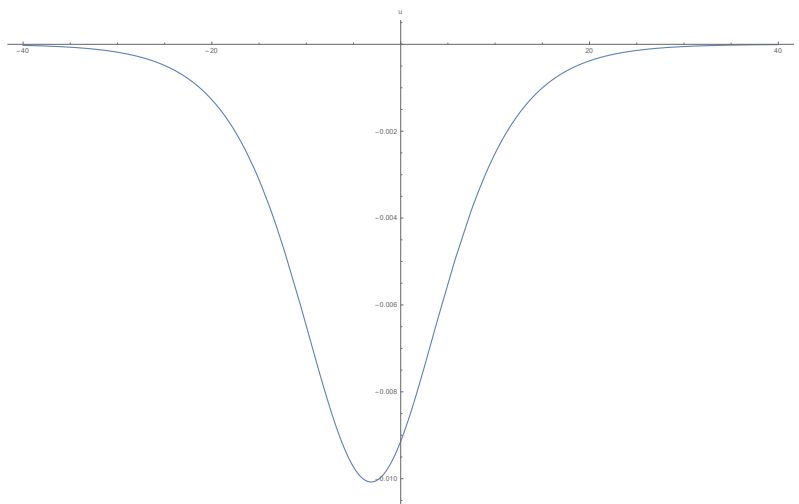


Figure 3.4: Solitary wave solution $u_5(x, 1, 1)$ of Eq.(3.11).

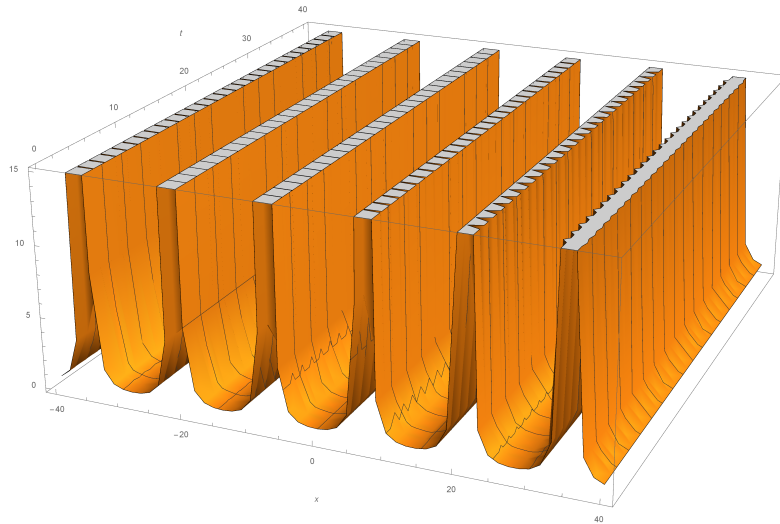


Figure 3.5: Periodic wave solution $u_6(x, 1, t)$ of Eq.(3.11).

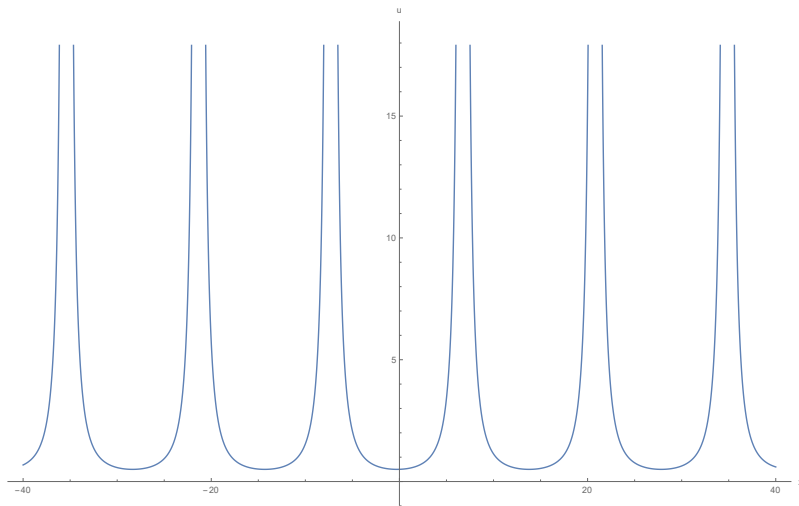


Figure 3.6: Periodic wave solution $u_6(x, 1, 1)$ of Eq.(3.11).

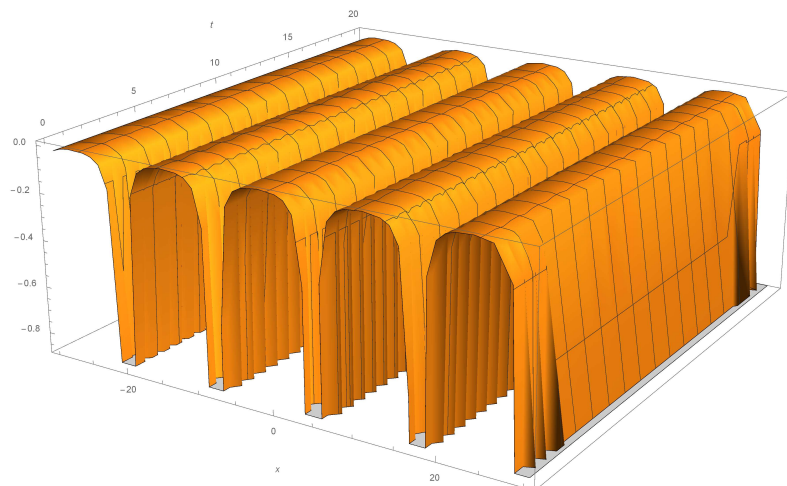


Figure 3.7: Periodic wave solution $u_{10}(x, 1, t)$ of Eq.(3.12).

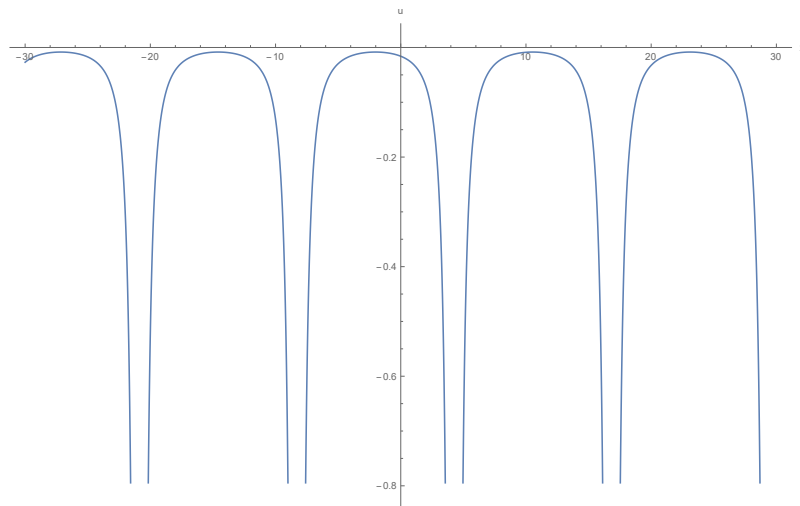


Figure 3.8: Periodic wave solution $u_{10}(x, 1, 1)$ of Eq.(3.12).

4. Conclusion

In this paper, the conformable space-time fractional ANNV equations have been solved by using the simplified $\tan(\frac{\phi(\xi)}{2})$ -expansion method (SITEM). Simulations of the kink wave, solitary wave and periodic wave solutions of the conformable space-time fractional ANNV equations have been obtained. Note that SITEM has been applied to the Kundu-Eckhaus equation for the parameter $p = 0$ in [26] and Konopelchenko-Dubrovsky equations for the nonzero parameter p in [27]. To our knowledge, conformable fractional ANNV equations have been solved for only time fractional case. In our work, SITEM has been applied to both space and time fractional ANNV equations.

References

- [1] Y. Y. Wang, Y. P. Zhang, C. Q. Dai, *Re-study on localized structures based on variable separation solutions from the modified tanh-function method*, *Nonlinear Dyn.* **83** (2016), 1331-1339.
- [2] D. J. Ding, D. Q. Jin, C. Q. Dai, *Analytical Solutions of Differential-Difference Sine-Gordon Equation*, *Thermal Science*, **21** (2017), 1701-1705.
- [3] C. Q. Dai, J. Liu, Y. Fan, D. G. Yu, *Two-dimensional localized Peregrine solution and breather excited in a variable-coefficient nonlinear Schrödinger equation with partial nonlocality*, *Nonlinear Dyn.*, **88** (2017), 1373-1383.
- [4] C. Q. Dai, G. Q. Zhou, *Exotic interactions between solitons of the (2 + 1)-dimensional asymmetric Nizhnik-Novikov-Veselov system*, *Chinese Phys.*, **16** (2007), 1201-1208.
- [5] T. Hong, Y. Z. Wang, Y. S. Huo, *Bogoliubov quasiparticles carried by dark solitonic excitations in nonuniform Bose Einstein condensates*, *Chin. Phys. Lett.*, **15** (1998), 550-552.
- [6] G. C. Das, *Explosion of soliton in a multicomponent plasma*, *Phys. Plasmas*, **4** (1997), 2095-2100.
- [7] S. Y. Lou, *A direct perturbation method: Nonlinear Schrödinger equation with loss*, *Chin. Phys. Lett.*, **16** (1999), 659-661.
- [8] C. Q. Dai, S. S. Wu, X. Cen, *New exact solutions of the (2+1)-dimensional asymmetric Nizhnik-Novikov-Veselov system*, *Int. J. Theor. Phys.*, **47** (2008), 1286-1293.
- [9] C. Q. Dai, Y. Y. Wang, *New variable separation solutions of the (2 + 1)-dimensional asymmetric Nizhnik-Novikov-Veselo system*, *Nonlinear Anal.*, **71** (2009), 1496-1503.
- [10] S. Zhang, T. C. Xia, *A generalized auxiliary equation method and its application to (2+1)-dimensional asymmetric Nizhnik-Novikov-Vesselov equations*, *J. Phys. A: Math. Theor.*, **40** (2007), 227-248.
- [11] A. Borhanifar, M. M. Kabir, L. M. Vahdat, *New periodic and soliton wave solutions for the generalized Zakharov system and (2 + 1)-dimensional Nizhnik-Novikov-Veselov system*, *Chaos Soliton Fractals*, **42** (2009), 1646-1654.
- [12] C. Deng, *New abundant exact solutions for the (2 + 1)-dimensional generalized Nizhnik-Novikov-Veselo system*, *Commun. Nonlinear Sci. Numer. Simula.*, **15** (2010), 3349-3357.
- [13] E. Yusufoglu, A. Bekir, *Exact solutions of coupled nonlinear evolution equations*, *Chaos Soliton Fractals*, **37** (2008), 842-848.
- [14] Y. J. Ren, H. Q. Zhang, *A generalized F-expansion method to find abundant families of Jacobi Elliptic Function solutions of the (2 + 1)-dimensional Nizhnik-Novikov-Veselov equation*, *Chaos Soliton Fractals*, **27** (2006), 959-979.
- [15] J. Tang, F. Han, M. Zhao, W. Fu, *Travelling wave solutions for the (2 + 1) dimensional Nizhnik-Novikov-Veselov equation*, *Appl. Math. Comput.*, **218** (2012), 11083-11088.
- [16] Y. Chen, Z. Z. Dong, *Symmetry reduction and exact solutions of the generalized Nizhnik-Novikov-Veselov equation*, *Nonlinear Anal.*, **71** (2009), 810-817.
- [17] A. M. Wazwaz, *Structures of multiple soliton solutions of the generalized, asymmetric and modified Nizhnik-Novikov-Veselov equations*, *Appl. Math. Comput.*, **218** (2012), 11344-11349.
- [18] L. M. Yan, F. S. Xu, *Generalized Exp-Function Method for Non-Linear Space-Time Fractional Differential Equations*, *Thermal Science*, **18** (2014), 1573-1576.
- [19] O. Guner, *New travelling wave solutions for fractional regularized long-wave equation and fractional coupled Nizhnik-Novikov-Veselov equation*, *J. Optim. Control Theor. Appl.*, **8** (2018), 63-72.
- [20] Y. Liu, L. Yan, *SSolutions of fractional Konopelchenko-Dubrovsky and Nizhnik-Novikov-Veselov equations using a generalized fractional subequation method*, *Abstr. Appl. Anal.*, **2013** (2013), Article ID 839613, 7 pages, doi:10.1155/2013/839613.
- [21] O. Tasbozan, Y. Cenesiz, A. Kurt, D. Baleanu, *New analytical solutions for conformable fractional PDEs arising in mathematical physics by exp-function method*, *Open Phys.*, **15** (2017), 647-651.
- [22] A. Kurt, O. Tasbozan, D. Baleanu, *New solutions for conformable fractional Nizhnik- Novikov-Veselov system via G'/G expansion method and homotopy analysis methods*, *Opt. Quant. Electron.*, **49**(333) (2017), 1-16.
- [23] J. Manafian, M. Foroutan, *Application of $\tan(\phi(\xi)/2)$ -expansion method for the time-fractional Kuramoto-Sivashinsky equation*, *Opt. Quant. Electron.*, **49**(272) (2017), 1-18.
- [24] J. Manafian, M. Lakestani, *Optical soliton solutions for the Gerdjikov-Ivanov model via $\tan(\phi(\xi)/2)$ -expansion method*, *Optik*, **127** (2016), 9603-9620.
- [25] J. Manafian, M. F. Aghdaei, M. Zadahmad, *Analytic study of sixth-order thin-film equation by $\tan(\phi(\xi)/2)$ -expansion method*, *Opt. Quant. Electron.*, **48** (2016), 410-424.
- [26] H. Liu, T. Zhang, *A note on the improved $\tan(\phi(\xi)/2)$ -expansion method*, *Optik*, **131** (2017), 273-278.
- [27] H. C. Yaslan, A. Girgin, *Sitem for the conformable space-time fractional coupled kd equations*, *J. Eng. Tech. Appl. Sci.*, **3** (2018), 223-233.
- [28] R. Khalil, M. A. Horani, A. Yousef, M. Sababheh, *A new definition of fractional derivative*, *J. Comput. Appl. Math.* **264** (2014), 65-70.

- [29] M. Boiti, J. J. P. Leon, M. Manna, F. Pempinelli, *On the spectral transform of a Korteweg-de Vries equation in two spatial dimensions*, Inverse Probl., **2** (1986), 271-279.

Some Exact Bianchi Types Cosmological Models in $f(R, T)$ Theory of Gravity

Abdulvahid Harunbhai Hasmani¹ and Ahmed Mohammed Al-Haysah^{1*}

¹Department of Mathematics, Sardar Patel University, Vallabh Vidyanagar-388120 Gujarat, India

^{1*}Department of Mathematics, Faculty of Education and Sciences-Rada'a, Albaydha University, Albaydha, Yemen

*Corresponding author E-mail: alhaysah2010@gmail.com

Article Info

Keywords: Bianchi types-III, V, VI₀ & VI_h, $f(R, T)$ theory of gravity, Cosmic time, Cosmological constant, Exact solutions, Hubble parameter, Variational principle

2010 AMS: 83D05, 83F05, 83C15

Received: 21 June 2018

Accepted: 30 April 2019

Available online: 26 December 2019

Abstract

In this paper, we attempt to study spatially homogeneous Bianchi types-III, V, VI₀ & VI_h cosmological models in $f(R, T)$ theory of gravity. Here the models are obtained by assuming forms of the function $f(R, T)$ as $f(R, T) = R + 2f(T)$ and $f(R, T) = f_1(R) + f_2(T)$. The exact solutions of Einstein's field equations (EFEs) have been obtained for two different types of physically viable cosmologies using a special form of Hubble parameter (HP). The physical and geometrical properties of these models have been discussed and expressions for the Ricci scalar R in each case are obtained.

1. Introduction

General relativity (GR) or Einstein's theory of gravitation is the most successful theory in application to cosmology. Until recently, our mental picture of the universe was based more on our philosophical prejudices (or religious beliefs) than on observational data [1]. Cosmology is a study of the origin, structure evolution, and fate of the universe as a whole based on interpretations of astronomical observations at different wave-lengths through laws of physics. Relativistic cosmological models are described as the exact solutions of the EFEs that help in understanding the important features of our universe. Many generalizations of EFEs have been proposed in last few decades. Einstein's general theory of relativity (GR) is one of the most beautiful structures of theoretical physics. Among several theories of gravitation, GR has been designated as the most successful one. In fact, GR is regarded as a geometric theory of gravitation.

Einstein's theory of gravitation is characterized by mathematical elegance and outstanding formal beauty using tools of Riemannian geometry. It is also realized that it leads to gravitational action. In 1917, Einstein introduced the cosmological constant Λ as the universal repulsion to make the universe static in accordance with a generally accepted picture of that time.

Einstein's theory is modified in several ways for better understanding. The bimetric theory, scalar-tensor theory, etc to name a few. A modification was given in $f(R, T)$ theory [2, 3]. The $f(R, T)$ theory of gravitation is one of the most popular alternatives to Einstein's theory of gravitation. Harko et al. (2011) [4] proposed another extension of standard GR, called the $f(R, T)$ theory of gravity, by introducing an arbitrary function of the Ricci scalar R and the trace T of the energy-momentum tensor. The field equations are derived from the Hilbert-Einstein type variational principle [5, 6]. In $f(R, T)$ theory we assume that the gravitational part of the action still depends on a generic function of the Ricci scalar R , but also presents a generic dependence on T [7]. Such a dependence on T would come from the consideration of quantum effects [8]. In reality, $f(R, T)$ theory provides an alternative way to explain the current cosmic acceleration with no need of introducing either the existence of extra spatial dimension or an exotic component like dark energy [9, 10]. In this theory, the gravitational Lagrangian S_m is given by an arbitrary function of the Ricci scalar R and trace T . This theory can be applied to explore various issues of current interests and may lead to some good inferences [11].

Bianchi types models have a vital role in the description and understanding of the early stages of evolution of the universe. In view of the observation of microwave background radiation, it is found that the universe is not isotropic [3, 12, 13]. Thus, the study of Bianchi types-III, V, VI₀ & VI_h cosmological models is important in the sense that these models are homogeneous and anisotropic, from which the process of isotropization of the universe is studied through the passage of time.

In this paper, an attempt has been made to investigate the exact solutions for Bianchi types-III, V, VI₀ & VI_h cosmological models in the framework of two cases of $f(R, T)$ theory of gravity. The physical and geometrical behaviors of such models have also been discussed.

2. $f(R, T)$ theory of gravity

The $f(R, T)$ theory is a modification of GR. The field equations of $f(R, T)$ theory are derived from a Hilbert-Einstein type variational principle.

The action for modified $f(R, T)$ theory of gravity is given by

$$S = \frac{1}{16\pi} \int f(R, T) \sqrt{-g} d^4x + \int S_m \sqrt{-g} d^4x, \quad (2.1)$$

where $f(R, T)$ is an arbitrary smooth function of Ricci scalar R and the trace T of energy-momentum tensor. S_m is the matter Lagrangian density. The matter energy-momentum tensor T_{ij} from the Lagrangian S_m is defined as [14],

$$T_{ij} = \frac{-2}{\sqrt{-g}} \frac{\partial(\sqrt{-g} S_m)}{\partial g^{ij}}. \quad (2.2)$$

Let us assume that the dependence of matter Lagrangian density S_m is merely on the metric tensor g_{ij} instead of its derivatives. In this case, Equation (2.2) becomes

$$T_{ij} = g_{ij} S_m - 2 \frac{\partial S_m}{\partial g^{ij}}. \quad (2.3)$$

The variations of the metric determinant and Ricci scalar R are

$$\partial(\sqrt{-g}) = -\frac{1}{2} \sqrt{-g} g_{ij} \partial g^{ij}, \quad (2.4)$$

$$\partial(R) = \partial(g^{ij} R_{ij}) = R_{ij} \partial g^{ij} + g_{ij} \nabla^k \nabla_k \partial g^{ij} - \nabla_i \nabla_j \partial g^{ij}. \quad (2.5)$$

The field equations of $f(R, T)$ theory are obtained by varying the action S in Equation (2.1) and using the properties given in Equations (2.4) and (2.5)

$$\frac{\partial f(R, T)}{\partial R} R_{ij} - \frac{1}{2} f(R, T) g_{ij} + (g_{ij} \nabla^k \nabla_k - \nabla_i \nabla_j) \frac{\partial f(R, T)}{\partial R} = 8\pi T_{ij} - \frac{\partial f(R, T)}{\partial T} (T_{ij} + \Theta_{ij}), \quad i, j, k = 1, 2, 3, 4, \quad (2.6)$$

where ∇_i denotes the covariant derivative. We define the variation of T with respect to the metric tensor as

$$\frac{\partial(g^{kl} T_{kl})}{\partial g^{ij}} = T_{ij} + \Theta_{ij}, \quad (2.7)$$

where

$$\Theta_{ij} = g^{kl} \frac{\partial T_{kl}}{\partial g^{ij}}. \quad (2.8)$$

It is clear from Equations (2.3) and (2.7), the tensor Θ_{ij} give in Equation (2.8) lead to

$$\Theta_{ij} = -2T_{ij} + g_{ij} S_m - 2g^{kl} \frac{\partial^2 S_m}{\partial g^{ij} \partial g^{kl}}. \quad (2.9)$$

Note that when $f(R, T) = f(R)$, then Equations (2.6) reduces to the field equations of $f(R)$ gravity. Contraction of Equation (2.6) gives the following relation between the Ricci scalar R and the trace T of the stress-energy tensor

$$\frac{\partial f(R, T)}{\partial R} R + 3 \nabla^k \nabla_k \frac{\partial f(R, T)}{\partial R} - 2f(R, T) = 8\pi T - \frac{\partial f(R, T)}{\partial T} T - \frac{\partial f(R, T)}{\partial T} \Theta, \quad (2.10)$$

with $\Theta = g^{ij} \Theta_{ij}$, Equation (2.10) gives a relation between Ricci scalar R and the trace T of energy-momentum tensor T_{ij} . In the other way the matter Lagrangian S_m , can be taken as $S_m = -p$. Then with the use of Equation (2.9), we obtain Θ_{ij} as

$$\Theta_{ij} = -2T_{ij} - p g_{ij}. \quad (2.11)$$

Using Equation (2.11) in Equation (2.6) the field equations become

$$\frac{\partial f(R, T)}{\partial R} R_{ij} - \frac{1}{2} f(R, T) g_{ij} + (g_{ij} \nabla^k \nabla_k - \nabla_i \nabla_j) \frac{\partial f(R, T)}{\partial R} = \left(8\pi + \frac{\partial f(R, T)}{\partial T} \right) T_{ij} + \frac{\partial f(R, T)}{\partial T} p g_{ij}. \quad (2.12)$$

Following, Harko et al. (2011) [4] to obtain some particular classes of $f(R, T)$ modified gravity models by specifying functional forms of $f(R, T)$ as

$$f(R, T) = \begin{cases} R + 2f(T), \\ f_1(R) + f_2(T), \\ f_1(R) + f_2(R) f_3(T). \end{cases} \quad (2.13)$$

In this paper, the attempt is to explore the first and the second cases of Equation (2.13) to study the exact solutions for Bianchi-III, V, VI₀ & VI_h in $f(R, T)$ theory of gravity.

3. The metric and the field equations

The spatially homogeneous (SH) and anisotropic Bianchi types space-times are given by,

$$ds^2 = dt^2 - A_1^2 dx^2 - e^{-2x} A_2^2 dy^2 - e^{-2mx} A_3^2 dz^2, \quad (3.1)$$

where A_1, A_2 and A_3 are called cosmic scale factors which are functions of time t , so the equation (3.1) represents different Bianchi types as,

1. Bianchi type-III if $m = 0$,
2. Bianchi type-V if $m = 1$,
3. Bianchi type-VI₀ if $m = -1$,
4. Bianchi type-VI_h for all other $m = h = -1$.

The computation of Ricci tensor R_{ij} and its spur was done using Mathematica [15] and [16]; the non-vanishing independent components are,

$$R_{11} = 1 + m^2 + A_1 \left[\dot{A}_1 \left(-\frac{\dot{A}_2}{A_2} - \frac{\dot{A}_3}{A_3} \right) - \ddot{A}_1 \right], \quad (3.2)$$

$$R_{14} = \frac{(m+1)\dot{A}_1}{A_1} - \frac{\dot{A}_2}{A_2} - \frac{m\dot{A}_3}{A_3}, \quad (3.3)$$

$$R_{22} = \frac{e^{-2x} A_2 \left[-(m+1)A_2 A_3 - A_1 (\dot{A}_2 (A_3 \dot{A}_1 + A_1 \dot{A}_3) + A_1 A_3 \dot{A}_2) \right]}{A_1^2 A_3}, \quad (3.4)$$

$$R_{33} = \frac{e^{-2mx} A_3 \left[-A_1^2 \dot{A}_2 \dot{A}_3 + A_2 (m(m+1)A_3 - A_1 (\dot{A}_1 \dot{A}_3 + A_1 \dot{A}_3)) \right]}{A_1^2 A_2}, \quad (3.5)$$

$$R_{44} = \frac{\dot{A}_1}{A_1} + \frac{\dot{A}_2}{A_2} + \frac{\dot{A}_3}{A_3}, \quad (3.6)$$

and

$$R = 2 \left[\frac{\ddot{A}_1}{A_1} + \frac{\ddot{A}_2}{A_2} + \frac{\ddot{A}_3}{A_3} + \frac{\dot{A}_1 \dot{A}_2}{A_1 A_2} + \frac{\dot{A}_1 \dot{A}_3}{A_1 A_2 A_3} + \frac{\dot{A}_2 \dot{A}_3}{A_2 A_3} - \frac{m^2 + m + 1}{A_1^2} \right], \quad (3.7)$$

where an overhead dot denotes derivative with respect to time t . The energy-momentum tensor for a perfect fluid is given by

$$T_{ij} = (\rho + p)u_i u_j - p g_{ij}, \quad (3.8)$$

where ρ is the proper energy density, p is the isotropic pressure and $u_i = (0, 0, 0, 1)$ is 4-velocity of the fluid particles which satisfies the condition $u^i u_i = 1$. The EFEs are given by

$$R_{ij} - \frac{1}{2} R g_{ij} = -8\pi T_{ij} + \Lambda g_{ij}, \quad (3.9)$$

where Λ is the cosmological constant. The average scale factor $a(t)$ and spatial volume V are defined by

$$V = a^3 = \prod_{i=1}^3 A_i. \quad (3.10)$$

Mean HP is given by

$$H = \frac{1}{3} \frac{\dot{V}}{V} = \frac{\dot{a}}{a} = \frac{1}{3} \sum_{i=1}^3 H_i = \frac{1}{3} \left(\frac{\dot{A}_1}{A_1} + \frac{\dot{A}_2}{A_2} + \frac{\dot{A}_3}{A_3} \right), \quad (3.11)$$

in which HPs in the directions of x, y and z -axes are obtained as

$$H_i = \frac{\dot{A}_i}{A_i}, \quad i = 1, 2, 3 \quad (\text{no sum}). \quad (3.12)$$

The scalar expansion θ is given by

$$\theta = \left(\frac{\dot{A}_1}{A_1} + \frac{\dot{A}_2}{A_2} + \frac{\dot{A}_3}{A_3} \right) = 3H.$$

Moreover, the shear σ^2 is given by

$$\sigma^2 = \frac{1}{2} \sigma_{ij} \sigma^{ij} = \frac{1}{2} \left[\sum_{i=1}^3 H_i^2 - 3H^2 \right],$$

the shear parameter is given by

$$\Sigma^2 = \Sigma_+^2 + \Sigma_-^2 = \frac{\sigma^2}{3H^2} = \frac{1}{6} \Sigma_{ij} \Sigma^{ij}, \quad \text{with } \Sigma_{ij} = \frac{\sigma_{ij}}{H}.$$

The density parameter Ω is given by

$$\Omega = 1 - \Sigma^2 - K \geq 0,$$

where the curvature parameter K is given by

$$K = \frac{{}^3R}{6H^2} = \frac{1}{12} \left(\sum_i N_i^2 - 2 \sum_{i < j} N_i N_j \right), \quad i, j = 1, 2, 3, \tag{3.13}$$

i.e.,

Group class	Bianchi type	N_1	N_2	N_3
Class A, ($a = 0$)	VI_0	0	+	-
	V	0	0	0
Class B, ($a \neq 0$)	VI_h	0	-	+
	III	0	+	-

Table 1: Canonical Structure Constants for Different Bianchi Types

The three structure constants N_1, N_2 and N_3 are the eigenvalue of the symmetric matrix, $N^{ij} = \text{diag}(N_1, N_2, N_3)$. In another way, we can get the form

$$\Omega + K + \Sigma^2 = 1.$$

An important observable quantity in cosmology is deceleration parameter (DP) defined as

$$q = -1 - \frac{\dot{H}}{H^2} = -\frac{\ddot{a}a}{\dot{a}^2}. \tag{3.14}$$

The evolution of H is describe by

$$\dot{H} = -(1 + q)H^2.$$

It is worth mentioning here that “the name DP and the negative sign are historical. Initially, q was supposed to be positive but recent observations from the supernova experiments suggest that it is negative”. To solve an integral part in the aforementioned equation, we may refer to the power-law assumption. Many kinds of researchers have used the power-law relation. For instance, Johri and Desikan [17] in the context of Robertson-Walker Brans-Dicke models, have already used the power-law relation between scale factor and scalar field. We use a well-known relation [18] between the mean HP and average scale factor a , given as

$$H = la^{-n}, \quad \forall n, \tag{3.15}$$

where $l > 0$. This is an important relation because it gives the constant value of the DP. Using Equations (3.11) and (3.15), we get

$$\dot{a} = la^{1-n}, \tag{3.16}$$

and consequently, from Equation (3.14) the DP turns out to be

$$q = n - 1,$$

which is obviously a constant. Integrating Equation (3.16), it follows that

$$a = \begin{cases} k_1 e^{lt}, & \text{for } n = 0, \\ (nlt + k_2)^{\frac{1}{n}}, & \text{for } n \neq 0, \end{cases} \tag{3.17}$$

where k_1 and k_2 are constants of integration, thus we obtain two values of the average scale factor a , that correspond to two different models of the universe. In this paper, we consider the average scale factor a when $n = 0$ in the first case of $f(R, T)$ theory and $n \neq 0$ in the second case of $f(R, T)$ theory.

4. Exact solutions for some Bianchi types

Here we first develop some important cosmological parameters and EFEs for Bianchi types III, V, VI_0 & VI_h space-times and then find the exact solutions of EFEs for constant and non-constant curvature case.

4.1. Solution for $f(R, T) = R + 2\lambda T$

We consider the case in which the function $f(R, T)$ is given by $f(R, T) = R + 2\lambda T$, where λ is a constant. Thus the field Equation (2.12) take the form

$$G_{ij} = R_{ij} - \frac{1}{2}Rg_{ij} = (8\pi + 2\lambda)T_{ij} + \lambda(2p + T)g_{ij}. \tag{4.1}$$

This form looks like EFEs in GR, the term $\lambda(2p + T)$ may play the role of cosmological parameter Λ of the GR field equations, that is

$$\Lambda = \Lambda(T) = \lambda(2p + T),$$

which supports the suggestion by Poplawski [19] where the dependence of the cosmological parameter Λ on T . The researchers like Magnano [20] have suggested that the $\Lambda(T)$ gravity is more general than the gravity in Palatini $f(R)$ theory and could be reduced to it if the pressure of the matter is neglected. Considering the perfect fluid case, the trace $T = \rho - 3p$, hence Equation (4.8) becomes

$$\Lambda = \lambda(\rho - p).$$

Thus we rewrite Equation (4.1) as

$$R_{ij} - \frac{1}{2}Rg_{ij} = (8\pi + 2\lambda)T_{ij} + \Lambda g_{ij}. \tag{4.2}$$

Now using Equations (4.2), and (3.2) to (3.9) we obtain a set of differential equations for Bianchi types-III, V, VI₀ & VI_h space-times

$$\begin{aligned} \frac{\ddot{A}_2}{A_2} + \frac{\ddot{A}_3}{A_3} + \frac{\dot{A}_2\dot{A}_3}{A_2A_3} - \frac{m}{A_1^2} &= (8\pi + 2\lambda)p - \Lambda, \\ \frac{\dot{A}_1}{A_1} + \frac{\ddot{A}_2}{A_2} + \frac{\dot{A}_1\dot{A}_2}{A_1A_2} - \frac{1}{A_1^2} &= (8\pi + 2\lambda)p - \Lambda, \\ \frac{\dot{A}_1}{A_1} + \frac{\ddot{A}_3}{A_3} + \frac{\dot{A}_1\dot{A}_3}{A_1A_3} - \frac{m^2}{A_1^2} &= (8\pi + 2\lambda)p - \Lambda, \\ \frac{\dot{A}_1\dot{A}_2}{A_1A_2} + \frac{\dot{A}_2\dot{A}_3}{A_2A_3} + \frac{\dot{A}_1\dot{A}_3}{A_1A_3} - \frac{m^2 + m + 1}{A_1^2} &= -\Lambda - (8\pi + 2\lambda)\rho, \\ (m + 1)\frac{\dot{A}_1}{A_1} - \frac{\dot{A}_2}{A_2} - \frac{m\dot{A}_3}{A_3} &= 0. \end{aligned} \tag{4.3}$$

Integrating Equation (4.3) and absorbing the integrating constant into A_2 or A_3 , we get

$$A_1^{m+1} = A_2A_3^m. \tag{4.4}$$

Using Equation (3.10) in Equation (4.4) we get

$$A_1^{m+2} = a^3A_3^{m-1}. \tag{4.5}$$

4.1.1. Cosmological solutions

We now obtain physically factual cosmological models to describe the decelerating and accelerating phases of the universe. Setting $A_3 = V^d$, where d is any constant, then from Equation (4.5), we get

$$\begin{aligned} A_1^{m+2} &= a^3V^{d(m-1)}, \\ &= a^{3(1+md-d)}. \end{aligned} \tag{4.6}$$

Here we will consider the value of average scale factor a for $n = 0$ only (see (3.17)). Using Equations (3.10), (3.17), (4.3) and (4.6) the metric coefficients $A_i (i = 1, 2, 3)$ turn out to be

$$A_i(t) = \left(k_1 e^{lt}\right)^{\xi_i}, \quad i = 1, 2, 3 \text{ (no sum)}, \tag{4.7}$$

where

$$\xi_1 = \frac{3(1+md-d)}{m+2}, \quad \xi_2 = \frac{3(1+m-d-2md)}{m+2}, \quad \xi_3 = 3d.$$

Using these in (3.1), we get the following form of the metric (3.1) as

$$ds^2 = dt^2 - \left(k_1 e^{lt}\right)^{\xi_1} dx^2 - e^{-2x} \left(k_1 e^{lt}\right)^{\xi_2} dy^2 - e^{-2mx} \left(k_1 e^{lt}\right)^{\xi_3} dz^2.$$

4.1.2. Physical and geometrical properties of the solution

In this subsection, we will compute the relevant physical and geometrical properties of the space-time. The necessary computations were done using Mathematica, necessary programming was done by us. The spatial volume and the average scale factor $a(t)$ are

$$V = (k_1 e^{lt})^3 = a^3.$$

Mean HP and DP are

$$H = l, \quad q = \frac{-\ddot{a}}{aH^2} = -1,$$

from Equation (3.12), the HPs in the directions of x, y and z -axes are

$$H_i = \frac{\dot{A}_i}{A_i} = l \xi_i, \quad i = 1, 2, 3 \text{ (no sum)}.$$

The scalar expansion is

$$\theta = 3l = 3H.$$

The shear scalar is

$$\begin{aligned} \sigma^2 &= \frac{l^2}{2} [\xi_1^2 + \xi_2^2 + \xi_3^2 - 3], \\ &= \frac{l^2}{(m+2)^2} [3(1-3d)^2(m^2+m+1)]. \end{aligned}$$

The shear parameter is given by

$$\begin{aligned} \Sigma^2 &= \frac{1}{6} [\xi_1^2 + \xi_2^2 + \xi_3^2 - 3], \\ &= \frac{1}{3(m+2)^2} [3(1-3d)^2(m^2+m+1)]. \end{aligned}$$

In this subsection, we take $\lambda = 0.1, l = 5, m = 0, \pm 1, n = 0.5, d = 0.1$ and $k_1 = 1$, for all graphs. The energy density ρ in the model is obtained as

$$\begin{aligned} \rho &= \frac{1}{8(8\pi^2 + 6\lambda\pi + \lambda^2)} \left[\frac{9l^2\lambda \left(-3dm(1+m) + (1+m)^2 + 3d^2(1+m+m^2) \right)}{(m+2)^2} \right. \\ &\quad \left. - \frac{9l^2(8\pi + 3\lambda) \left(1+m-d(-2+3d)(1+m+m^2) \right)}{(m+2)^2} - \frac{\lambda m - (8\pi + 3\lambda)(m^2+m+1)}{(k_1 e^{lt})^{\frac{6(1+md-d)}{(m+2)}}} \right]. \end{aligned}$$

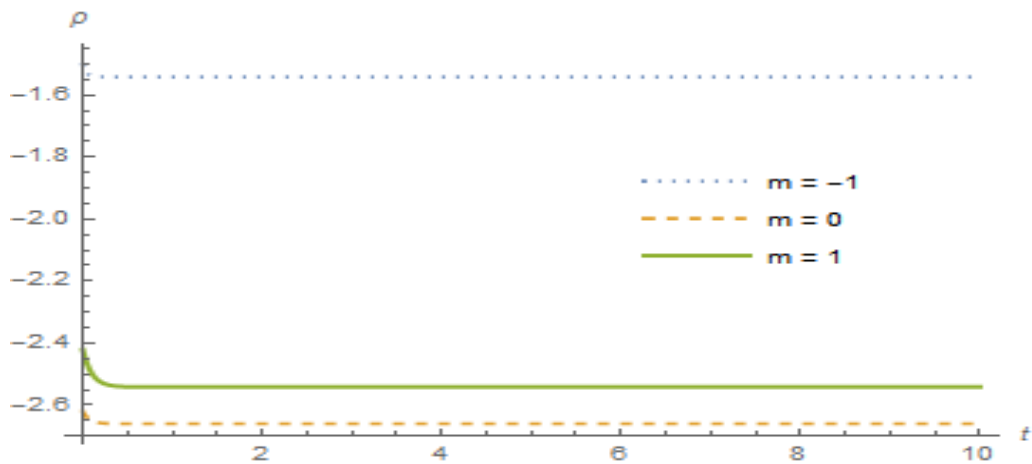


Figure 4.1: The Evolution of Energy Density ρ Versus Cosmic Time t

Figure 4.1, shows ρ as a decreasing function for $0 \leq t < 1$ and constant for $t \geq 1$. The expressions for isotropic pressure p in the model is given by

$$\begin{aligned} p &= \frac{1}{8(8\pi^2 + 6\lambda\pi + \lambda^2)} \left[\frac{9l^2(8\pi + 3\lambda) \left(-3dm(1+m) + (1+m)^2 + 3d^2(1+m+m^2) \right)}{(m+2)^2} \right. \\ &\quad \left. - \frac{9l^2\lambda \left(1+m-d(-2+3d)(1+m+m^2) \right)}{(m+2)^2} - \frac{m(8\pi + 3\lambda) - (m^2+1)\lambda}{(k_1 e^{lt})^{\frac{6(1+md-d)}{(m+2)}}} \right]. \end{aligned}$$

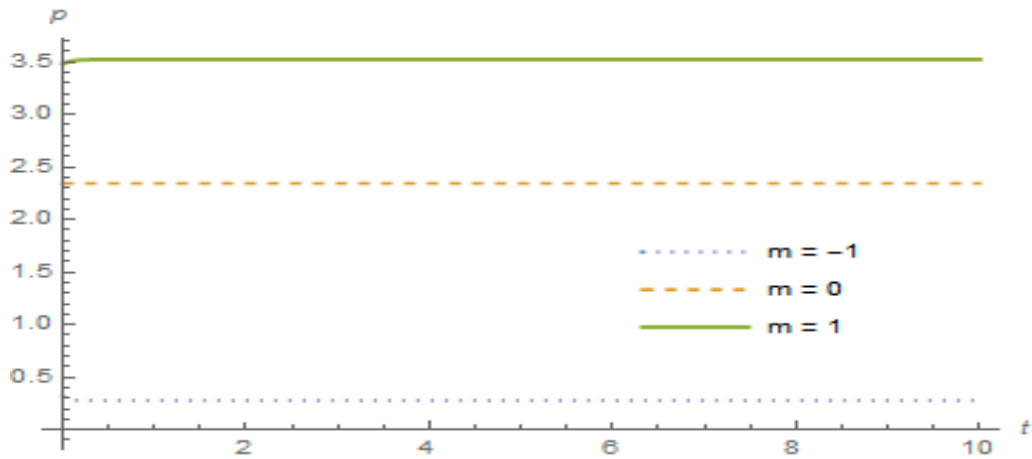


Figure 4.2: The Evolution of Pressure p Versus Cosmic Time t

From Figure 4.2, we observe that the pressure is an increasing function for $0 \leq t < 1$ and constant for $t \geq 1$. The cosmological parameter Λ is

$$\Lambda = \frac{\lambda}{8(8\pi^2 + 6\lambda\pi + \lambda^2)} \left[\frac{-9l^2(8\pi + 2\lambda) \left(6d^2 + 6md^2 + 6m^2d^2 + m + m^2 - 5m^2d - 5md - 2d \right)}{(m+2)^2} - \frac{(8\pi + 3\lambda)(m^2 + 2m + 1) - \lambda(m^2 + m + 1)}{(k_1 e^{lt})^{\frac{6(1+md-d)}{(m+2)}}} \right].$$

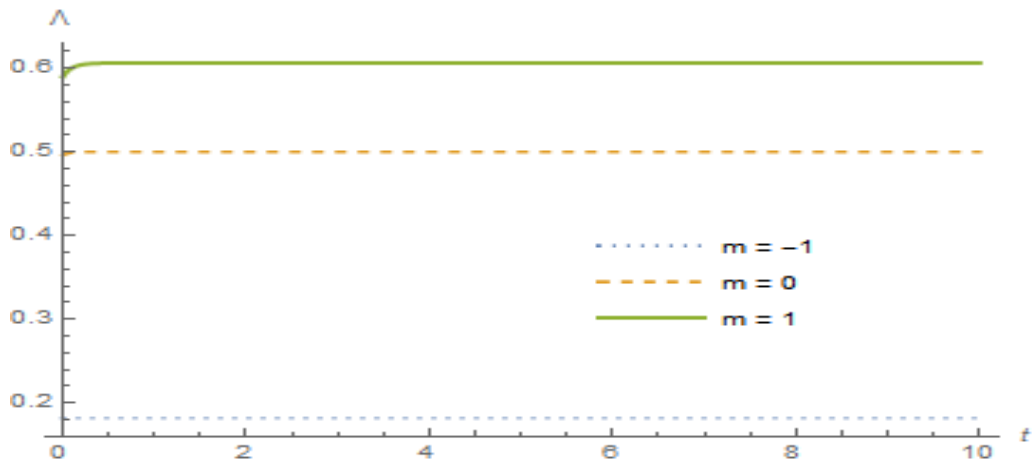


Figure 4.3: The Evolution of Cosmological Constant Λ Versus Cosmic Time t

From Figure 4.3, we observe that the cosmological term Λ is an increasing function for $0 \leq t < 1$ and constant for $t \geq 1$. The density parameter Ω is given by

$$\Omega = 1 - \frac{1}{3(m+2)^2} \left[3(1 - 3d)^2(m^2 + m + 1) \right] - K \geq 0,$$

where K is the curvature parameter, as defined in Equation (3.13). The Ricci scalar R for Bianchi types-III, V, VI₀ & VI_h cosmological models are given by Equations (3.7) and (4.7), it follows that

$$R = \frac{2l^2}{(m+2)^2} \left[(27 - 18d - 18md + 27m + 27d^2 + 27md^2) + m^2(9 - 18d + 27d^2) \right] - 2(m^2 + m + 1) \left(k_1 e^{lt} \right)^{\frac{-6(1+md-d)}{(m+2)}}.$$

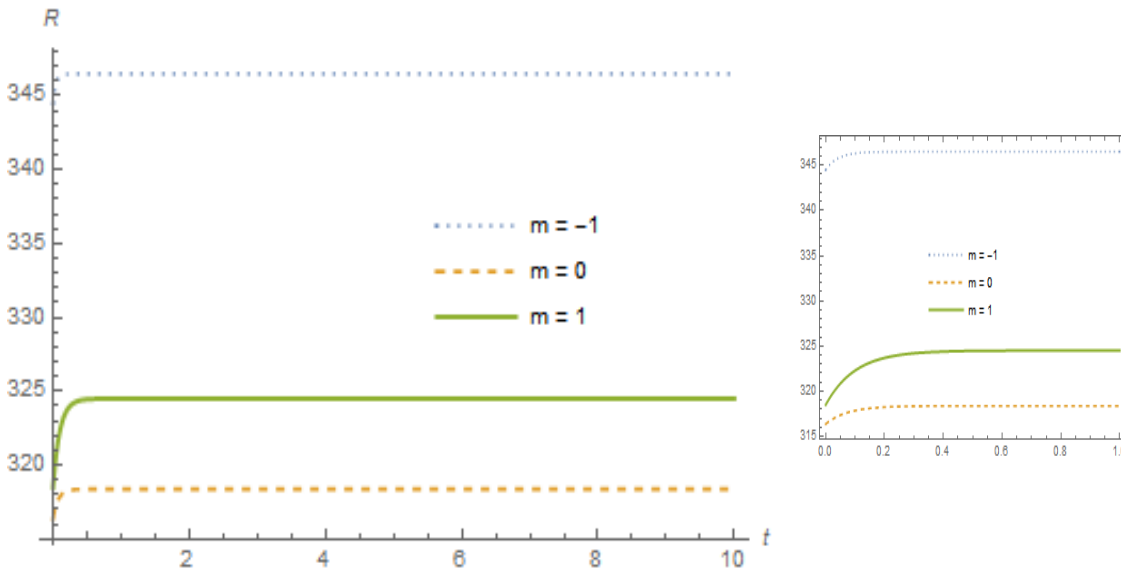


Figure 4.4: The Evolution of Ricci Scalar R Versus Cosmic Time t

From Figure 4.4, we observe that the Ricci scalar R is an increasing function for $0 \leq t < 1$ and constant for $t \geq 1$. The function $f(R, T)$ of Ricci scalar R and the trace T , can be found as

$$f(R, T) = R + 2\lambda(\rho - 3p).$$

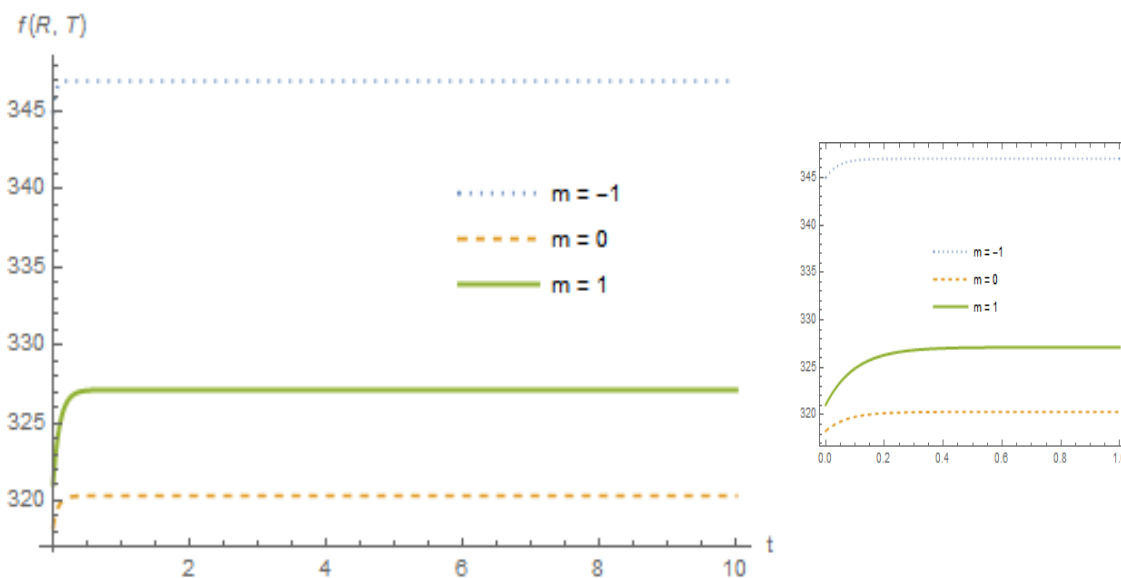


Figure 4.5: The Evolution of $f(R, T)$ Versus Cosmic Time t

Figure 4.5, shows that the $f(R, T)$ is an increasing function for $0 \leq t < 1$ and constant for $t \geq 1$.

4.2. Solution for $f(R, T) = \lambda(R + T)$

We consider the case in which the function $f(R, T)$ is given by $f(R, T) = \lambda(R + T)$, where λ is an arbitrary parameter. Thus the field equation (2.12) take the form

$$\lambda R_{ij} - \frac{1}{2}\lambda(R + T)g_{ij} + (g_{ij}\nabla^k\nabla_k - \nabla_i\nabla_j)\lambda = (8\pi + \lambda)T_{ij} + \left(p + \frac{1}{2}T\right)\lambda g_{ij},$$

setting $(g_{ij}\nabla^k\nabla_k - \nabla_i\nabla_j)\lambda = 0$, we get

$$\lambda R_{ij} - \frac{1}{2}\lambda R g_{ij} = (8\pi + \lambda)T_{ij} + \left(p + \frac{1}{2}T\right)\lambda g_{ij}. \tag{4.8}$$

The Einstein tensor G_{ij} is defined by

$$G_{ij} = R_{ij} - \frac{1}{2}R g_{ij}.$$

Equation (4.8) becomes

$$\lambda G_{ij} = (8\pi + \lambda)T_{ij} + \left(p + \frac{1}{2}T\right)\lambda g_{ij}. \tag{4.9}$$

This form looks like EFEs in GR, we choose a negative small value for the arbitrary λ so that we have the same sign of the RHS of Equation (4.9) we keep this choice of λ throughout the discussion. The term $(p + \frac{1}{2}T)$ can now be regarded as a cosmological parameter Λ . Hence

$$\Lambda = p + \frac{1}{2}T,$$

so Equation (4.9) becomes

$$G_{ij} = R_{ij} - \frac{1}{2}Rg_{ij} = \frac{(8\pi + \lambda)}{\lambda}T_{ij} + \Lambda g_{ij}, \tag{4.10}$$

which supports the suggestion by Poplawski [19] where the dependence of the cosmological parameter Λ on T . The researchers like Magnano [20] have suggested that the Λ gravity is more general than the gravity in Palatini $f(R)$ theory and could be reduced to it if the pressure of matter is neglected. Considering the perfect fluid case, the trace $T = \rho - 3p$, hence

$$\Lambda = \frac{1}{2}(\rho - p).$$

The field equations, in this case, are similar to those written earlier (4.3) to (4.3) with only change due to rights side of (4.10), thus the coefficient $(8\pi + 2\lambda)$ is replaced by $(\frac{8\pi + 2\lambda}{\lambda})$. The field equation for G_{14} is same as Equation (4.3). Also following same procedure we get relations (4.4) and (4.5).

4.2.1. Cosmological solutions

We now obtain physically factual cosmological models to describe the decelerating and accelerating phases of the universe. Setting $A_3 = V^d$, where d is any constant, then from Equation (4.5), we get

$$\begin{aligned} A_1^{m+2} &= a^3 V^{d(m-1)} \\ &= a^{3(1+md-d)}. \end{aligned} \tag{4.11}$$

Here we will consider the value of average scale factor a for $n \neq 0$ only. Using Equations (3.10), (3.17), (4.3) and (4.11) the metric coefficients A_i ($i = 1, 2, 3$) turn out to be

$$A_i(t) = (nlt + k_2)^{\frac{\xi_i}{n}}, i = 1, 2, 3 \text{ (no sum)}, \tag{4.12}$$

where

$$\xi_1 = \frac{3(1+md-d)}{m+2}, \quad \xi_2 = \frac{3(1+m-d-2md)}{m+2}, \quad \xi_3 = 3d.$$

Using these in (3.1), we get the following form of the metric (3.1)

$$ds^2 = dt^2 - (nlt + k_2)^{\frac{\xi_1}{n}} dx^2 - e^{-2x}(nlt + k_2)^{\frac{\xi_2}{n}} dy^2 - e^{-2mx}(nlt + k_2)^{\frac{\xi_3}{n}} dz^2.$$

4.2.2. Physical and geometrical properties of the solution

In this subsection, we will compute the relevant physical and geometrical properties of the space-time. The necessary computations were done using Mathematica, necessary programming was done by us. The spatial volume and the average scale factor $a(t)$ are

$$V = (nlt + k_2)^{\frac{3}{n}} = a^3.$$

In this subsection, we take $\lambda = 0.1$, $l = 5$, $m = 0, \pm 1$, $n = 0.5$, $d = 0.1$ and $k_2 = 1$ for all graphs.

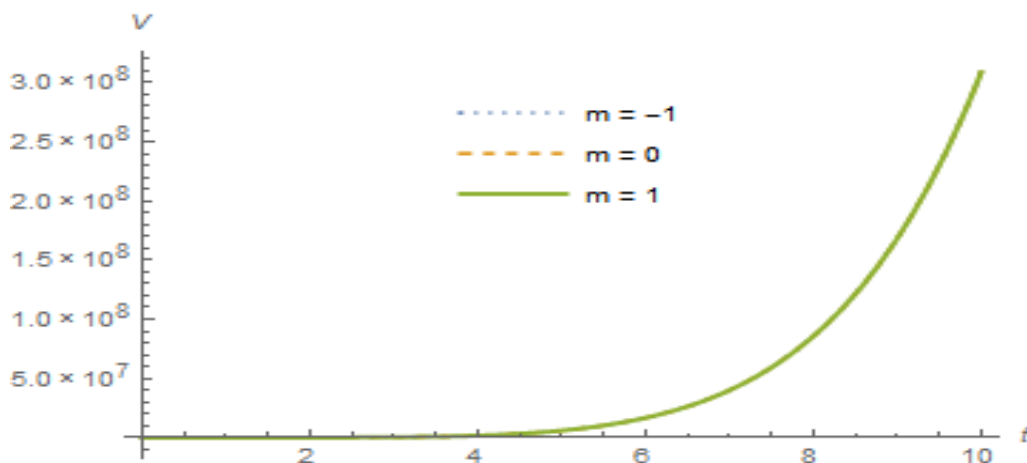


Figure 4.6: The Evolution of Volume V Versus Cosmic Time t

Figure 4.6, shows that volume V is an increasing function of time t . Mean HP and DP are

$$H = \frac{l}{nlt + k_2}, \quad q = \frac{-\ddot{a}}{aH^2} = n - 1,$$

in which HPs in the directions of x, y and z -axes are

$$H_i = \frac{\dot{A}_i}{A_i} = \frac{\xi_i l}{nlt + k_2}, \quad i = 1, 2, 3 \text{ (no sum)}.$$

The scalar expansion becomes

$$\theta = \frac{3l}{nlt + k_1}.$$

The shear scalar is

$$\begin{aligned} \sigma^2 &= \frac{l^2}{2(nlt + k_2)^2} [\xi_1^2 + \xi_2^2 + \xi_3^2 - 3] \\ &= \frac{l^2}{(m+2)^2(nlt + k_2)^2} [3(1-3d)^2(m^2 + m + 1)]. \end{aligned}$$

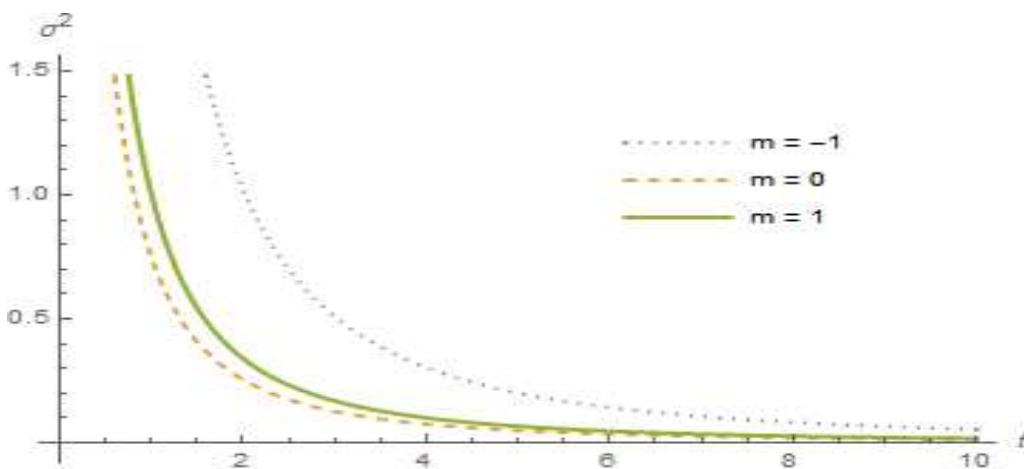


Figure 4.7: The Evolution of Shear Scalar σ^2 Versus Cosmic Time t

Figure 4.7, shows σ^2 as a decreasing function of time t . The shear parameter is given by

$$\begin{aligned} \Sigma^2 &= \frac{1}{6} [\xi_1^2 + \xi_2^2 + \xi_3^2 - 3], \\ &= \frac{1}{3(m+2)^2} [3(1-3d)^2(m^2 + m + 1)]. \end{aligned}$$

The energy density ρ in the model is obtained as

$$\rho = -\frac{9\lambda l^2(1+m-d(-2+3d)(1+m+m^2))}{2(4\pi+\lambda)(m+2)^2(nlt+k_2)^2} - \frac{\lambda^2}{6(4\pi+\lambda)^2} \left[\frac{3l^2(3-n)}{(nlt+k_2)^2} - \frac{2(m^2+m+1)}{(nlt+k_2)^{\frac{6(1+md-d)}{n(m+2)}}} \right] + \frac{\lambda(m^2+m+1)}{2(4\pi+\lambda)(nlt+k_2)^{\frac{6(1+md-d)}{n(m+2)}}}.$$

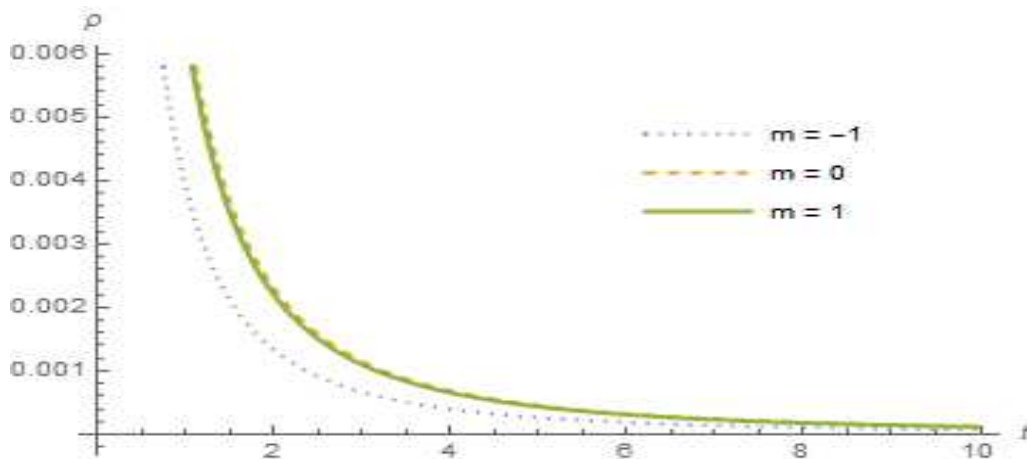


Figure 4.8: The Evolution of Energy Density ρ Versus Cosmic Time t

Figure 4.8, shows that energy density ρ is a decreasing function of time t . The expressions for isotropic pressure p in the model is given by

$$p = -\frac{9\lambda l^2(1+m-d(-2+3d)(1+m+m^2))}{2(4\pi+\lambda)(m+2)^2(nlt+k_2)^2} + \frac{\lambda(16\pi+3\lambda)}{6(4\pi+\lambda)^2} \left[\frac{3l^2(3-n)}{(nlt+k_2)^2} - \frac{2(m^2+m+1)}{(nlt+k_2)^{\frac{6(1+md-d)}{n(m+2)}}} \right] + \frac{\lambda(m^2+m+1)}{2(4\pi+\lambda)(nlt+k_2)^{\frac{6(1+md-d)}{n(m+2)}}}.$$

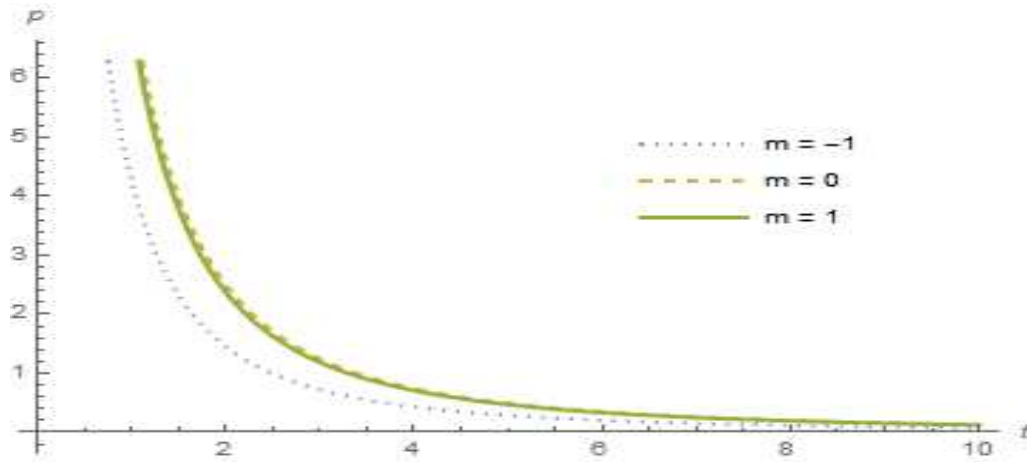


Figure 4.9: The Evolution of Pressure p Versus Cosmic Time t

Figure 4.9, shows that the pressure is a decreasing function of time. The cosmological parameter Λ is

$$\Lambda = \frac{1}{2}(\rho - p) = \frac{\lambda}{6(4\pi+\lambda)} \left[\frac{3l^2(3-n)}{(nlt+k_2)^2} - \frac{2(m^2+m+1)}{(nlt+k_2)^{\frac{6(1+md-d)}{n(m+2)}}} \right].$$

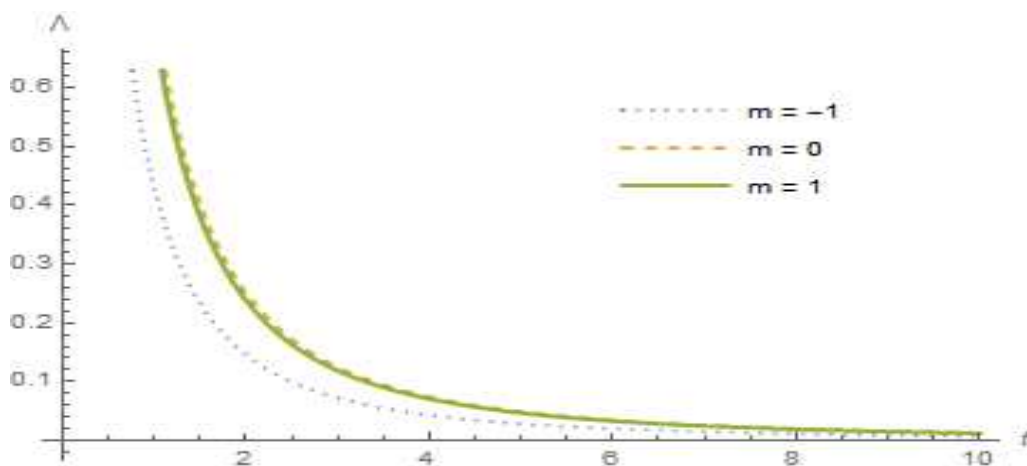


Figure 4.10: The Evolution of Cosmological Constant Λ Versus Cosmic Time t

Figure 4.10, shows that the cosmological term Λ is a decreasing function of time t . The density parameter Ω , is given by

$$\Omega = 1 - \frac{1}{3(m+2)^2} \left[3(1-3d)^2(m^2+m+1) \right] - K \geq 0,$$

where K is the curvature parameter, as defined in Equation (3.13). The Ricci scalar R for Bianchi types-III, V, VI₀ & VI_h cosmological models are given by Equations (3.7) and (4.12) it follows that

$$\begin{aligned} R &= -\frac{2l^2}{(nlt+k_2)^2} \left[\xi_1^2 + \xi_2^2 + \xi_3^2 - n(\xi_1 + \xi_2 + \xi_3) + (\xi_1 \xi_2 + \xi_1 \xi_3 + \xi_2 \xi_3) \right] - 2(m^2+m+1)(nlt+k_2)^{-\frac{2\xi_1}{n}}, \\ &= \frac{2l^2}{(m+2)^2(nlt+k_2)^2} \left[(m+1)(27-18d+27d^2-12n) + m^2(9-18d+27d^2-3n) \right] - 2(m^2+m+1)(nlt+k_2)^{-\frac{6(1+md-d)}{n(m+2)}}. \end{aligned}$$

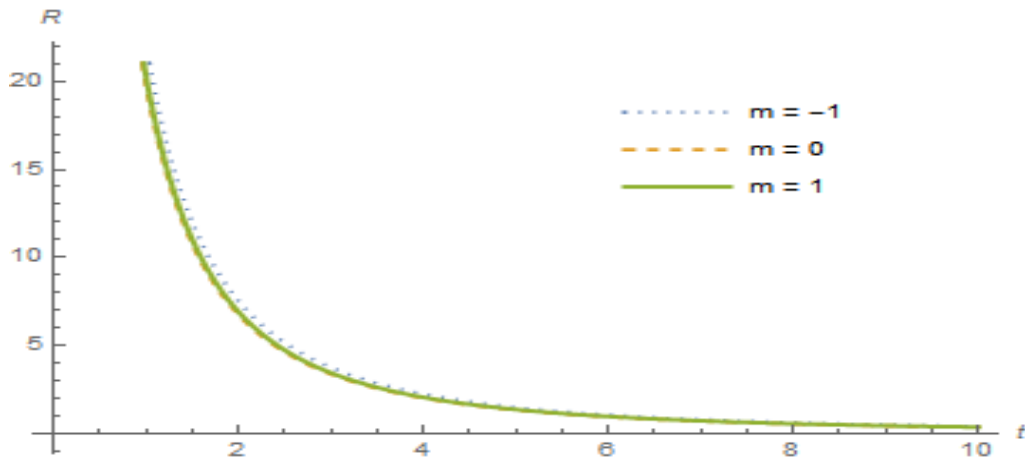


Figure 4.11: The Evolution of Ricci Scalar R Versus Cosmic Time t

Figure 4.11, shows that the curvature is positive through the whole evolution of the universe. The function $f(R, T)$ of Ricci scalar R and the trace T can be found as

$$f(R, T) = \lambda_1 R + \lambda_2 (\rho - 3p).$$

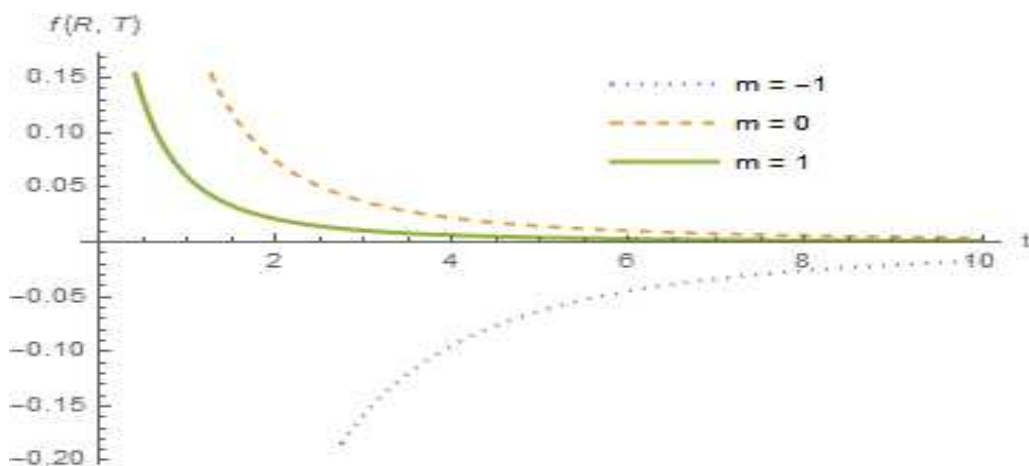


Figure 4.12: The Evolution of $f(R, T)$ Versus Cosmic Time t

Figure 4.12, shows that the $f(R, T)$ is an increasing function when $m = 0, 1$ and decreasing function when $m = -1$ of time t .

5. Conclusion

In this paper, we have extended the study of exact solutions of EFEs for Bianchi types-III, V, VI₀ & VI_h space-times in $f(R, T)$ theory and obtained the exact solutions corresponding to singularity point $n \neq 0$, and regular point $n = 0$. The exact solutions to the corresponding field equations are obtained in quadrature form. The behaviors of the cosmological parameter Λ have been discussed in each case. We have also examined the well-known physical and geometrical properties of our models in two different viable cosmologies. It is shown that our models represent expanding, shearing, non-rotating and accelerating universe in each case. In the first case of $f(R, T)$ theory, when $n = 0$ with $a = k_1 e^{lt}$, the model has no singularity point. The volume V is finite and blows to infinite at $t \rightarrow \infty$. The generalized HP H is constant and accordingly, expansion scalar θ is constant. The HPs H_i , $i = 1, 2, 3$ are finite for all finite values of t . The shear scalar σ^2 and shear parameter Σ^2 are constant as $t \rightarrow \infty$. The energy density ρ (Figure 4.1) is constant as $t \rightarrow \infty$ and the Figure 4.1, shows that ρ is negative, its physical interpretation may be debatable however this is mathematically consistent. The isotropic pressure p (Figure 4.2), density parameter Ω and Ricci scalar R (Figure 4.4) are constant as $t \rightarrow \infty$. The function $f(R, T)$ of the Ricci scalar R and trace T is finite (Figure 4.5) at non-singularity.

In the second case of $f(R, T)$ theory, when $n \neq 0$ with $a = (nlt + k_2)^{\frac{1}{n}}$, it is observed that the spatial volume $V \rightarrow \infty$ as $t \rightarrow \infty$ (Figure 4.6), and the volume scalar factor vanishes at the singularity point. The generalized HP is zero at the singularity. The expansion scalar $\theta \rightarrow 0$ as $t \rightarrow \infty$, as well as it is observed that θ starts with infinite value at $t = 0$ and then rapidly becomes constant after some finite time. The direction HPs H_i , $i = 1, 2, 3$ are zero at the singularity point. The shear scalar σ^2 (Figure 4.7) and shear parameter Σ^2 are zero as $t \rightarrow \infty$. The isotropic pressure p (Figure 4.9), energy density ρ (Figure 4.8) are constant at $t \rightarrow \infty$. The Ricci scalar R is infinite $t \rightarrow \infty$ (Figure 4.11). The density parameter Ω is constant as $t \rightarrow \infty$. The function $f(R, T)$ of the Ricci scalar R and trace T is infinite (Figure 4.12) at the singularity.

Acknowledgement

The authors are thankful to the University Grant Commission, India for providing financial support under UGC-SAP-DRS(III) provided to the Department of Mathematics, Sardar Patel University, Vallabh Vidyanagar, where the work was carried out. AMA is also thankful to the Al-Baydha University, and Government of the Republic of Yemen for providing financial support. The authors are also thankful to the anonymous referees for their critical comments that improved quality of the manuscript a lot.

References

- [1] S. Cotsakis, E. Papantonopoulos, *Cosmological Crossroads: An Advanced Course in Mathematical, Physical and String Cosmology*, Springer Sci. & Business Media, 2002.
- [2] P. Agrawal, D. Pawar, *Plane symmetric cosmological model with quark and strange quark matter in $f(R, T)$ theory of gravity*, J. Astrophys. Astr., **38**(2) (2017), 1-7, <https://doi.org/10.1007/s12036-016-9420-y>.
- [3] R. Chaubey, A. Shukla, *A new class of Bianchi cosmological models in $f(R, T)$ gravity*, Astrophys. Space Sci., **343**(1) (2013), 415-422, <https://doi.org/10.1007/s10509-012-1204-5>.
- [4] T. Harko, F. S. Lobo, S. Nojiri, S. D. Odintsov, *$f(R, T)$ gravity*, Phys. Rev. D, **84**(2) (2011), 024020-1 to 024020-14.
- [5] T. Harko, F. S. Lobo, *Generalized dark gravity*, Int. J. of Modern Phys. D, **21**(11) (2012), 1242019-1 to 1242019-8, <https://doi.org/10.1142/S0218-271812420199>.
- [6] P. Sahoo, B. Mishra, G. C. Reddy, *Axially symmetric cosmological model in $f(R, T)$ gravity*, Eur. Phys. J. Plus, **129**(3) (2014), 1-8, <https://doi.org/10.1140/epjp/i2014-14049-7>.
- [7] P. Moraes, P. Sahoo, *The simplest non-minimal matter-geometry coupling in the $f(R, T)$ cosmology*, The Eur. Phys. J. C, **77**(7) (2017), 1-8, <https://doi.org/10.1140/epjc/s10052-017-5062-8>.
- [8] K. Adhav, *LRS Bianchi type-I cosmological model in $f(R, T)$ theory of gravity*, Astrophys. Space Sci., **339**(2) (2012), 365-369, <https://doi.org/10.1007/s10509-011-09638>.
- [9] D. Pawar, P. Arawal, *Dark energy cosmological model in $f(R, T)$ theory of gravity*, Prespacetime J., **6**(3) (2015), 719-732.
- [10] D. Pawar, P. Agrawal, *Role of constant deceleration parameter in cosmological model filled with dark energy in $f(R, T)$ theory*, Bulg. J. of Phys., **43**(2), (2016), 148-155.
- [11] D. Pawar, G. Bhuttampalle, P. Agrawal, *Kaluza-klein string cosmological model in $f(R, T)$ theory of gravity*, New Astronomy, **65** (2018), 1-6, <https://doi.org/10.1016/j.newast.2018.05.002>.
- [12] R. S. Kumar, *Some exact cosmological models in modified theories of gravitation*, Ph.D. Thesis, Acharya Nagarjuna Uni., 2013.
- [13] D. Pawar, P. Arawal, *Magnetized domain wall in $f(R, T)$ theory of gravity*, New Astronomy, **54** (2017), 56-60, <https://doi.org/10.1016/j.newast.2017.01.006>.
- [14] L. D. Landau, *The Classical Theory of Fields*, Elsevier, 2013.
- [15] A. H. Hasmani, G. Rathva, *Algebraic computations in general relativity using mathematica*, Prajn. J. of Pure & Appl. Sci., **15** (2007), 77-81.
- [16] A. H. Hasmani, *Algebraic computation of newmann-penrose scalars in general relativity using mathematica*, J. of Sci. **1** (2010), 82-83.
- [17] V. Johri, K. Desikan, *Cosmological models with constant deceleration parameter in Brans-Dicke theory*, Gen. Relat. Gravit., **26**(12) (1994), 1217-1232, <https://doi.org/10.1007/BF0210671>.
- [18] M. S. Berman, *A special law of variation for hubbles parameter*, Nuov. Cim. B, **74**(2) (1983), 182-186, <https://doi.org/10.1007/BF02721676>.
- [19] N. J. Poplawski, *The present universe in the Einstein frame, metrica affine $R + 1/R$ gravity*, Class. Quantum Grav., **23**(15) (2006), 4819-4827, <https://doi.org/10.1088/0264-9381/23/15/003>.
- [20] G. Magnano, *Are there metric theories of gravity other than general relativity*, Gen. Relat. & Gravi. Phys., (1995), arXiv:gr-qc/9511027v2.

Analysis of the Convergence and Periodicity of a Rational Difference Equation

Mohammed B. Almatrafi^{1*} and Marwa M. Alzubaidi²

¹Department of Mathematics, College of Science, Taibah University, Al-Madinah Al-Munawarah, Saudi Arabia

²Department of Mathematics, College of Duba, University of Tabuk, Saudia Arabia

*Corresponding author E-mail: mmutrafi@taibahu.edu.sa

Article Info

Keywords: Difference equation, Equilibria, Global attractivity, Local stability, Periodicity

2010 AMS: 39A10

Received: 02 May 2019

Accepted: 28 July 2019

Available online: 26 December 2019

Abstract

The exact solutions of most difference equations cannot be obtained sometimes. This can be attributed to the fact that there is no a specific approach from which one can find the exact solution. Therefore, many researchers tend to study the qualitative behaviours of these equations. In this paper, we will investigate some qualitative properties such as local stability, global stability, periodicity and solutions of the following eighth order recursive equation

$$x_{n+1} = c_1x_{n-3} - \frac{c_2x_{n-3}}{c_3x_{n-3} - c_4x_{n-7}}, \quad n = 0, 1, \dots,$$

where the coefficients c_i , for all $i = 1, \dots, 4$, are assumed to be positive real numbers and the initial conditions x_i for all $i = -7, -6, \dots, 0$, are arbitrary non-zero real numbers.

1. Introduction

Nowadays, a huge number of researchers put a lot of effort to investigate the qualitative behaviours of some fractional recursive equations. Researchers examine some properties such as local stability, global stability, boundedness, periodicity and theoretical and numerical solutions to predict the future pattern of these equations. This development can be obviously seen in most recent studies. Take, for instance the following ones. Almatrafi et al. [1] discovered the stability, periodicity, boundedness and solutions of the following fourth order fractional difference equations

$$x_{n+1} = \frac{\alpha x_n x_{n-3}}{\pm \beta x_{n-3} \pm \gamma x_{n-2}}.$$

Cinar [2] obtained the solution of the second order recursive equation

$$x_{n+1} = \frac{ax_{n-1}}{1 + bx_n x_{n-1}}.$$

Elabbasy et al. [3] examined the qualitative behaviours of the recursive equation

$$x_{n+1} = ax_n - \frac{bx_n}{cx_n - dx_{n-1}}.$$

Garić-Demirović et al. [4] investigated the periodicity of the solution and the stability of the equilibrium point of the difference equation

$$x_{n+1} = \frac{Ax_n^2 + Bx_n x_{n-1} + Cx_{n-1}^2}{ax_n^2 + bx_n x_{n-1} + cx_{n-1}^2}.$$

In [5], the authors concerned with presenting the qualitative behaviour of the sixth order difference equation

$$x_{n+1} = \frac{Cx_{n-5}}{A + Bx_{n-2}x_{n-5}}.$$

Khyat et al. [6] analysed the properties of the following second order recursive equation

$$x_{n+1} = \frac{x_n}{Cx_{n-1}^2 + Dx_n + F}.$$

The investigation in [7] concentrates on showing the periodic character, semi-cycle character and global stability of the difference equation

$$x_{n+1} = \frac{\alpha + \beta x_n + \gamma x_{n-k}}{Bx_n + Cx_{n-k}}.$$

Simsek et al [8] obtained the expressions of the solutions of the fourth order difference equation

$$x_{n+1} = \frac{x_{n-3}}{1 + x_{n-1}}.$$

More results on the qualitative behaviours of some fractional difference equations can be obtained on refs. [9]-[19].

Our principal aim in this work is to discuss some mathematical properties such as local stability, global attractivity, periodic character and solutions of the eighth order difference equation

$$x_{n+1} = c_1 x_{n-3} - \frac{c_2 x_{n-3}}{c_3 x_{n-3} - c_4 x_{n-7}}, \quad n = 0, 1, \dots, \quad (1.1)$$

where the coefficients c_i , for all $i = 1, \dots, 4$, are assumed to be positive real numbers and the initial conditions are required to be arbitrarily real numbers. Moreover, theoretical and numerical solutions to a special case of Eq.(1.1) will be shown in this paper.

2. Local stability of the equilibrium point

The main duty in this section is to analyse the behaviour of the solutions in the neighbourhood of the equilibrium point. The equilibrium point of Eq.(1.1) is given by

$$\bar{x} = c_1 \bar{x} - \frac{c_2 \bar{x}}{c_3 \bar{x} - c_4 \bar{x}}.$$

Hence,

$$\bar{x} = \frac{c_2}{(1 - c_1)(c_4 - c_3)}, \quad c_1 \neq 1, c_3 \neq c_4.$$

Next, we assume that a function $h : (0, \infty)^2 \rightarrow (0, \infty)$ is defined by the form

$$h(y, z) = c_1 y - \frac{c_2 y}{c_3 y - c_4 z}. \quad (2.1)$$

Then,

$$\frac{\partial h(y, z)}{\partial y} = c_1 - \frac{c_2(c_3 y - c_4 z) - c_2 c_3 y}{(c_3 y - c_4 z)^2} = c_1 + \frac{c_2 c_4 z}{(c_3 y - c_4 z)^2}, \quad (2.2)$$

$$\frac{\partial h(y, z)}{\partial z} = -\frac{c_2 c_4 y}{(c_3 y - c_4 z)^2}. \quad (2.3)$$

We now calculate Eq.(2.2) and Eq.(2.3) at \bar{x} as follows:

$$\begin{aligned} \frac{\partial h(\bar{x}, \bar{x})}{\partial y} &= c_1 + \frac{c_2 c_4 \bar{x}}{(c_3 \bar{x} - c_4 \bar{x})^2} = c_1 + \frac{c_4(1 - c_1)}{c_4 - c_3} := -p_1, \\ \frac{\partial h(\bar{x}, \bar{x})}{\partial z} &= -\frac{c_2 c_4 \bar{x}}{(c_3 \bar{x} - c_4 \bar{x})^2} = -\frac{c_4(1 - c_1)}{c_4 - c_3} := -p_2. \end{aligned}$$

Thus, the linearised equation of Eq. (1.1) around \bar{x} is given by the form:

$$u_{n+1} + p_1 u_{n-3} + p_2 u_{n-7} = 0.$$

Theorem 2.1. *Let*

$$|c_4 - c_1 c_3| + c_4 |1 - c_1| < |c_4 - c_3|.$$

Then, the equilibrium point of Eq.(1.1) is locally asymptotically stable.

Proof. Theorem A in [12] guarantees that the equilibrium point of Eq.(1.1) is locally asymptotically stable if

$$|p_1| + |p_2| < 1,$$

which leads to

$$\left| -\left(c_1 + \frac{c_4(1-c_1)}{c_4-c_3} \right) \right| + \left| \frac{c_4(1-c_1)}{c_4-c_3} \right| < 1.$$

Therefore,

$$|c_1(c_4-c_3) + c_4(1-c_1)| + c_4|1-c_1| < |c_4-c_3|.$$

Or,

$$|c_4 - c_1c_3| + c_4|1-c_1| < |c_4-c_3|.$$

The proof is complete. \square

3. Global stability of the equilibrium point

In this section, we will present a specific condition under which the equilibrium point is a global stable.

Theorem 3.1. *The equilibrium point of Eq.(1.1) is a global attractor if $c_1 < 1$.*

Proof. Assume that $a, b \in \mathbb{R}$ and let $h : [a, b]^2 \rightarrow [a, b]$ be a function defined by Eq.(2.1). Then, the function h is increasing in y and decreasing in z . Next, we suppose that (ϕ, ψ) is a solution to the following system:

$$\phi = h(\phi, \psi), \quad \psi = h(\psi, \phi).$$

Thus,

$$\begin{aligned} \phi &= h(\phi, \psi) = c_1\phi - \frac{c_2\phi}{c_3\phi - c_4\psi}, \\ \psi &= h(\psi, \phi) = c_1\psi - \frac{c_2\psi}{c_3\psi - c_4\phi}. \end{aligned}$$

Simplifying this gives us

$$c_3\phi^2 - c_4\phi\psi = c_1c_3\phi^2 - c_1c_4\phi\psi - c_2\phi \quad (3.1)$$

$$c_3\psi^2 - c_4\phi\psi = c_1c_3\psi^2 - c_1c_4\phi\psi - c_2\psi \quad (3.2)$$

Subtracting Eq.(3.2) from Eq.(3.1) yields

$$c_3(\phi^2 - \psi^2) = c_1c_3(\phi^2 - \psi^2) + c_2(\psi - \phi).$$

Therefore,

$$(\phi - \psi) \left[c_3(1-c_1)(\phi + \psi) + c_2 \right] = 0.$$

Hence, if $c_1 < 1$, then $\phi = \psi$. As a result, Theorem B in [20] assures that the equilibrium point is a global attractor. \square

4. Periodicity of the solutions

This section is devoted to study the periodicity of the solution of Eq.(1.1).

Theorem 4.1. *Eq.(1.1) has no prime period two solutions.*

Proof. Suppose that Eq.(1.1) has prime period two solutions on the form:

$$\dots, t, \tau, t, \tau, \dots,$$

where $t \neq \tau$. Then, Eq.(1.1) leads to

$$\begin{aligned} t &= c_1t - \frac{c_2t}{c_3t - c_4t}, \\ \tau &= c_1\tau - \frac{c_2\tau}{c_3\tau - c_4\tau}. \end{aligned}$$

Therefore,

$$\begin{aligned} (1-c_1)t &= -\frac{c_2}{c_3-c_4}, \\ (1-c_1)\tau &= -\frac{c_2}{c_3-c_4}. \end{aligned}$$

This exactly implies that $t = \tau$, which contradicts our assumption. \square

5. Special case of Eq.(1.1)

We now turn to solve the following difference equation theoretically.

$$x_{n+1} = x_{n-3} - \frac{x_{n-3}}{x_{n-3} - x_{n-7}}, \quad n = 0, 1, \dots \tag{5.1}$$

Theorem 5.1. Let $\{x_n\}_{n=-7}^\infty$ be a solution to Eq.(5.1) and assume that $x_{-7} = \alpha, x_{-6} = \beta, x_{-5} = \gamma, x_{-4} = \delta, x_{-3} = \kappa, x_{-2} = \lambda, x_{-1} = \mu, x_0 = \rho$. Then, for $n = 0, 1, 2, \dots$, the solution of Eq.(5.1) is given by the following formulas:

$$\begin{aligned} x_{8n-7} &= -\frac{[(n-1)\alpha - n\kappa][\alpha - \kappa + n]}{\alpha - \kappa}, & x_{8n-6} &= -\frac{[(n-1)\beta - n\lambda][\beta - \lambda + n]}{\beta - \lambda}, \\ x_{8n-5} &= -\frac{[(n-1)\gamma - n\mu][\gamma - \mu + n]}{\gamma - \mu}, & x_{8n-4} &= -\frac{[(n-1)\delta - n\rho][\delta - \rho + n]}{\delta - \rho}, \\ x_{8n-3} &= -\frac{[n\alpha - (n+1)\kappa][\alpha - \kappa + n]}{\alpha - \kappa}, & x_{8n-2} &= -\frac{[n\beta - (n+1)\lambda][\beta - \lambda + n]}{\beta - \lambda}, \\ x_{8n-1} &= -\frac{[n\gamma - (n+1)\mu][\gamma - \mu + n]}{\gamma - \mu}, & x_{8n} &= -\frac{[n\delta - (n+1)\rho][\delta - \rho + n]}{\delta - \rho}. \end{aligned}$$

Proof. It can be easily seen that the solution is true at $n = 0$. Now, we suppose that $n > 0$ and assume that the relations are satisfied at $n - 1$ as follows:

$$\begin{aligned} x_{8n-15} &= -\frac{[(n-2)\alpha - (n-1)\kappa][\alpha - \kappa + n - 1]}{\alpha - \kappa}, & x_{8n-14} &= -\frac{[(n-2)\beta - (n-1)\lambda][\beta - \lambda + n - 1]}{\beta - \lambda}, \\ x_{8n-13} &= -\frac{[(n-2)\gamma - (n-1)\mu][\gamma - \mu + n - 1]}{\gamma - \mu}, & x_{8n-12} &= -\frac{[(n-2)\delta - (n-1)\rho][\delta - \rho + n - 1]}{\delta - \rho}, \\ x_{8n-11} &= -\frac{[(n-1)\alpha - n\kappa][\alpha - \kappa + n - 1]}{\alpha - \kappa}, & x_{8n-10} &= -\frac{[(n-1)\beta - n\lambda][\beta - \lambda + n - 1]}{\beta - \lambda}, \\ x_{8n-9} &= -\frac{[(n-1)\gamma - n\mu][\gamma - \mu + n - 1]}{\gamma - \mu}, & x_{8n-8} &= -\frac{[(n-1)\delta - n\rho][\delta - \rho + n - 1]}{\delta - \rho}. \end{aligned}$$

Next, it can be obviously observed from Eq.(5.1) that

$$\begin{aligned} x_{8n-7} &= x_{8n-11} - \frac{x_{8n-11}}{x_{8n-11} - x_{8n-15}} \\ &= -\frac{[(n-1)\alpha - n\kappa][\alpha - \kappa + n - 1]}{\alpha - \kappa} - \frac{-\frac{[(n-1)\alpha - n\kappa][\alpha - \kappa + n - 1]}{\alpha - \kappa}}{-\frac{[(n-1)\alpha - n\kappa][\alpha - \kappa + n - 1]}{\alpha - \kappa} + \frac{[(n-2)\alpha - (n-1)\kappa][\alpha - \kappa + n - 1]}{\alpha - \kappa}} \\ &= -\frac{[(n-1)\alpha - n\kappa][\alpha - \kappa + n - 1]}{\alpha - \kappa} + \frac{[(n-1)\alpha - n\kappa]}{\kappa - \alpha} \\ &= -\frac{[(n-1)\alpha - n\kappa][\alpha - \kappa + n]}{\alpha - \kappa}. \\ x_{8n-6} &= x_{8n-10} - \frac{x_{8n-10}}{x_{8n-10} - x_{8n-14}} \\ &= -\frac{[(n-1)\beta - n\lambda][\beta - \lambda + n - 1]}{\beta - \lambda} - \frac{-\frac{[(n-1)\beta - n\lambda][\beta - \lambda + n - 1]}{\beta - \lambda}}{-\frac{[(n-1)\beta - n\lambda][\beta - \lambda + n - 1]}{\beta - \lambda} + \frac{[(n-2)\beta - (n-1)\lambda][\beta - \lambda + n - 1]}{\beta - \lambda}} \\ &= -\frac{[(n-1)\beta - n\lambda][\beta - \lambda + n - 1]}{\beta - \lambda} + \frac{[(n-1)\beta - n\lambda]}{\lambda - \beta} \\ &= -\frac{[(n-1)\beta - n\lambda][\beta - \lambda + n]}{\beta - \lambda}. \end{aligned}$$

Other formulas can be proved in a similar way. Thus, the remaining proofs will be omitted. □

6. Numerical examples

In order to confirm our theoretical work, we will illustrate some figures that show the behaviour of the solutions according to the previous conditions.

Example 6.1. The local stability of the equilibrium point is depicted in this example under the values $c_1 = 0.3$, $c_2 = 0.1$, $c_3 = 8$, $c_4 = 1$, $x_{-7} = 0.001$, $x_{-6} = -0.02$, $x_{-5} = -0.03$, $x_{-4} = 0.02$, $x_{-3} = -0.04$, $x_{-2} = 0.021$, $x_{-1} = -0.01$, $x_0 = -0.02$. See Figure 6.1.

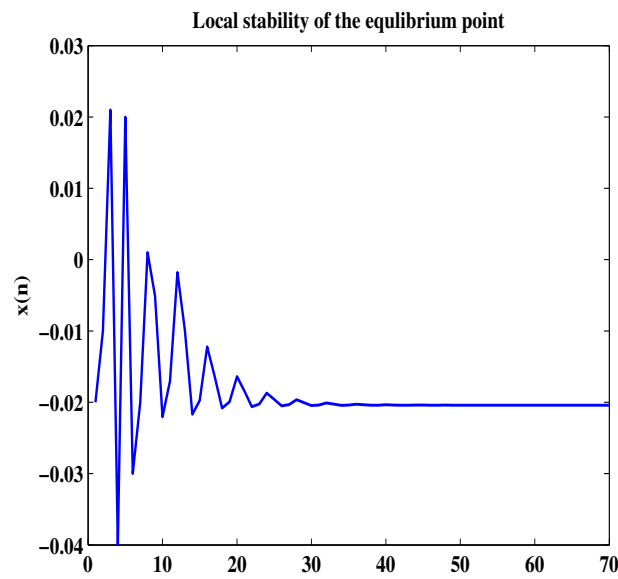


Figure 6.1: Local Stability of The Equilibrium Point.

Example 6.2. The global stability of the equilibrium point is given in Figure 6.2 according to the following data. $c_1 = 0.4$, $c_2 = 0.2$, $c_3 = 8$, $c_4 = 1$, $x_{-7} = 0.1$, $x_{-6} = -0.2$, $x_{-5} = 6$, $x_{-4} = -5$, $x_{-3} = 3$, $x_{-2} = -1$, $x_{-1} = 1$, $x_0 = -0.2$.

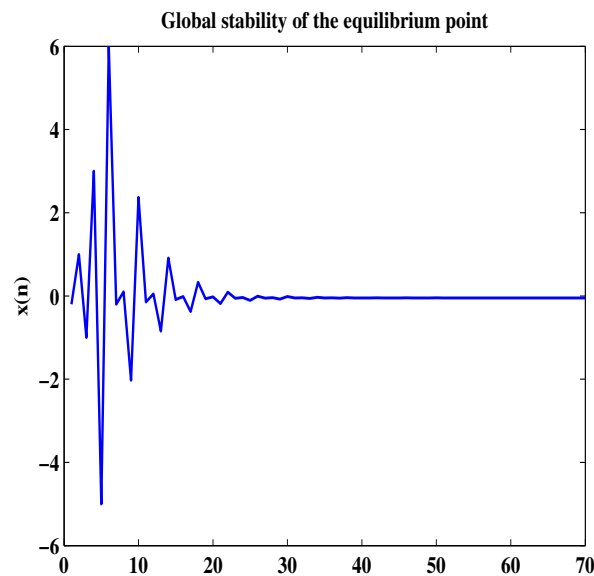


Figure 6.2: Global Stability of The Equilibrium Point.

Example 6.3. In Figure 6.3, we plot another behaviour of the solutions of Eq.(1.1). Here, we assume that $c_1 = 0.6$, $c_2 = 0.2$, $c_3 = 4$, $c_4 = 0.2$, $x_{-7} = -1$, $x_{-6} = -0.2$, $x_{-5} = 0.2$, $x_{-4} = 1$, $x_{-3} = 0.1$, $x_{-2} = -0.5$, $x_{-1} = 0.25$, $x_0 = -0.3$.

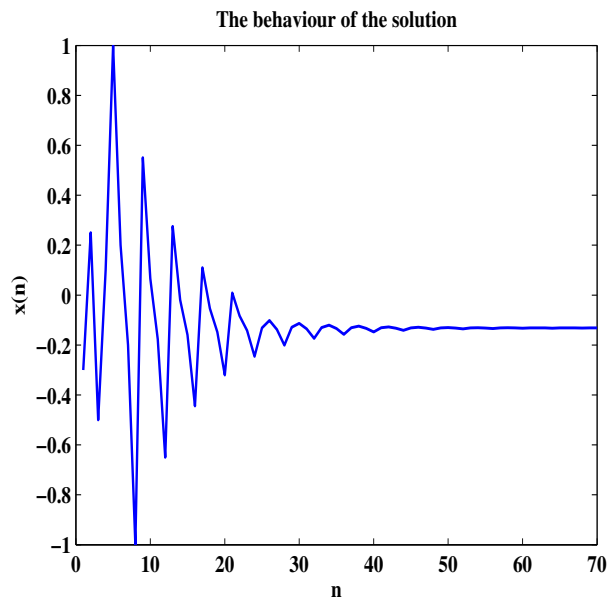


Figure 6.3: Solution of Eq.(1.1).

Example 6.4. Figure 6.4 shows the solution of the special case equation when we take $x_{-7} = -0.8$, $x_{-6} = 0.2$, $x_{-5} = 0.7$, $x_{-4} = 1.5$, $x_{-3} = -0.1$, $x_{-2} = 0.5$, $x_{-1} = 0.12$, $x_0 = -1$.

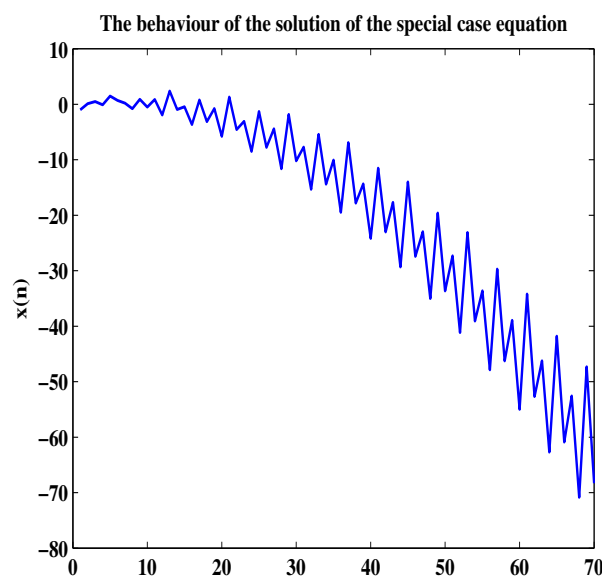


Figure 6.4: Solution of the Special Case Equation.

7. Conclusion

In this work, we have explored the stability and periodicity of Eq.(1.1) and analysed the solutions of Eq.(5.1). Section 2 highlighted a condition under which the equilibrium point of Eq.(1.1) is locally asymptotically stable. Following this, we have shown that the equilibrium point is a global stable if $c_1 < 1$, as pictured in Figure 6.2. In Section 4, it has been proved that Eq.(1.1) has no prime period two solutions. Finally, the analytical and numerical solutions of Eq.(5.1) has been provided in Theorem 5.1 and Section 6, respectively.

References

- [1] M. B. Almatrafi, E. M. Elsayed, F. Alzahrani, *Qualitative behavior of two rational difference equations*, Fundam. J. Math. Appl., **1**(2) (2018), 194-204.
- [2] C. Cinar, *On the positive solutions of the difference equation $x_{n+1} = ax_{n-1}/(1 + bx_n x_{n-1})$* , Appl. Math. Comput., **156** (2004), 587-590.
- [3] E. M. Elabbasy, H. El-Metwally, E. M. Elsayed, *On the difference equation $x_{n+1} = ax_n - (bx_n)/(cx_n - dx_{n-1})$* , Adv. Difference Equ., **2006** (2006), Article ID 82579, 1-10.
- [4] M. Garić-Demirović, M. Nurkanović, Z. Nurkanović, *Stability, periodicity and Neimark-Sacker bifurcation of certain homogeneous fractional difference equations*, Int. J. Difference Equ., **12**(1) (2017), 27-53.
- [5] M. Ghazel, E.M. Elsayed, A.E. Matouk, A.M. Mousallam, *Investigating dynamical behaviors of the difference equation $x_{n+1} = Cx_{n-5}/(A + Bx_{n-2}x_{n-5})$* , J. Nonlinear Sci. Appl., **10** (2017), 4662-4679.
- [6] T. Khyat, M. R. S. Kulenović, *The invariant curve caused by Neimark-Sacker bifurcation of a perturbed Beverton-Holt difference equation*, Int. J. Difference Equ., **12**(2) (2017), 267-280.
- [7] M. Saleh, N. Alkoumi, Aseel Farhat, *On the dynamic of a rational difference equation $x_{n+1} = \alpha + \beta x_n + \gamma x_{n-k}/Bx_n + Cx_{n-k}$* , Chaos, Solitons Fractals, **96**(2017), 76-84.
- [8] D. Simsek, C. Cinar, I. Yalcinkaya, *On the recursive sequence $x_{n+1} = \frac{x_n - 3}{1 + x_{n-1}}$* , Int. J. Contemp. Math. Sci., **1**(10) (2006), 475-480.
- [9] M. B. Almatrafi, E. M. Elsayed, *Solutions and formulae for some systems of difference equations*, MathLAB J., **1**(3) (2018), 356-369.
- [10] M. B. Almatrafi, E. M. Elsayed, Faris Alzahrani, *Qualitative behavior of a quadratic second-order rational difference equation*, Int. J. Adv. Math., **2019**(1) (2019), 1-14.
- [11] F. Belhannache, N. Touafek, R. Abo-zeid, *On a higher-order rational difference equation*, J. Appl. Math. & Informatics, **34**(5-6) (2016), 369-382.
- [12] E. M. Elabbasy, H. El-Metawally, E. M. Elsayed, *On the difference equation $x_{n+1} = (ax_n^2 + bx_{n-1}x_{n-k})/(cx_n^2 + dx_{n-1}x_{n-k})$* , Sarajevo J. Math., **4**(17) (2008), 1-10.
- [13] M. A. El-Moneam, E.M.E. Zayed, *Dynamics of the rational difference equation*, Inform. Sci. Letters, **3**(2) (2014), 45-53.
- [14] A. Khaliq, Sk.S. Hassan, *Dynamics of a rational difference equation $x_{n+1} = ax_n + (\alpha + \beta x_{n-k})/(A + Bx_{n-k})$* , Int. J. Adv. Math., **2018**(1) (2018), 159-179.
- [15] V. L. Kocic, G. Ladas, *Global Behaviour of Nonlinear Difference Equations of Higher Order with Applications*, Kluwer Academic Publishers, Dordrecht, 1993.
- [16] Y. Kostrov, Z. Kudlak, *On a second-order rational difference equation with a quadratic term*, Int. J. Difference Equ., **11**(2) (2016), 179-202.
- [17] K. Liu, P. Li, F. Han, W. Zhong, *Global dynamics of nonlinear difference equation $x_{n+1} = A + x_n/x_{n-1}x_{n-2}$* , J. Comput. Anal. Appl., **24**(6) (2018), 1125-1132.
- [18] S. Moranjkicić, Z. Nurkanović, *Local and global dynamics of certain second-order rational difference equations containing quadratic terms*, Adv. Dyn. Syst. Appl., **12**(2) (2017), 123-157.
- [19] M. Saleh, M. Aloqeili, *On the rational difference equation $y_{n+1} = A + \frac{y_n - k}{y_n}$* , Appl. Math. Comput. **171**(1) (2005), 862-869.
- [20] E. M. Elsayed, *Dynamics of recursive sequence of order two*, Kyungpook Math. J., **50** (2010), 483-497.



Bayesian Analysis of the Discrete Two-Parameter Bathtub Hazard Distribution

Ammar M. Sarhan¹

¹Department of Mathematics and Statistics, Faculty of Science, Dalhousie University, Halifax, Canada

Article Info

Keywords: Data analysis, Maximum likelihood estimator, Probability models, Reliability measures

2010 AMS: 46N30, 90B25

Received: 28 May 2019

Accepted: 18 September 2019

Available online: 26 December 2019

Abstract

A new discrete two-parameter bathtub hazard distribution is proposed by Sarhan [1]. This paper uses Bayes method to estimate the two unknown parameters and the reliability measures of this distribution. The joint posterior distribution of the model parameters cannot be obtained in a convenient form. Therefore, numerical techniques are needed. We apply four Bayesian numerical methods to get random draws from the joint posterior distribution to be used to estimate the model parameters and its reliability measures without deriving the actual joint posterior distribution. It is assumed here that the two model parameters are priori independent random variables with beta and gamma distributions. Two scenarios for the hyperparameters are applied to compare their contributions on the Bayesian inferences. Two real data sets are re-analyzed using the Bayesian techniques applied here. A simulation study is performed to investigate the properties of the methods applied.

1. Introduction

It is very common that the researchers in the fields of reliability analysis and life testing experiments use continuous lifetime distributions to study the reliability of a system, see for example Gnedenko and Ushakov [2], Lawless [3], Sinha [4], and Kapur and Lamberson [5]. Sometimes, in practice, it is impossible to test the underlying system on a continuous scale. For example, the lifetime of the switch in the case of an on/off-switching unit, the number of cycles prior to failure of an equipment which operates in cycles, the lifetime (in days/weeks) of systems that are placed on the life test. In such situations, discrete lifetime distributions might be more appropriate.

Recently, Sarhan [1] proposed a discrete two-parameter distribution that displays bathtub shaped hazard function in addition to the increasing and decreasing shapes. The bathtub hazard shape property allows this model to fit a number of real datasets in reliability analysis. Sarhan [1] used $DTPBT(q, \beta)$ to denote this distribution, where q and β are the model parameters. He discussed some statistical properties of the $DTPBT(q, \beta)$ and used some frequentest techniques such as quantile, least squares and maximum likelihood method to do inference on the two unknown parameters of the proposed model. Also, he used the model to analyze two real datasets and compared the proposed model with the discrete Weibull, (Nakagaw and Osaki [6]), discrete modified Weibull DMW (Nooghabi et al. [7]), discrete additive Weibull DAddW (Bebbington et al. [8]) and discrete reduced modified Weibull DRMW (Almalki and Nadarajah [9]). He concluded that the DTPBT model performed better fit than all of these above mentioned models.

The main goal of this current paper is to use Bayesian method to do inference on the DTPBT model. We use Bayesian method to estimate the model parameters (in point and interval). Also, we use Bayesian method to report on the reliability measures of the model. It is assumed here that the two parameters q and β are independent variables, where q follows beta priori distribution with hyperparameters (a_1, a_2) and β follows a gamma priori distribution with hyperparameters (b_1, b_2) . Two scenarios for the hyperparameters (a_1, a_2) and (b_1, b_2) are proposed and a comparison between them is discussed. The posterior distribution of the vector of the two unknown parameters $\theta = (q, \beta)$, given the available data, cannot be derived in a convenient form. Therefore, numerical approaches for Bayesian analysis are needed. In this paper, we will apply: (1) the accept-reject (AR) technique, (2) the sampling importance resampling (SIR) method, and (3) two versions of Monte Carlo Markov chain (MCMC) algorithm to get random draws from the joint posterior distribution. Once the random draws from the joint posterior distribution are obtained, we can perform any Bayesian analysis we wish for the model parameters or any of the model reliability measures.

One of the advantages of the Bayesian methods applied here is that they do not require the posterior distribution of (q, β) to be in an explicit form.

The rest of the paper is organized as follows. In Section 2 we give a brief description of the DTPBT. In Section 3, we present the joint posterior distribution of $\theta = (q, \beta)$ and discuss the Bayes analysis. Three main numerical methods to draw random samples from the joint posterior distribution are discussed in Section 4. In Section 5, two real data sets are analyzed using the proposed methods. A simulation study is carried out in section 6. Finally, section 7 concludes the paper and discusses some future work.

2. The DTPBT(q, β) distribution

The discrete random variable X is said to have a discrete two-parameter bathtub hazard distribution, with parameters q and β , if its probability mass function takes the following form, Sarhan [1],

$$p(x; q, \beta) = \frac{1}{q} \left[q^{e^{(x-1)\beta}} - q^{e^{x\beta}} \right], \quad x = 1, 2, \dots, 0 < q < 1, \beta > 0.$$

The survival function (sf) of X is

$$S(x; q, \beta) = q^{e^{x\beta}} - 1, \quad x = 1, 2, \dots, 0 < q < 1, \beta > 0.$$

The cumulative distribution function (cdf) of X is

$$F(x; q, \beta) = 1 - q^{e^{x\beta}} - 1, \quad x = 1, 2, \dots, 0 < q < 1, \beta > 0.$$

The hazard rate function (hrf) of X is

$$h(x; q, \beta) = 1 - q^{e^{x\beta}} - e^{-(x-1)\beta}, \quad x = 1, 2, \dots, 0 < q < 1, \beta > 0.$$

Sarhan [1] shows that the hazard function can be increasing/decreasing or bathtub shaped based on the values of the model parameters. Example of the different shapes of the hazard rate function are provided in Figure 2.1 when (q, β) is $(0.9, 0.2)$ increasing, $(0.9, 0.3)$ bathtub and $(0.9, 0.9)$ decreasing. The variety of the shape of hazard function, specifically the bathtub shaped, allows the DTPBT distribution to fit various number of discrete real datasets.

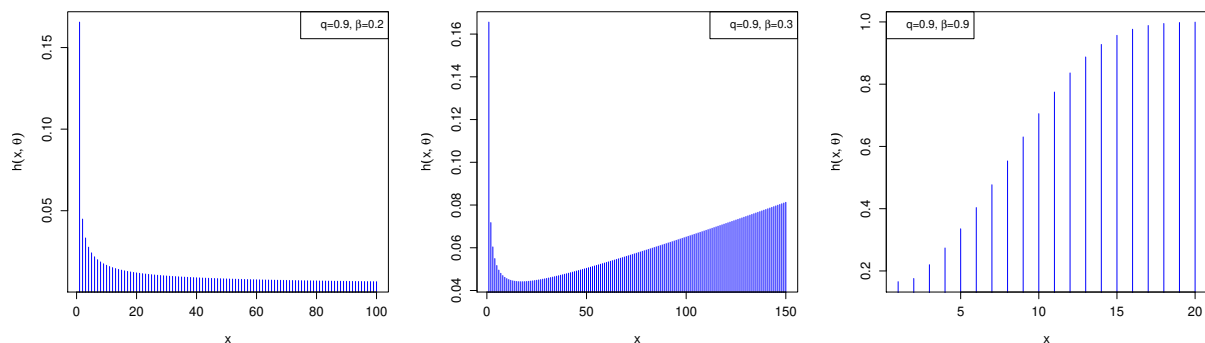


Figure 2.1: The hazard rate function of the DTPBT distribution when (q, β) is [from the left to right] $(0.9, 0.2)$, $(0.9, 0.3)$ and $(0.9, 0.9)$.

3. Bayes analysis

Let X_1, X_2, \dots, X_n be a simple random sample from DTPBT(q, β). The likelihood function of this sample is

$$L(\underline{x}; q, \beta) = \frac{1}{q^n} \prod_{i=1}^n \left[q^{e^{(x_i-1)\beta}} - q^{e^{x_i\beta}} \right], \quad (3.1)$$

where \underline{x} represents the observations of the simple random sample. Let us assume that q and β be independent random variables with priori $\text{beta}(a_1, a_2)$ and $\text{gamma}(b_1, b_2)$ distributions, respectively. That is, the joint prior density of (q, β) , up to a constant, is

$$g(q, \beta) \propto q^{a_1-1} (1-q)^{a_2-1} \beta^{b_1-1} e^{-b_2\beta}, \quad 0 < q < 1; \beta > 0. \quad (3.2)$$

The hyperparameters $a_j, b_j > 0, j = 1, 2$, will be subjectively selected based on the priori information on q and β when it is available. Applying Bayes' theorem using the likelihood function (3.1) and the joint prior density function (3.2), we get the joint posterior density function of (q, β) , given the data, up to a constant, as

$$g(q, \beta | \underline{x}) \propto q^{-n+a_1-1} (1-q)^{a_2-1} \beta^{b_1-1} e^{-b_2\beta} \prod_{i=1}^n \left[q^{e^{(x_i-1)\beta}} - q^{e^{x_i\beta}} \right], \quad 0 < q < 1; \beta > 0. \quad (3.3)$$

Under the squared error loss, which is adopted here,

1. The Bayes estimates of q and β are the posterior means given by

$$\hat{q} = \int_0^1 q g_q(q|\underline{x}) dq \quad \text{and} \quad \hat{\beta} = \int_0^\infty \beta g_\beta(\beta|\underline{x}) d\beta, \tag{3.4}$$

where $g_q(q|\underline{x})$ and $g_\beta(\beta|\underline{x})$ are the marginal posterior density functions of q and β , respectively.

2. The Bayes estimate of a real-valued function of the $\vartheta = (q, \beta)$, say $w(q, \beta)$, is the posterior mean of $w(q, \beta)$, that is

$$\hat{w}(q, \beta) = \int_0^\infty \int_0^1 w(q, \beta) g(q, \beta|\underline{x}) dq d\beta. \tag{3.5}$$

The joint posterior distribution (3.3) is in an inconvenient form as well as the normalized constant can not be derived theoretically. Therefore, the marginal posterior densities $g_q(q|\underline{x})$ and $g_\beta(\beta|\underline{x})$ cannot be derived explicitly, and so the integrals in (3.4) and (3.5) cannot be calculated analytically. Accordingly, we will use numerical approaches to perform Bayes analysis for the model parameters and its reliability measures. For the numerical techniques applied in this paper, it is more convenient to reparametrize the two parameters $q \in (0, 1)$ and $\beta > 0$ to be both real-valued by using the expressions $\theta_1 = \log\left(\frac{q}{1-q}\right)$ and $\theta_2 = \log(\beta)$. The joint posterior density function of $\theta = (\theta_1, \theta_2)$, given data, is

$$g_\theta(\theta_1, \theta_2|\underline{x}) = g\left(\frac{1}{1+e^{-\theta_1}}, e^{\theta_2}|\underline{x}\right) \frac{e^{\theta_2-\theta_1}}{(1+e^{-\theta_1})^2}, \quad -\infty < \theta_1, \theta_2 < \infty.$$

Also, for the numerical approaches which will be applied here, it is helpful to use the natural logarithm of the joint posterior density of θ , which is given by

$$\log g_\theta(\theta_1, \theta_2|\underline{x}) = \log g\left(\frac{1}{1+e^{-\theta_1}}, e^{\theta_2}|\underline{x}\right) + \theta_2 - \theta_1 - 2\log(1+e^{-\theta_1}). \tag{3.6}$$

4. Bayesian numerical techniques

In this section we discuss how to use four Bayesian numerical approaches that will help us to overcome the main difficulties in Bayes analysis. These techniques allow us to get random draws from the joint posterior distribution without deriving its explicit form. These techniques require only to write the posterior density function up to a constant as given in (3.3). For simplicity, in the rest of the paper, we use ϑ to denote the vector of the two unknown parameters, namely $\vartheta = (q, \beta)$.

Accept-Reject method (AR): The AR method is a general technique that can be used to generate independent random draws from probability distributions. It is one of the most useful techniques for simulating random draws from a variety of probability distributions. For more information on the AR method, we refer to Givens and Hoeting [10], Monahan [11], and Robert and Casella [12].

The main goal of using the AR method is to generate independent random draws from the posterior probability density (3.3). The basic idea in the AR method is to find a proposal, say $p(\vartheta)$, that satisfies: (1) easy to simulate from, (2) mimics the posterior distribution, and (3) there exists a positive constant M such that $\frac{g(\vartheta|\text{data})}{p(\vartheta)} \leq M$ for all ϑ . The following steps summarize the AR algorithm:

1. Specify the size of desired random draws m .
2. Simulate ϑ from the proposal $p(\vartheta)$.
3. Calculate the ratio $R = \frac{g(\vartheta|\text{data})}{Mp(\vartheta)}$.
4. Generate a random value U from uniform distribution on the unit interval.
5. If $U \leq R$ accept ϑ as a random draw from $g(\vartheta|\text{data})$; otherwise reject it.
6. Repeat steps 2-5 until m draws are accepted.

We will use the bivariate t distribution with a small degrees of freedom as a proposal since smaller degrees of freedom provide a heavy tailed proposal and therefore it would be more likely to find the upper bound constant M .

The location and variance-covariance matrix of the proposal distribution can be found as those we obtain by using normal approximation to the logarithm of the joint posterior distribution of the real-valued vector θ , given in (3.6). Let $\kappa(\theta) = \log g_\theta(\theta|\text{data})$ and $\tilde{\theta}$ be its mode. The second-order Taylor series expansion of $\kappa(\theta)$ about $\tilde{\theta}$ is

$$\kappa(\theta) \approx \kappa(\tilde{\theta}) + \frac{1}{2} (\theta - \tilde{\theta})^T \kappa''(\tilde{\theta}) (\theta - \tilde{\theta}),$$

where $\kappa''(\tilde{\theta})$ is the Hessian of $\kappa(\theta)$ evaluated at $\tilde{\theta}$. The above expansion of $\kappa(\theta)$ can be approximated by multivariate normal distribution with mean $\mu = \tilde{\theta}$ and variance-covariance matrix $\Sigma = \left(-\kappa''(\tilde{\theta})\right)^{-1}$. To apply this normal approximation, we need the mode $\tilde{\theta}$, that can be estimated by using Newton's method. Newton's method starts with a guess mode $\theta^{(0)}$, then estimates the mode at the i th iteration by

$$\theta^{(i)} = \theta^{(i-1)} - \left(\kappa''(\theta^{(i-1)})\right)^{-1} \kappa'(\theta^{(i-1)}),$$

where $\kappa'(\theta^{(i-1)})$ and $\kappa''(\theta^{(i-1)})$ are the gradient and Hessian of $\kappa(\theta)$ at the iteration $i - 1$. These iterations are repeated until convergence. The constant M can be found by maximizing $D(\theta) = \kappa(\theta) - \log p(\theta)$ with respect to θ . Again, Newton's method can be used to obtain $\log M$ as the mode of $D(\theta)$, then calculate M .

Sampling Importance Resampling Method (SIR): Sampling importance resampling (SIR) method is an alternative general method for simulating independent random draws from a general posterior distribution. As in the AR method, SIR requires a proposal that mimics the target posterior distribution but it does not require the bound constant M . We will use the same proposal as in the AR method. The SIR method can be implemented by applying the following algorithm:

1. Simulated m draws from the proposal density $p(\vartheta)$, say $\vartheta^{(1)}, \dots, \vartheta^{(m)}$
2. Compute the weights for the draws $w_j = \frac{g(\vartheta^{(j)}|\text{data})}{p(\vartheta^{(j)})}$, $i = 1, \dots, m$
3. Convert the weights to probabilities $w_i^* = \frac{w_i}{\sum_{j=1}^m w_j}$, $i = 1, \dots, m$
4. Simulate m random draws with replacement from the discrete distribution $\{\vartheta^{(i)}, w_i^*\}_{i=1}^m$, say $\vartheta^{*1}, \dots, \vartheta^{*m}$.

Then the set of random draws $\{\vartheta^{*1}, \dots, \vartheta^{*m}\}$ is approximately distributed according to the actual posterior distribution $g(\vartheta|\text{data})$.

Markov Chain Monte Carlo method (MCMC): Markov Chain Monte Carlo (MCMC) methods have been extensively used to become one of the most useful computational tools in the modern Bayesian data analysis. MCMC is very general and flexible technique to simulate a sequence of nonindependent draws from a probability distribution. MCMC method begins with an initial value $\vartheta^{(0)}$ and a mechanism for drawing the i -th value in the sequence $\vartheta^{(i)}$ given the $(i-1)$ st value $\vartheta^{(i-1)}$. This mechanism consists of: (1) a proposal probability distribution $p(\vartheta^*|\vartheta)$ that produces a candidate value ϑ^* given a current ϑ , and (2) calculate an acceptance probability P of accepting the candidate ϑ^* as the next value in the sequence. A general reference for the MCMC is Gelman et al. [13].

The following steps can be followed to implement the Metropolis-Hastings algorithm:

1. Specify the sequence size $m > 1$.
2. Choose an initial value $\vartheta^{(0)} = (\vartheta_1^{(0)}, \vartheta_2^{(0)})'$.
3. For $i = 1, \dots, m$ repeat the following steps
 - i. Set $\vartheta^{(i)} = \vartheta^{(i-1)}$.
 - ii. Generate a candidate value ϑ^* from a proposal distribution $p(\vartheta^*|\vartheta^{(i)})$.
 - iii. Calculate the ratio $r_i = \frac{g(\vartheta^*|\text{data})/p(\vartheta^*|\vartheta^{(i)})}{g(\vartheta^{(i)}|\text{data})/p(\vartheta^{(i)}|\vartheta^*)}$.
 - iv. Set $\vartheta^{(i)} = \vartheta^*$ with probability $P_i = \min\{1, r_i\}$; otherwise keep $\vartheta^{(i)}$ as is.

Metropolis-Hastings algorithm (MHA) uses different proposals. However, we will use two different chains: (1) independence chain (IND), in which the acceptance ratio is $r_i = \frac{g(\vartheta^*|\text{data})p(\vartheta^{(i)})}{g(\vartheta^{(i)}|\text{data})p(\vartheta^*)}$, and (2) random walk chain (RWC), in which the acceptance ratio is $r_i = \frac{g(\vartheta^*|\text{data})}{g(\vartheta^{(i)}|\text{data})}$. The MHA generates random draws from the target distribution regardless of the proposal $p(\vartheta^*|\vartheta)$. However, the choice of the proposal is important since a poor choice considerably delays the convergence towards the target distribution. We will use the same proposal as that we use in the AR.

5. Data analysis

We use the four previously discussed Bayesian numerical methods to analyze the same two real datasets that were analyzed by Sarhan [1].

5.1. Electronic devices data:

In this dataset, 18 electronic devices were put on a life test and their lifetimes (in days) were observed as 5, 11, 21, 31, 46, 75, 98, 122, 145, 165, 196, 224, 245, 293, 321, 330, 350, 420. Wang [14] showed that this data have a bathtub hazard shape and used the additive Burr XII distribution to analyze it. Sarhan [1] applied different frequentest methods to re-analyze this dataset using the DTPBT distribution. In this section, we apply Bayes methods discussed here to analyze this dataset using the DTPBT distribution. Also, we estimate the model reliability measures.

Figure 5.1 [left panel] displays the contour plots for the log-posterior density function of (q, β) , which shows that the posterior distribution is right skewed and therefore normal approximation to the log-posterior distribution is not appropriate. This is one of the reasons to transform the two parameters q from $(0, 1)$ interval to the real valued interval using $\theta_1 = \log\left(\frac{q}{1-q}\right)$ and β from $(0, \infty)$ domain to real valued domain using $\theta_2 = \log\beta$. Using this transformation, the log-posterior density function becomes more symmetric as shown in Figure 5.1 [right panel] and therefore normal approximation for $\log g_\theta(\theta|\text{data})$ is appropriate. This will allow us to use the mode and variance covariance matrix for the normal approximation as the location and scale parameters for a symmetric proposal distribution. In this study, we use bivariate t distribution with 4 degrees of freedom as a proposal in all four Bayesian numerical methods.

We used beta and gamma prior distributions for the two unknown parameters q and β , respectively, under two scenarios: (1) Poor/weak prior information, in which we assume that all hyperparameters are equal and equal to 0.001, this indicates that prior mean of q is 0.5 and standard deviation of 0.4995, while β has a prior mean of 1 and variance of 1000; (2) Good prior information: we use the posterior mean and posterior variance, that are obtained by using scenario 1, as prior mean and variance for each parameter then get a new set of hyperparameters $a_1 = 168.594, a_2 = 1.419, b_1 = 141.829$ and $b_2 = 472.326$. As a quick diagnostic test for the effect of the prior information, we provided the contour plots for the log-likelihood function and the log-posterior density function of (q, β) using each scenario along with the contour plots for the log-prior density function of (q, β) using each scenario as displayed in Figure 5.2. Despite of scenario 1 provides a very skewed prior distribution, it slightly improves the skewness of the likelihood function. Scenario 2 is more symmetric and less distributed which leads to a less skewness in the joint posterior distribution of (q, β) with more precision in the sense of having narrower contour.

Using scenario 1, the acceptance rates for the accept-reject (AR), random walk (RW) and independent chain (IND) Markov Chain Monte Carlo are 10.81%, 46.67% and 67.46%, respectively. The AR methods has the lowest acceptance rate, then the RW and the INC has the

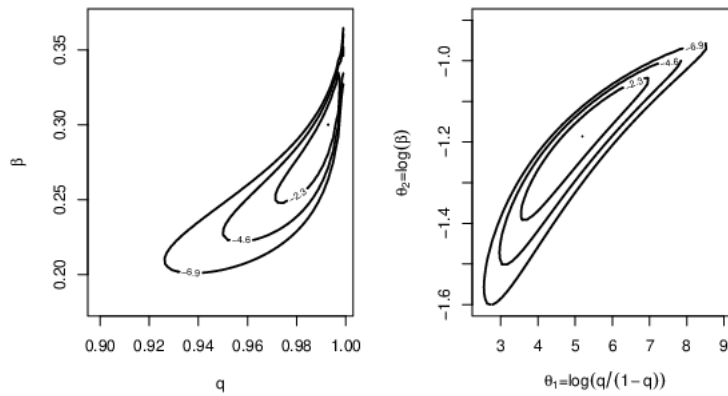


Figure 5.1: The contour plots for the log-posterior of (q, β) [left panel] and for $\left(\log\left(\frac{q}{1-q}\right), \log\beta\right)$ [right panel], using non informative priors (scenario 1) of the hyperparameters.

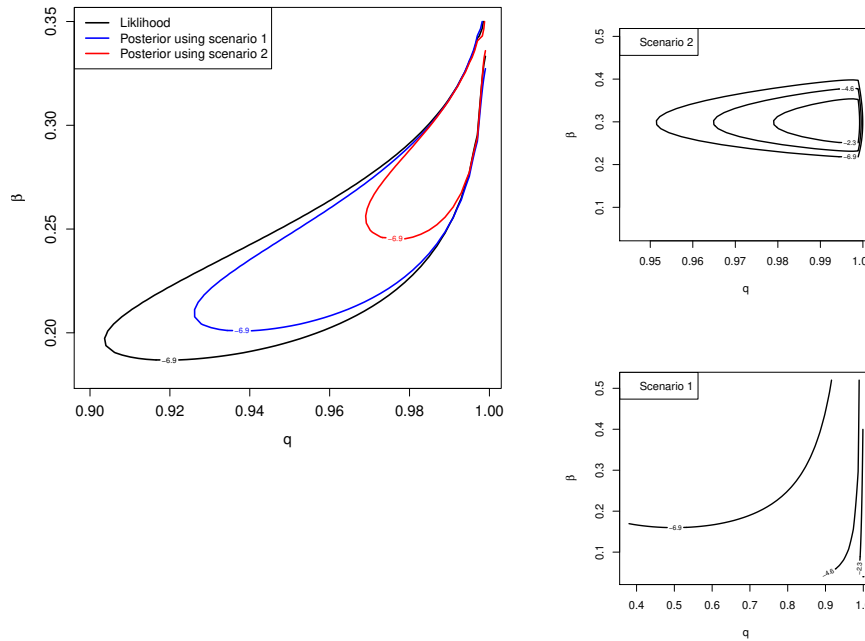


Figure 5.2: The contour plots [left panel] for the log-likelihood and for the log-posterior functions of (q, β) using non informative priors (scenario 1) and informative priors (scenario 2); and the contour plots for the log-prior density using scenario 1 [bottom-right] and scenario 2 [top-right].

largest acceptance rate. The accept reject method is the slowest method comparing to the other three techniques applied here. The fastest one is the SIR method. The posterior mean, mode and 95% credible interval for the two parameters q and β using the four techniques are displayed in Table 1. The four techniques provide very similar results. However the INC provides more precise credible interval but the SIR is more faster and provides independent draws. Therefore, we would recommend SIR algorithm, for the underling distribution, over all other techniques discussed here.

Using scenario 2, the acceptance rates for AR, RW and IND algorithms are respectively 52.3%, 50.8% and 78.12%, which are generally higher than those for scenario 1. The acceptance rate corresponding to AR is increased by more than 40% using scenario 2. Furthermore, as expected, scenario 2 provides better Bayesian inferences for q and β than scenario 1 in the sense of providing narrower credible intervals. However, all Bayesian point estimates are very similar.

The four numerical techniques are performed using prior scenario 1 to get 10,000 draws from the posterior distribution of the transformed parameters $\theta = (\theta_1, \theta_2)$. Figure 5.3 shows the posterior contours along with the draws obtained using the four methods. Using the inverse transformations of θ_1 and θ_2 , $q = (1 + e^{-\theta_1})^{-1}$ and $\beta = e^{\theta_2}$, we get random draws from the marginal posterior distributions of q and β , given data, respectively. Figure 5.4 shows the marginal posterior densities of q and β using the four techniques. To see how good the draws that are obtained from the MCMC, RW and IND chains, we provide some diagnostic tests; the trace plots and autocorrelation plots for θ_1 and θ_2 using the whole chains and the last 70% of the chains. From these plots, we can see that there is a good mix of the draws and the Lag

declines rapidly in addition to the high acceptance rates of both two chains. The trace plots show that the early 27% of the chain were not plausible values from the posterior distribution. That is why we discarded the early 30% of the chain and used the last 70% as draws from the actual posterior distribution. Also, the ACF plots show high correlation in the chain over the early 30% (burn-in period), then declines rapidly in the last 70%.

Parameter	Method	Mean	Median	2.5th	97.5th	Width
Scenario 1						
q	SIR	0.991305	0.993312	0.972841	0.998798	0.025956
	AR	0.991379	0.993427	0.972511	0.998784	0.026273
	RW	0.991258	0.993529	0.970904	0.998572	0.027668
	IND	0.991850	0.993608	0.974821	0.998804	0.023983
β	SIR	0.298777	0.299823	0.246841	0.345158	0.098318
	AR	0.299521	0.300323	0.247899	0.346341	0.098442
	RW	0.299066	0.300799	0.245420	0.342906	0.097486
	IND	0.300765	0.300979	0.252553	0.346116	0.093563
Scenario 2						
q	SIR	0.992372	0.992988	0.983703	0.997554	0.013852
	AR	0.992372	0.993072	0.983525	0.997504	0.013978
	RW	0.992154	0.993034	0.981538	0.998019	0.025692
	IND	0.992357	0.993032	0.983500	0.997490	0.013990
β	SIR	0.298861	0.298871	0.269706	0.328245	0.058540
	AR	0.299227	0.299151	0.269963	0.328406	0.058443
	RW	0.285673	0.298209	0.001915	0.330015	0.082522
	IND	0.298920	0.299080	0.269414	0.328720	0.059306

Table 1: The posterior mean, median, 2.5th, 97.5th percentiles (the bounds of the 95% credible interval) and the credible intervals' widths of q and β , using scenarios 1 and 2.

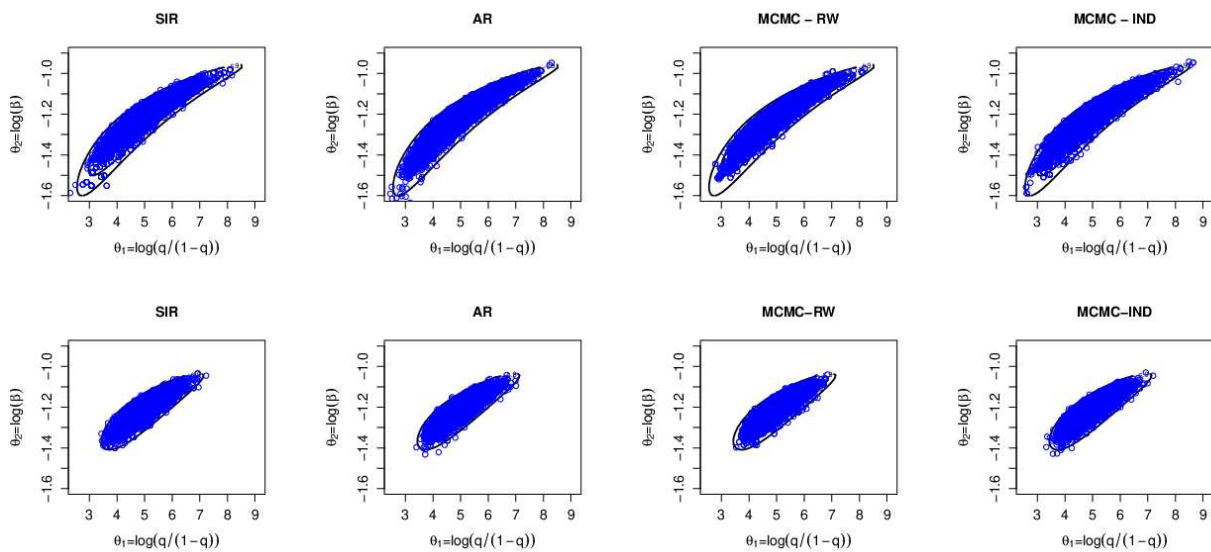


Figure 5.3: The contour plots for the log-posterior of $(\log(\frac{q}{1-q}), \log \beta)$ along with the draws obtained from the joint posterior distribution using SIR, AR, MCMC-RW and MCMC-IND methods using scenario 1 [top row] and scenario 2 [bottom row].

We can use the draws that were simulated from the joint posterior distribution of (q, β) , by following the adopted technique, to get random draws from the posterior distribution of any reliability measure we wish without deriving the actual posterior distribution of that measure. As examples, we calculate the basic Bayes analysis for the probability mass function and the reliability function of the model at a given value x_0 , e.g., the sample mean, using each adopted technique in this paper using the two scenarios of the hyperparameters. Table 2 shows the posterior mean, median, the limits of a 95% credible interval of each measure.

Figure 5.6 displays the Bayes estimate of the posterior probability density function of $P(X = x_0)$, when $x_0 = 172$ 'the sample mean', using the four techniques applied here and the two scenarios of the hyperparameters. As expected, the posterior distribution of $p(172)$ using prior scenario 1 has more spread than that obtained using prior scenario 2.

Both the two prior scenarios provide similar results for the probability mass and survival functions that shows the robustness of the Bayesian analysis.

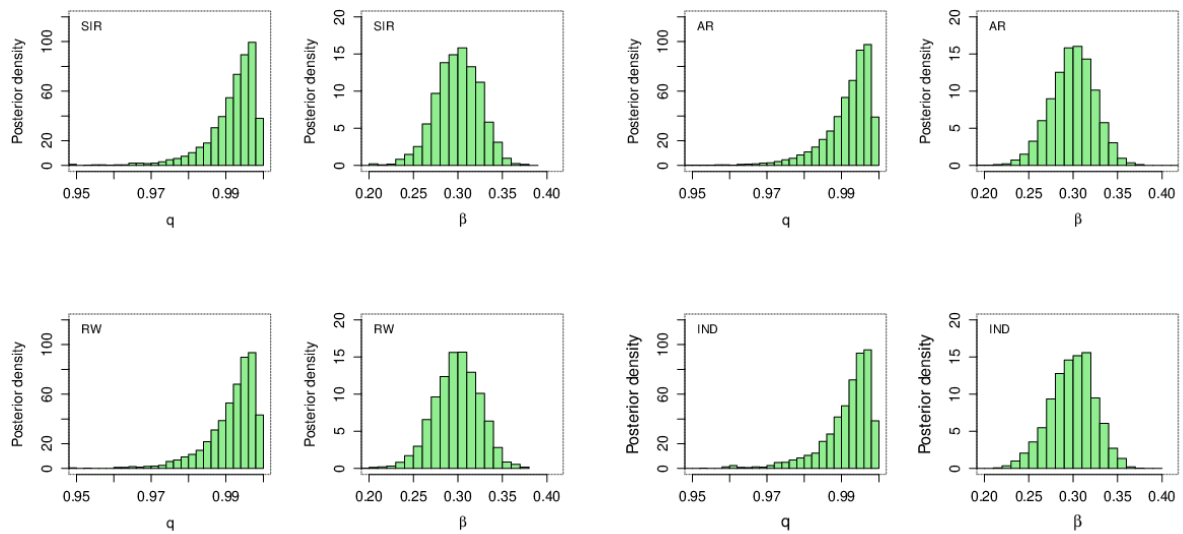


Figure 5.4: The approximated marginal posterior density functions of q and β using SIR (top left), AR (top right), RW (bottom left) and IND (bottom right) methods, using scenario 1 of the hyperparameters.

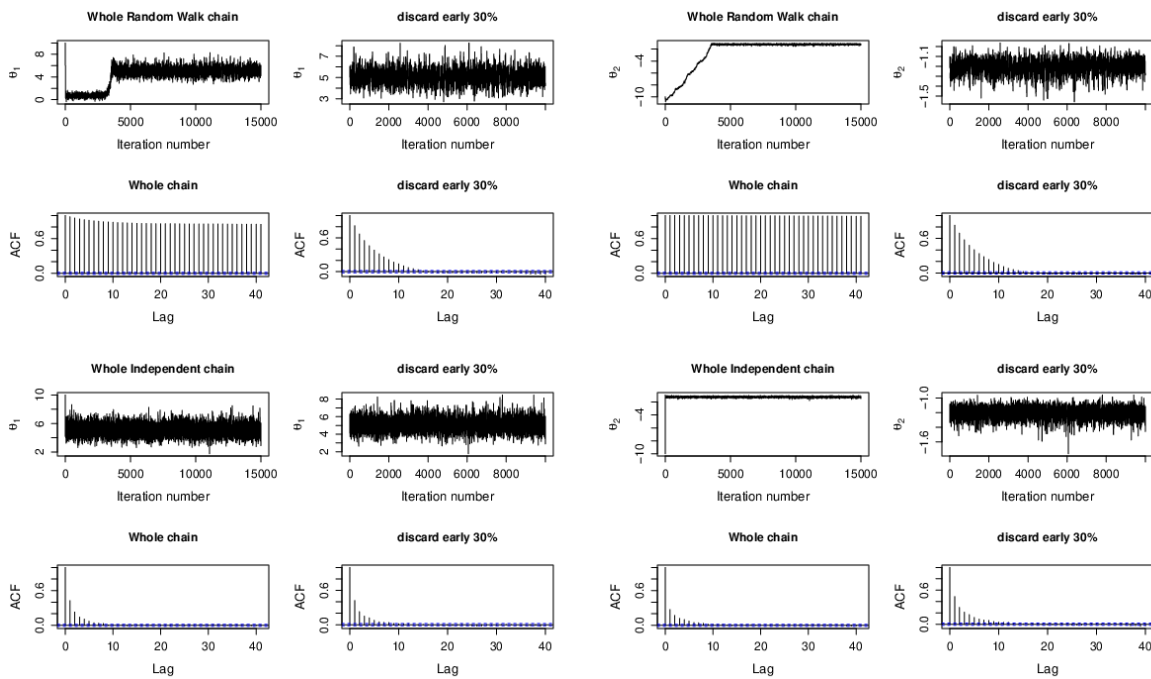


Figure 5.5: The trace and autocorrelation plots for the transformed parameters using RW [top two rows] and IND [bottom two rows]

5.2. Aarset data:

Aarset data [15] consist of the failure times (in weeks) of 50 devices put on a life test. The TTT-Transform plot for this dataset shows that it has a bathtub-shape. Nooghabi et al. [7] used the DMW distribution, Xie and Lai [16] used DAddW, and Almalki and Nadarajah [9] used DRMW to analyze this data set and reported that all of these distributions fit the data well. Sarhan [1] used the DTPBT distribution to analyze this dataset and compared it with those models mentioned above and reported that the DTPBT was better.

In the first dataset, all Bayesian point estimates were very similar using both scenarios of the hyperparameters. Therefore, in this dataset, we implement all the Bayesian techniques adopted here using only scenario 1 of the hyperparameters. Table 3 presents the posterior mean, median and the limits of the 95% credible interval along with its width of the model parameters and the probability mass function and survival function of a random selected device evaluated at 46 weeks (the sample mean). As in the first dataset, all the Bayesian methods, we applied here, give similar results.

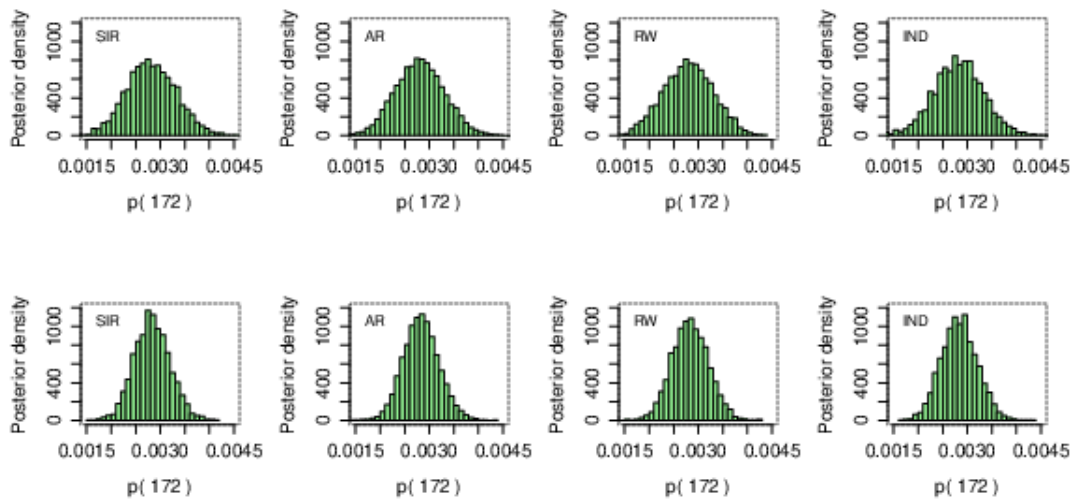


Figure 5.6: The approximated posterior density function of $p(172) = P(X = 172)$ using the four techniques SIR, AR, RW, IND by applying scenario 1 [top row] and scenario 2 [bottom row].

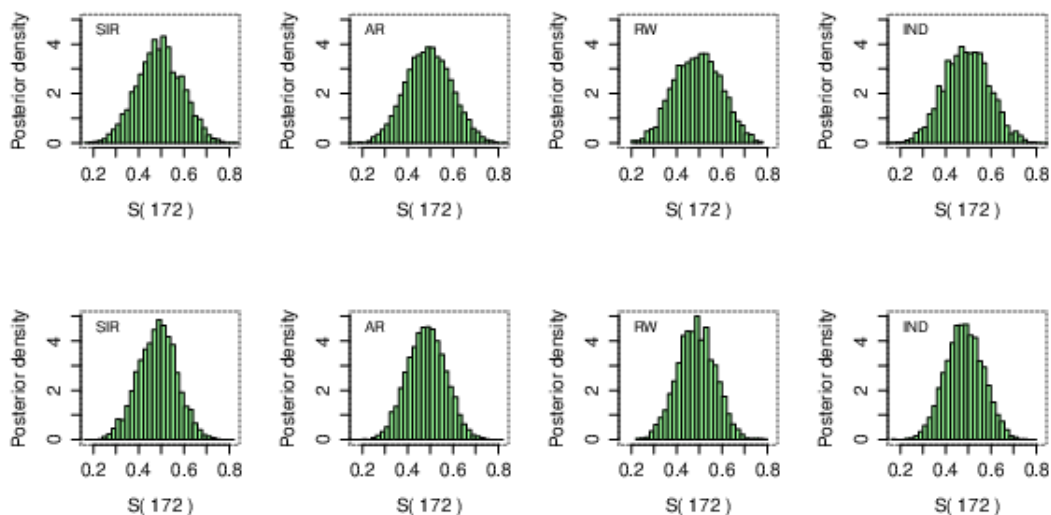


Figure 5.7: The approximated posterior density function of $S(172)$ using the four techniques SIR, AR, RW, IND [from left to right] using scenario 1 [top row] and scenario 2 [bottom row].

6. Simulation results

In order to compare the performance of the four numerical methods applied here, a simulation study is implemented according to the following scheme:

1. Specify the actual value of the vector of model parameters $\vartheta = (q, \beta)$
2. Specify the sample size n
3. Generate a random sample with size n from the $DTPBT(q, \beta)$
4. For the random sample obtained in step 3,
 - (a) generate m random draws from the joint posterior distribution by applying each of the four simulation techniques described in this article (AR, SIR, RW and IND)
 - (b) use the random draws obtained in (a), using every technique, to calculate the Bayes estimate and 95% Bayesian probability interval 'BPI' for q and β
 - (c) for every parameter, calculate: (i) the bias 'exact - estimate' and (ii) an indicator $C = 1$ if the BPI captures the actual value and 0, otherwise.
5. Repeat Steps 3 and 4, N times, then calculate the mean squared errors 'MSE' and the coverage probability 'CP' for every parameter,

Measure	Method	Mean	Median	2.5th	97.5th	Width
Scenario 1						
$p(172)$	SIR	0.00282	0.00281	0.00187	0.00380	0.00193
	AR	0.00282	0.00282	0.00190	0.00379	0.00190
	RW	0.00280	0.00280	0.00186	0.00379	0.00193
	IND	0.00280	0.00281	0.00183	0.00381	0.00198
$S(172)$	SIR	0.49126	0.49213	0.29913	0.68191	0.38278
	AR	0.49275	0.49159	0.30592	0.68669	0.38077
	RW	0.49433	0.49505	0.30318	0.68154	0.37836
	IND	0.49251	0.49329	0.30049	0.68598	0.38549
Scenario 2						
$p(172)$	SIR	0.00282	0.00281	0.00215	0.00357	0.00142
	AR	0.00283	0.00282	0.00214	0.00357	0.00143
	RW	0.00283	0.00282	0.00216	0.00359	0.00143
	IND	0.00283	0.00284	0.00212	0.00357	0.00145
$S(172)$	SIR	0.48475	0.48378	0.32239	0.65225	0.32986
	AR	0.48338	0.48283	0.32064	0.64691	0.32627
	RW	0.48597	0.48429	0.32773	0.65650	0.32877
	IND	0.48487	0.48356	0.32330	0.64864	0.32534

Table 2: Posterior mean, median, 2.5th, 97.5th percentiles (the bounds of the credible interval) and the credible intervals' widths of $p(172)$ and $S(172)$ using prior scenarios 1 and 2.

Parameter	Method	Mean	Median	2.5th	97.5th	Width
q	SIR	0.97704	0.97872	0.95273	0.99130	0.03857
	AR	0.97703	0.97875	0.95344	0.99124	0.03780
	RW	0.97647	0.97809	0.95143	0.99112	0.03969
	IND	0.97684	0.97849	0.95263	0.99082	0.03819
β	SIR	0.34020	0.34047	0.29433	0.38290	0.08857
	AR	0.34059	0.34093	0.29685	0.38268	0.08582
	RW	0.33885	0.33872	0.29409	0.38228	0.08819
	IND	0.33976	0.34042	0.29456	0.38087	0.08631
$p(46)$	SIR	0.01012	0.01008	0.00759	0.01279	0.00520
	AR	0.01013	0.01011	0.00769	0.01275	0.00505
	RW	0.01004	0.00998	0.00750	0.01266	0.00516
	IND	0.01010	0.01009	0.00758	0.01269	0.00511
$S(46)$	SIR	0.43495	0.43291	0.32432	0.55333	0.22901
	AR	0.43374	0.43318	0.31956	0.55621	0.23665
	RW	0.43293	0.43273	0.31709	0.54725	0.23016
	IND	0.43276	0.43372	0.31980	0.54828	0.22847

Table 3: The posterior mean, median, 2.5th, 97.5th percentiles and the credible intervals' widths of q , β and $p(46)$ and $S(46)$ using prior scenarios 1.

using each technique, according to

$$MSE = \frac{\sum_{i=1}^N (\text{Exact} - \text{Estimated}_i)^2}{N}, CP = \frac{\sum_{i=1}^N C_i}{N}$$

here Estimated_i and C_i are the estimated value and the value of the indicator C obtained in the i -th iteration.

We implemented the above algorithm using scenario 1 of hyperparameters with $N = 10000$, $m = 10000$, for different sample size $n = 25, 50, 75$, and 100 , and different sets of parameters' values $\vartheta = (0.9, 0.2), (0.9, 0.3)$ and $(0.9, 0.9)$. The choice of the parameters' value was to reflect different shapes of the hazard function (decreasing, bathtub and increasing) of the DTPBT model. Table 4 summarizes the obtained results, from which we can conclude that: (1) the MSE decreases with the sample size for every parameter using all four numerical methods applied in this paper, (2) the MSE corresponding to each parameter is almost the same for each method, (3) the CP corresponding to each parameter using all four methods gets closer to the nominated confidence level when the sample size gets bigger.

7. Conclusion

Bayesian inferences of the two parameters of the discrete tow-parameter bathtub distribution and its reliability measures are discussed in this paper. The joint posterior distribution of the two parameters has no explicit form. To overcome this problem, four numerical Bayesian computation techniques (accept-reject, sampling-importance resampling and two versions of Markov chain Monte Carlo) are adopted. The two parameters are assumed to be independent and beta and gamma priori distributed with known hyperparameters. Two scenarios of the hyperparameters are discussed and we showed that the Bayes analysis is robust for the choice of the hyperparameters. We re-analyzed two real datasets using the four Bayesian numerical techniques applied here. Finally, we performed a simulation study to investigate the properties of the four Bayesian methods.

As a future work, the methods discussed in this paper can be used under different types of data sets with different testing scenarios such as progressively censored data, competing risks data and/or masked data.

Parameter	Case 1: $(q, \beta) = (0.9, 0.2)$								
	n	MSE				CP			
		AR	SIR	RW	IND	AR	SIR	RW	IND
q	15	0.00196	0.00197	0.00198	0.00186	0.891	0.894	0.895	0.869
	20	0.00145	0.00144	0.00145	0.00137	0.927	0.929	0.921	0.911
	25	0.00108	0.00107	0.00108	0.00107	0.932	0.933	0.929	0.927
	50	0.00057	0.00056	0.00056	0.00056	0.932	0.930	0.932	0.926
	75	0.00040	0.00041	0.00041	0.00040	0.922	0.928	0.924	0.931
	100	0.00031	0.00031	0.00031	0.00031	0.925	0.937	0.925	0.930
β	15	0.00125	0.00125	0.00125	0.00100	0.902	0.903	0.907	0.858
	20	0.00078	0.00077	0.00077	0.00065	0.929	0.928	0.924	0.900
	25	0.00049	0.00049	0.00049	0.00047	0.940	0.941	0.941	0.922
	50	0.00025	0.00025	0.00025	0.00024	0.930	0.932	0.934	0.931
	75	0.00017	0.00017	0.00017	0.00016	0.919	0.921	0.920	0.921
	100	0.00012	0.00012	0.00012	0.00012	0.928	0.929	0.929	0.928
Case 2: $(q, \beta) = (0.9, 0.3)$									
q	15	0.00201	0.00201	0.00202	0.00193	0.894	0.908	0.901	0.869
	20	0.00143	0.00142	0.00142	0.00138	0.911	0.913	0.917	0.894
	25	0.00118	0.00117	0.00116	0.00115	0.921	0.922	0.916	0.909
	50	0.00059	0.00059	0.00059	0.00059	0.930	0.932	0.930	0.932
	75	0.00038	0.00038	0.00038	0.00038	0.938	0.941	0.937	0.938
	100	0.00031	0.00031	0.00031	0.00031	0.923	0.927	0.930	0.924
β	15	0.00260	0.00261	0.00259	0.00204	0.930	0.925	0.922	0.874
	20	0.00172	0.00172	0.00169	0.00153	0.917	0.918	0.917	0.898
	25	0.00813	0.00814	0.00812	0.00742	0.914	0.912	0.916	0.905
	50	0.00325	0.00325	0.00326	0.00325	0.942	0.939	0.935	0.931
	75	0.00191	0.00190	0.00190	0.00189	0.941	0.944	0.941	0.944
	100	0.00152	0.00151	0.00152	0.00152	0.933	0.929	0.933	0.920
Case 3: $(q, \beta) = (0.9, 0.9)$									
q	15	0.00253	0.00254	0.00255	0.00252	0.886	0.882	0.882	0.862
	20	0.00164	0.00164	0.00165	0.00160	0.897	0.895	0.890	0.877
	25	0.00128	0.00127	0.00127	0.00125	0.903	0.896	0.901	0.895
	50	0.00057	0.00056	0.00057	0.00057	0.936	0.932	0.936	0.929
	75	0.00041	0.00041	0.00041	0.00041	0.925	0.931	0.925	0.935
	100	0.00029	0.00030	0.00029	0.00029	0.942	0.937	0.939	0.943
β	15	0.03212	0.03213	0.03208	0.03164	0.873	0.873	0.870	0.856
	20	0.02818	0.02818	0.02801	0.02464	0.895	0.895	0.882	0.869
	25	0.01787	0.01795	0.01757	0.01643	0.906	0.908	0.900	0.889
	50	0.00622	0.00622	0.00621	0.00616	0.929	0.928	0.935	0.931
	75	0.00415	0.00413	0.00413	0.00411	0.923	0.936	0.918	0.925
	100	0.00277	0.00278	0.00276	0.00277	0.931	0.931	0.930	0.935

Table 4: The MSE associated with the Bayes point estimate of the model parameters using each Bayesian simulation method and the coverage probability corresponding to the 95% credible intervals

References

- [1] A. M. Sarhan, *A two-parameter discrete distribution with a bathtub hazard shape*, Commun. Stat. Appl. Methods, **24**(1) (2017), 15-27.
- [2] B. Gnedenko, I. Ushakov, *Probabilistic Reliability Engineering*, John Wiley & Sons, New York, 1995.
- [3] J. F. Lawless, *Statistical Models and Methods for Lifetime Data*, John Wiley & Sons, New York, 1982.
- [4] S. K. Sinha, *Reliability and Life testing*, Wiley Eastern Ltd, New Delhi, 1986.
- [5] K. C. Kapur KC, L. R. Lamberson, *Reliability and in Engineering Design*, John Wiley & Sons, New York, 1976.
- [6] T. Nakagawa, S. Osaki, *The Discrete Weibull Distribution*, IEEE Trans. Reliab., **R-24**(5) (1975), 300-301.
- [7] M. S. Nooghabi, A. R. Roknabady G. H. Borzadaran, *Discrete modified Weibull distribution*, Metron, **LXIX** (2011), 207-222.
- [8] M. Bebbington, C-D Lai, M. Wellington, R. Zitakis, *The discrete additive Weibull distribution: A bathtub-shaped hazard for discontinuous failure data*, Reliab. Engrg. Syst. Safety, **106** (2012), 37-44.
- [9] S. J. Almalki, S. Nadarajah, *A new discrete modified Weibull distribution*, IEEE Trans. Reliab., **63**(1) (2014), 68-80.
- [10] G. Givens, J. Hoeting, *Computational Statistics*, Hoboken. NJ: John Wiley and Sons, 2005.
- [11] J. Monahan, *Numerical Methods of Statistics*, Cambridge: Cambridge University Press, 2001.
- [12] C. Robert, G. Casella, *Monte Carlo Statistical Methods*, New York: Springer, 2014.
- [13] A. Gelman, J. Carlin, H. Stern, D. Rubin, *Bayesian Data Analysis*, New York: Chapman and Hall, 2003.
- [14] F. K. Wang, *A new model with bathtub-shaped failure rate using an additive Burr XII distribution*, Reliab. Engrg. Syst. Safety, **70** (2000), 305-312.
- [15] M. V. Aarset, *How to identify a bathtub hazard rate*, IEEE Trans. Reliab., **R-36** (1987), 106-108.
- [16] M. Xie, C. D. Lai, *Reliability analysis using an additive Weibull model with bathtub-shaped failure rate function*, Reliab. Engrg. Syst. Safety, **52** (1995), 87-93.

2-Absorbing Semiprimary Fuzzy Ideal of Commutative Rings

Deniz Sönmez¹, Gürsel Yeşilot¹, Serkan Onar^{2*} and Bayram Ali Ersoy¹

¹Department of Mathematics, Faculty of Science and Arts, Yıldız Technical University, Turkey

²Management Information Systems, Gelişim University, Turkey

*Corresponding author E-mail: serkan10ar@gmail.com

Article Info

Keywords: 2-absorbing primary fuzzy ideals, 2-absorbing semiprimary fuzzy ideals

2010 AMS: 03E72, 08A72

Received: 01 July 2019

Accepted: 27 September 2019

Available online: 26 December 2019

Abstract

In this work, we introduce the notion of 2-absorbing semiprimary fuzzy ideal which is a generalization of semiprimary fuzzy ideal. Let R be a ring. Then the nonconstant fuzzy ideal μ is called a 2-absorbing semiprimary fuzzy ideal if $\sqrt{\mu}$ is a 2-absorbing fuzzy ideal of R . Furthermore, we give some fundamental results concerning these notions.

1. Introduction

Zadeh in 1965 introduced the fundamental concept of fuzzy set [1]. Focusing on the structure of ring, the paper of Liu [2], defining fuzzy ideals, initiated the investigation of rings by means of expanding the class of ideals with these fuzzy objects. Mukherjee and Sen have continued the study of fuzzy ideals by introducing the notion of prime fuzzy ideals [3]. Nowadays, fuzzy algebraic structures were developed and many interesting results were obtained. The concept of 2-absorbing ideals, which is a generalization of prime ideals [4] and 2-absorbing primary ideals, which is a generalization of primary ideals [5] were introduced. Although the prime fuzzy ideals and primary fuzzy ideals have been investigated [3, 6], the concept of 2-absorbing semiprimary fuzzy ideals have not been studied yet. In this study, we characterize the 2-absorbing semiprimary fuzzy ideals, some generalizations of 2-absorbing semiprimary fuzzy ideals and described some their properties. Recall from [4, 5] that a proper ideal I of R is called a 2-absorbing ideal if whenever $a, b, c \in R$ and $abc \in I$ then either $ab \in I$ or $ac \in I$ or $bc \in I$ and a proper ideal I of R is called a 2-absorbing primary ideal if whenever $a, b, c \in R$ and $abc \in I$ then either $ab \in I$ or $ac \in \sqrt{I}$ or $bc \in \sqrt{I}$. Recall also from [7] that a nonconstant fuzzy ideal μ of R is called a 2-absorbing fuzzy ideal of R if for any fuzzy points x_r, y_s, z_t of R , $x_r y_s z_t \in \mu$ implies that either $x_r y_s \in \mu$ or $x_r z_t \in \mu$ or $y_s z_t \in \mu$ and a nonconstant fuzzy ideal μ of R is called a 2-absorbing primary fuzzy ideal of R if for any fuzzy points x_r, y_s, z_t of R , $x_r y_s z_t \in \mu$ implies that either $x_r y_s \in \mu$ or $x_r z_t \in \sqrt{\mu}$ or $y_s z_t \in \sqrt{\mu}$. Based on these definitions, a nonconstant fuzzy ideal μ is called a 2-absorbing semiprimary fuzzy ideal if $\sqrt{\mu}$ is a 2-absorbing fuzzy ideal of R .

2. Preliminaries

We assume throughout that all rings are commutative with $1 \neq 0$. Unless stated otherwise $L = [0, 1]$ stands for a complete lattice. \mathbb{Z} denotes the ring of integers, $L(R)$ denotes the set of fuzzy sets of R and $LI(R)$ denotes the set of fuzzy ideals of R . For $\mu, \xi \in L(R)$, we say $\mu \subseteq \xi$ if and only if $\mu(x) \leq \xi(x)$ for all $x \in R$. When $r \in L$, $x, y \in R$ we define $x_r \in L(R)$ as follows :

$$x_r(y) = \begin{cases} x & \text{if } x = y, \\ 0 & \text{otherwise,} \end{cases}$$

and x_r is referred to as fuzzy point of R . Let I be an ideal of R . Then

$$\lambda_I = \begin{cases} 1 & \text{if } x \in I, \\ 0 & \text{otherwise,} \end{cases}$$

Definition 2.1. [2] A fuzzy subset μ of a ring R is called a fuzzy ideal of R if for all $x, y \in R$ the following conditions are satisfied :

- $\mu(x-y) \geq \mu(x) \wedge \mu(y), \forall x, y \in R$
- $\mu(xy) \geq \mu(x) \vee \mu(y), \forall x, y \in R$

Let μ be any fuzzy ideal of R ; $x, y \in R$, and 0 be the additive identity of R . Then it is easy to verify the following:

- (i) $\mu(0) \geq \mu(x)$, $\mu(x) = \mu(-x)$ and $\mu_t \subset \mu_s$ where $s, t \in \text{Im}(\mu)$ and $t > s$.
(ii) If $\mu(0) = \mu(x-y)$, then $\mu(x) = \mu(y)$, $\mu(x) = s$ iff $x \in \mu_s$ and $x \notin \mu_t, \forall t > s$.

Definition 2.2. [8] Let μ be any fuzzy ideal of R . The ideals $\mu_t, (\mu(0) \geq t)$ are called level ideals of μ .

Definition 2.3. [3] A fuzzy ideal μ of R is called prime fuzzy ideal if for any two fuzzy points x_r, y_s of R , $x_r y_s \in \mu$ implies either $x_r \in \mu$ or $y_s \in \mu$.

Definition 2.4. [6] Let μ be a fuzzy ideal of R . Then $\sqrt{\mu}$, called the radical of μ , is defined by $\sqrt{\mu}(x) = \bigvee_{n \geq 1} \mu(x^n)$.

Definition 2.5. [6] A fuzzy ideal μ of R is called primary fuzzy ideal if for any two fuzzy points x_r, y_s of R , $x_r y_s \in \mu$ implies either $x_r \in \mu$ or $y_s \in \sqrt{\mu}$.

Theorem 2.6. [6] Let μ be fuzzy ideal of a ring R . Then $\sqrt{\mu}$ is a fuzzy ideal of R .

Definition 2.7. [3] Let R be a ring. Then a nonconstant fuzzy ideal μ is said to be weakly completely prime fuzzy ideal iff for $x, y \in R$, $\mu(xy) = \max\{\mu(x), \mu(y)\}$.

Theorem 2.8. [9] Let $f: R \rightarrow S$ be a ring homomorphism and let μ be a fuzzy ideal of R such that μ is constant on $\text{Ker} f$ and ξ be a fuzzy ideal of S . Then,

- $\sqrt{f(\mu)} = f(\sqrt{\mu})$,
- $\sqrt{f^{-1}(\xi)} = f^{-1}(\sqrt{\xi})$.

Definition 2.9. [4] A nonzero proper ideal I of a commutative ring R with $1 \neq 0$ is called a 2-absorbing ideal if whenever $a, b, c \in R$ with $abc \in I$, then either $ab \in I$ or $ac \in I$ or $bc \in I$.

Definition 2.10. [5] A proper ideal I of R is called a 2-absorbing primary ideal of R if whenever $a, b, c \in R$ with $abc \in I$, then either $ab \in I$ or $ac \in \sqrt{I}$ or $bc \in \sqrt{I}$.

Definition 2.11. [10] A proper ideal I of R is called a 2-absorbing quasi primary ideal of R if whenever $a, b, c \in R$ with $abc \in I$, then either $ab \in \sqrt{I}$ or $ac \in \sqrt{I}$ or $bc \in \sqrt{I}$.

Theorem 2.12. [5] If I is a 2-absorbing primary ideal of R , then \sqrt{I} is a 2-absorbing ideal of R .

Definition 2.13. [11] An element $1 > \alpha \in L$ is called a 2-absorbing element if for any $x, y, z \in L$, $x \wedge y \wedge z < \alpha$ implies either $x \wedge y < \alpha$ or $x \wedge z < \alpha$ or $y \wedge z < \alpha$.

Lemma 2.14. [9] Let μ be a fuzzy ideal of R . Then for any positive integer n , $\sqrt{\mu^n} = \sqrt{\mu}$.

Lemma 2.15. [9] Let μ and λ be fuzzy ideals of R . If $\mu \subseteq \lambda$ then $\sqrt{\mu} \subseteq \sqrt{\lambda}$.

Theorem 2.16. [9] If μ and ξ are two fuzzy ideals of R , then $\sqrt{\mu \cap \xi} = \sqrt{\mu} \cap \sqrt{\xi} = \sqrt{\mu \xi}$

Theorem 2.17. [7] $f: R \rightarrow S$ be a ring homomorphism. If ξ is a 2-absorbing fuzzy ideal of S then $f^{-1}(\xi)$ is a 2-absorbing fuzzy ideal of R .

Theorem 2.18. [7] Let $f: R \rightarrow S$ be a surjective ring homomorphism. If μ is a 2-absorbing fuzzy ideal of R which is constant on $\text{Ker} f$ then $f(\mu)$ is a 2-absorbing fuzzy ideal of S .

3. 2-absorbing semiprimary fuzzy ideals

Before we investigate 2-absorbing semiprimary fuzzy ideals, we will give the characterization of cartesian product of some fuzzy ideals which will be used in next parts.

Definition 3.1. Let μ and α be two fuzzy ideals of R . The cartesian product of μ and α is defined by $\mu \times \alpha$ such that $(\mu \times \alpha)(x, y) = \mu(x) \wedge \alpha(y)$ [12]. In addition to this definition, if $(x_r, y_s) \in \mu \times \alpha$ for any fuzzy points x_r, y_s of R then $x_r \in \mu$ and $y_s \in \alpha$ so $r \wedge s \leq \mu \times \alpha(x, y) = \mu(x) \wedge \alpha(y)$.

Recall that if μ and α are fuzzy ideals of R then $\mu \times \alpha$ is a fuzzy ideal of $R \times R$.

Lemma 3.2. Let μ and α be two fuzzy ideals of R . Then $\sqrt{\mu \times \alpha} = \sqrt{\mu} \times \sqrt{\alpha}$

Proof. $\sqrt{\mu \times \alpha}(x, y) = \bigvee_{n \geq 1} \{(\mu \times \alpha)(x^n, y^n)\} = \bigvee_{n \geq 1} \{\mu(x^n) \wedge \alpha(y^n)\}$
 $= \bigvee_{n \geq 1} \{\mu(x^n)\} \wedge \bigvee_{n \geq 1} \{\alpha(y^n)\} = \sqrt{\mu}(x) \wedge \sqrt{\alpha}(y) = \sqrt{\mu} \times \sqrt{\alpha}(x, y)$ □

Lemma 3.3. Let $R = R_1 \times R_2$, where R_1 and R_2 are rings and μ be a nonconstant fuzzy ideal of R . If μ is a prime fuzzy ideal then either $\mu = \mu_1 \times \lambda_{R_2}$ for some prime fuzzy ideal μ_1 of R_1 or $\mu = \lambda_{R_1} \times \mu_2$ for some prime fuzzy ideal μ_2 of R_2 .

Proof. Assume that μ be a prime fuzzy ideal of R . Then there exist α and β fuzzy ideals of R_1, R_2 respectively such that $\mu = \alpha \times \beta$. Then for any fuzzy points x_r, y_s of R $(x_r, y_s) = (x_r, 1_1)(1_1, y_s) \in \mu = \alpha \times \beta$. So $(x_r, 1_1) \in \alpha \times \beta$ or $(1_1, y_s) \in \alpha \times \beta$ since μ is a prime fuzzy ideal. Thus we conclude that $\beta = \lambda_{R_2}$ and α is a prime fuzzy ideal or $\alpha = \lambda_{R_1}$ and β is a prime fuzzy ideal. □

Theorem 3.4. Let $R = R_1 \times R_2$, where R_1 and R_2 are commutative rings with nonzero identity. Let μ be a nonconstant fuzzy ideal of R . Then the following statements are equivalent:

- (1) μ is a semiprimary fuzzy ideal of R .
- (2) Either $\mu = \mu_1 \times \lambda_{R_2}$ for some semiprimary fuzzy ideal μ_1 of R_1 or $\mu = \lambda_{R_1} \times \mu_2$ for some semiprimary fuzzy ideal μ_2 of R_2 .

Proof. (1) \Rightarrow (2) Assume that μ is a semiprimary fuzzy ideal of R . Then $\mu = \mu_1 \times \mu_2$ for some fuzzy ideal μ_1 of R_1 and some fuzzy ideal μ_2 of R_2 . Since $\sqrt{\mu} = \sqrt{\mu_1} \times \sqrt{\mu_2}$ is a prime fuzzy ideal then by the previous lemma either $\sqrt{\mu_1} = \lambda_{R_1}$ so $\mu_1 = \lambda_{R_1}$ and $\sqrt{\mu_2}$ is a prime fuzzy ideal or $\sqrt{\mu_2} = \lambda_{R_2}$ so $\mu_2 = \lambda_{R_2}$ and $\sqrt{\mu_1}$ is a prime fuzzy ideal. Hence $\mu = \mu_1 \times \lambda_{R_2}$ for some semiprimary fuzzy ideal μ_1 or $\mu = \lambda_{R_1} \times \mu_2$ for some semiprimary fuzzy ideal μ_2 .

(2) \Rightarrow (1) It is clear that since $\sqrt{\mu} = \sqrt{\mu_1 \times \lambda_{R_2}} = \sqrt{\mu_1} \times \lambda_{R_2}$ is a prime fuzzy ideal of R if μ_1 is any semiprimary fuzzy ideal of R_1 . \square

Theorem 3.5. Let μ be a fuzzy ideal of R . If μ is a 2-absorbing then $\mu \times \lambda_R$ ($\lambda_R \times \mu$) is a 2-absorbing fuzzy ideal of $R \times R$.

Proof. Assume that $(x_r, a_k)(y_s, b_p)(z_t, c_h) \in \mu \times \lambda_R$ for any fuzzy points $x_r, y_s, z_t, a_k, b_p, c_h$ of R . Then $(x_r y_s z_t, a_k b_p c_h) \in \mu \times \lambda_R$ so $x_r y_s z_t \in \mu$ and $a_k b_p c_h \in \lambda_R$. Since μ is a 2-absorbing fuzzy ideal then $x_r y_s \in \mu$ or $x_r z_t \in \mu$ or $y_s z_t \in \mu$. Thus we get that $(x_r, a_k)(y_s, b_p) \in \mu \times \lambda_R$ or $(x_r, a_k)(z_t, c_h) \in \mu \times \lambda_R$ or $(y_s, b_p)(z_t, c_h) \in \mu \times \lambda_R$. Hence $\mu \times \lambda_R$ is a 2-absorbing fuzzy ideal.

By the similar way it can be seen that $\lambda_R \times \mu$ is a 2-absorbing fuzzy ideal of $R \times R$. \square

Definition 3.6. Let R be a ring. Then the nonconstant fuzzy ideal μ is said to be a 2-absorbing semiprimary fuzzy ideal if $\sqrt{\mu}$ is a 2-absorbing fuzzy ideal of R .

Example 3.7. (1) Every prime fuzzy ideal is a 2-absorbing semiprimary fuzzy ideal.

(2) Every primary fuzzy ideal is a 2-absorbing semiprimary fuzzy ideal.

(3) Every semiprimary fuzzy ideal is a 2-absorbing semiprimary fuzzy ideal.

Proposition 3.8. Let μ be a nonconstant fuzzy ideal of R . Then the following assertions are equivalent.

- (i) μ is a 2-absorbing semiprimary fuzzy ideal.
- (ii) If $x_r y_s z_t \in \mu$ for any fuzzy points x_r, y_s, z_t of R then $x_r y_s \in \sqrt{\mu}$ or $x_r z_t \in \sqrt{\mu}$ or $y_s z_t \in \sqrt{\mu}$.

Corollary 3.9. If μ is 2-absorbing primary fuzzy ideal then μ is 2-absorbing semiprimary fuzzy ideal.

But, as indicated in the following example, the converse of Corollary 3.9 is not true.

Example 3.10. Let $R = \mathbb{Z}$, the ring of integers. Define the fuzzy ideal μ of Z by

$$\mu(x) = \begin{cases} 1 & x \in 36Z, \\ 1/2 & x \in 6Z - 36Z, \\ 0 & \text{otherwise.} \end{cases}$$

Since $2_1 3_1 \notin \mu$, $2_1 1_{\frac{1}{2}} \notin \sqrt{\mu}$ and $3_1 1_{\frac{1}{2}} \notin \sqrt{\mu}$ while $2_1 3_1 1_{\frac{1}{2}} \in \mu$, then μ is not 2-absorbing primary fuzzy ideal. However, it is easy to see that μ is 2-absorbing semiprimary fuzzy ideal, since $\sqrt{\mu} = \lambda_{6Z}$ where it is a 2-absorbing fuzzy ideal of Z .

Remark 3.11. In Example 2.7 [5], it is proved that a 2-absorbing semiprimary ideal is not necessarily a 2-absorbing primary ideal. In the following theorem we show under what conditions a 2-absorbing semiprimary (fuzzy) ideal is a 2-absorbing primary (fuzzy) ideal. Note that if μ is a semiprime fuzzy ideal of R , then we have $\sqrt{\mu} = \mu$.

Theorem 3.12. Let R be a ring. Then the following statements hold:

- (1) Let μ be a semiprime fuzzy ideal of R . Then μ is a 2-absorbing primary fuzzy ideal if and only if it is 2-absorbing semiprimary fuzzy ideal.
- (2) Let I be a semiprime ideal of R . Then I is a 2-absorbing primary ideal if and only if it is 2-absorbing semiprimary ideal.

Proof. (1) We show that only sufficient conditions. Let μ be semiprime fuzzy ideal. If μ is 2-absorbing semiprimary fuzzy ideal and $x_r y_s z_t \in \mu$ for any x_r, y_s, z_t fuzzy points of R , then $x_r y_s \in \sqrt{\mu}$ or $x_r z_t \in \sqrt{\mu}$ or $y_s z_t \in \sqrt{\mu}$. Since μ is semiprime fuzzy ideal then $\sqrt{\mu} = \mu$ so $x_r y_s \in \mu = \sqrt{\mu}$ or $x_r z_t \in \sqrt{\mu}$ or $y_s z_t \in \sqrt{\mu}$. Hence we get that μ is a 2-absorbing primary fuzzy ideal of R .

(2) We omit the proof since it is clear by (1). \square

Theorem 3.13. Let μ be a fuzzy ideal of R . If μ is a 2-absorbing semiprimary then μ_t is a 2-absorbing semiprimary ideal of R for any $t \in [0, \mu(0)]$.

Proof. If μ is a 2-absorbing semiprimary then $\sqrt{\mu}$ is a 2-absorbing fuzzy ideal of R . By [7, Lemma 3.3], $\sqrt{\mu_t} = \sqrt{\mu}$ is also 2-absorbing ideal. Hence μ_t is 2-absorbing semiprimary ideal of R . \square

Theorem 3.14. Let μ_1 be ξ_1 -semiprimary fuzzy ideal of R and μ_2 be ξ_2 -semiprimary fuzzy ideal of R . Then the following statements hold.

- (i) $\mu_1 \mu_2$ is a 2-absorbing semiprimary fuzzy ideal of R .
- (ii) $\mu_1 \cap \mu_2$ is a 2-absorbing semiprimary fuzzy ideal of R .

Proof. Since $\sqrt{\mu_1} = \xi_1$ and $\sqrt{\mu_2} = \xi_2$ are prime fuzzy ideals then $\sqrt{\mu_1 \mu_2} = \sqrt{\mu_1 \cap \mu_2} = \sqrt{\mu_1} \cap \sqrt{\mu_2}$ is 2-absorbing fuzzy ideal of R . Hence $\mu_1 \cap \mu_2$ and $\mu_1 \mu_2$ are 2-absorbing semiprimary fuzzy ideal. \square

Theorem 3.15. Let μ be a nonconstant fuzzy ideal. If $\mu_* = \{x \in R : \mu(x) > 0\}$ is a 2-absorbing semiprimary ideal of R where $\mu(0) = 1$ and $|Im\mu| = 2$ then μ is a 2-absorbing semiprimary fuzzy ideal of R .

Proof. Assume that $\mu(0) = 1, Im\mu = \{1, \alpha\}$ and μ_* is a 2-absorbing semiprimary ideal.

Let $x_r y_s z_t \in \mu$ but $x_r y_s \notin \sqrt{\mu}, y_s z_t \notin \sqrt{\mu}$ and $x_r z_t \notin \sqrt{\mu}$. Then $r \wedge s \wedge t \leq \mu(xyz)$ and $r \wedge s > \sqrt{\mu}(xy), s \wedge t > \sqrt{\mu}(yz), r \wedge t > \sqrt{\mu}(xz)$. Thus for all $n \in \mathbb{Z}^+, r \wedge s > \mu(x^n y^n), s \wedge t > \mu(y^n z^n)$ and $r \wedge t > \mu(x^n z^n)$. By our assumption we get that $\mu(x^n y^n) = \mu(y^n z^n) = \mu(x^n z^n) = \alpha$ so $xy, yz, xz \notin \mu_*$. However, $\alpha < r \wedge s \wedge t \leq \mu(xyz) = 1$ so $xy, yz, xz \notin \sqrt{\mu_*}$ and $xyz \in \mu_*$. But this contradicts that μ_* is 2-absorbing semiprimary ideal. Hence μ is a 2-absorbing semiprimary fuzzy ideal. \square

Theorem 3.16. Let I be a 2-absorbing quasi primary ideal of R and $\alpha \in [0, 1)$ be any arbitrary. If μ is the fuzzy ideal of R defined by

$$\mu(x) = \begin{cases} 1 & x \in I, \\ \alpha & x \notin I, \end{cases}$$

for all $x \in R$, then μ is a 2-absorbing semiprimary fuzzy ideal of R .

Proof. Let I be a 2-absorbing primary ideal of R . Assume that $x_r y_s z_t \in \mu$ but $x_r y_s \notin \sqrt{\mu}$ and $x_r z_t \notin \sqrt{\mu}$ and $y_s z_t \notin \sqrt{\mu}$ for any $x, y, z \in R$. Then $\mu((xy)^n) \leq \sqrt{\mu}(xy) < r \wedge s$ and $\mu((yz)^n) \leq \sqrt{\mu}(yz) < s \wedge t$ and $\mu((xz)^n) \leq \sqrt{\mu}(xz) < r \wedge t$ for all $n \geq 1$. In this case $\mu((xy)^n) = \alpha$ and $(xy)^n \notin I$ so $xy \notin \sqrt{I}, \mu((yz)^n) = \alpha$ and $(yz)^n \notin I$ so $yz \notin \sqrt{I}, \mu((xz)^n) = \alpha$ and $(xz)^n \notin I$ so $xz \notin \sqrt{I}$. Since I is 2-absorbing semiprimary ideal of R then we get $xyz \notin I$ and so $\mu(xyz) = \alpha$. By our assumption we get $(xyz)_{r \wedge s \wedge t} = x_r y_s z_t \in \mu$ and $r \wedge s \wedge t \leq \mu(xyz) = \alpha$. Thus $\alpha < r \wedge s, \alpha < s \wedge t$ and $\alpha < r \wedge t$ so $\alpha < r \wedge s \wedge t$, which is a contradiction. Hence μ is a 2-absorbing semiprimary fuzzy ideal of R . \square

Theorem 3.17. Let $f : R \rightarrow S$ be a ring homomorphism. If ξ is a 2-absorbing semiprimary fuzzy ideal of S then $f^{-1}(\xi)$ is a 2-absorbing semiprimary fuzzy ideal of R .

Proof. Let ξ be a 2-absorbing semiprimary fuzzy ideal of S . We show that $\sqrt{f^{-1}(\xi)}$ is a 2-absorbing fuzzy ideal of R . Since $\sqrt{f^{-1}(\xi)} = f^{-1}(\sqrt{\xi})$ and $\sqrt{\xi}$ is a 2-absorbing fuzzy ideal then the inverse image of $\sqrt{\xi}$ is also 2-absorbing fuzzy ideal by [7, Theorem 31]. Hence $f^{-1}(\xi)$ is a 2-absorbing semiprimary fuzzy ideal of R . \square

Theorem 3.18. Let $f : R \rightarrow S$ be a surjective ring homomorphism. If μ is a 2-absorbing semiprimary fuzzy ideal of R which is constant on $\text{Ker}f$ then $f(\mu)$ is a 2-absorbing semiprimary fuzzy ideal of S .

Proof. Assume that μ is a 2-absorbing semiprimary fuzzy ideal of R which is constant on $\text{Ker}f$. Then $\sqrt{\mu}$ is a 2-absorbing fuzzy ideal of R such that $\sqrt{\mu}$ is also constant on $\text{Ker}f$. By [7, Theorem 32], $f(\sqrt{\mu}) = \sqrt{f(\mu)}$ is a 2-absorbing fuzzy ideal of S . \square

Theorem 3.19. If f is a homomorphism from a ring R onto a ring S , then the mapping $\mu \rightarrow f(\mu)$ defines a one-to-one correspondence between the set of all 2-absorbing semiprimary fuzzy ideals of R which is constant on $\text{Ker}f$ and the set of all 2-absorbing semiprimary fuzzy ideals of S .

Definition 3.20. Let μ be a 2-absorbing semiprimary fuzzy ideal of R . Then $\gamma = \sqrt{\mu}$ is a 2-absorbing fuzzy ideal. We say that μ is a γ -2-absorbing semiprimary fuzzy ideal of R .

Theorem 3.21. Let $\mu_1, \mu_2, \dots, \mu_n$ be γ -2-absorbing semiprimary fuzzy ideals of R for some 2-absorbing fuzzy ideal γ of R . Then $\mu = \bigcap_{i=1}^n \mu_i$ is a γ -2-absorbing semiprimary fuzzy ideal of R .

Proof. Let $\mu_i, i \in \{1, 2, \dots, n\}$ be γ -2-absorbing semiprimary fuzzy ideals of R . Then $\sqrt{\bigcap_{i=1}^n \mu_i} = \bigcap_{i=1}^n \sqrt{\mu_i} = \gamma = \sqrt{\mu}$ is a 2-absorbing fuzzy ideal. Hence μ is a γ -2-absorbing primary fuzzy ideal of R . \square

Theorem 3.22. Let R_1 and R_2 be commutative rings with nonzero identity and μ be a nonconstant fuzzy ideal of R_1 (of R_2). If μ is a 2-absorbing semiprimary fuzzy ideal of R_1 (of R_2) then $\mu \times \lambda_{R_2}$ ($\lambda_{R_1} \times \mu$) is a 2-absorbing semiprimary fuzzy ideal of $R_1 \times R_2$.

Proof. Assume that μ is a 2-absorbing semiprimary fuzzy ideal. Since $\sqrt{\mu}$ is a 2-absorbing fuzzy ideal then $\sqrt{\mu \times \lambda_{R_2}} = \sqrt{\mu} \times \lambda_{R_2}$ is a 2-absorbing fuzzy ideal of $R_1 \times R_2$. Hence we get $\mu \times \lambda_{R_2}$ is a 2-absorbing semiprimary fuzzy ideal of $R_1 \times R_2$. \square

Corollary 3.23. Let $R = R_1 \times R_2$ where R_1 and R_2 be two rings and μ be a nonconstant fuzzy ideal of R . Then the following statements are equivalent: (1) μ is a 2-absorbing semiprimary fuzzy ideal of R . (2) Either $\mu = \mu_1 \times \lambda_{R_2}$ for some 2-absorbing semiprimary fuzzy ideal μ_1 of R_1 , or $\mu = \lambda_{R_1} \times \mu_2$ for some 2-absorbing semiprimary fuzzy ideal μ_2 of R_2 , or $\mu = \mu_1 \times \mu_2$ for some 2-absorbing semiprimary fuzzy ideal of R_2 .

4. Conclusion

In this paper, we have characterized 2-absorbing semiprimary fuzzy ideals of a ring. Also the notions of 2-absorbing and 2-absorbing primary fuzzy ideals and their properties are proposed. Furthermore, the relationship between 2-absorbing semiprimary fuzzy ideals and 2-absorbing semiprimary ideals. Finally, we have examined that the properties of cartesian product of 2-absorbing semiprimary fuzzy ideals. To extend this study, one could study other algebraic structures and do some further study on the properties them.

Acknowledgement

This work was supported by Research Fund of the Yildiz Technical University. Project Number: 2015-01-03-DOP03.

References

- [1] L. A. Zadeh, *Fuzzy sets*, Inform. Control, **8** (1965), 338-353.
- [2] W. J. Liu, *Fuzzy invariant subgroups and fuzzy ideals*, Fuzzy Sets Syst., **8** (1982), 133-139.
- [3] T. K. Mukherjee, M.K. Sen, *Prime fuzzy ideals in rings*, Fuzzy Sets Syst. **32** (1989), 337-341.
- [4] A. Badawi, *On 2-absorbing ideals of commutative rings*, Bull. Austral. Math. Soc., **75**(3) (2007), 417-429.
- [5] A. Badawi, U. Tekir, E. Yetkin, *On 2-absorbing primary ideals in commutative rings*, Bull. Austral. Math. Soc., **51**(4) (2014), 1163-1173.
- [6] T. K. Mukherjee, M. K. Sen, *Primary fuzzy ideals and radical of fuzzy ideals*, Fuzzy Sets Syst., **56** (1993), 97-101.
- [7] D. Sönmez, G. Yeşilot, S. Onar, B. A. Ersoy, B. Davvaz, *On 2-absorbing primary fuzzy ideals of commutative rings*, Math. Probl. Eng., (2017), doi: 10.1155/2017/5485839.
- [8] V. N. Dixit, R. Kumar, N. Ajmal, *Fuzzy ideals and fuzzy prime ideals of a ring*, Fuzzy Sets Syst., **44** (1991), 127-138.
- [9] L. I. Sidky, S. A. Khatib, *Nil radical of fuzzy ideal*, Fuzzy Sets Syst., **47** (1992), 117-120.
- [10] S. Koc, R. N. Uregen, U. Tekir, *On 2-absorbing quasi primary submodules*, Filomat, **31** (2017), 2943-2950.
- [11] F. Callialp, E. Yetkin, U. Tekir, *On 2-absorbing primary and weakly 2-absorbing primary elements in multiplicative lattices*, Ital. J. Pure Appl. Math., **34** (2015), 263-276 .
- [12] B. A. Ersoy, *A generalization of cartesian product of fuzzy subgroups and ideals*, J. Appl. Sci., **3** (2003), 100-102.

Korovkin Type Approximation Theorem for Functions of Two Variables Through $\alpha\beta$ -Statistical Convergence

Selma Altundag^{1*} and Bayram Sozbir¹

¹Department of Mathematics, Faculty of Science and Arts, Sakarya University, Sakarya, Turkey

*Corresponding author E-mail: scaylan@sakarya.edu.tr

Article Info

Keywords: $\alpha\beta$ -statistical convergence, Double sequences, Korovkin type theorem, Lacunary statistical convergence, λ -statistical convergence, Statistical convergence

2010 AMS: 41A10, 41A36, 40A05, 40A30, 40G15

Received: 28 November 2019

Accepted: 22 December 2019

Available online: 26 December 2019

Abstract

In this paper, we introduce the concepts of $\alpha\beta$ -statistical convergence and strong $\alpha\beta$ -summability of double sequences and investigate the relation between these two new concepts. Moreover, statistical convergence and $\alpha\beta$ -statistical convergence of double sequences are compared under some certain assumptions. Finally, as an application, we prove Korovkin type approximation theorem for a function of two variables by using the notion of $\alpha\beta$ -statistical convergence.

1. Introduction

The idea of statistical convergence for sequences of real and complex numbers was introduced by Fast [1] and Steinhaus [2] independently in the same year 1951 as follows. Let $K \subseteq \mathbb{N}$, the set of natural numbers and $K_n = \{k \leq n : k \in K\}$. Then the natural density of K is defined by $\delta(K) = \lim_n n^{-1} |K_n|$ if the limit exists, where $|K_n|$ denotes the cardinality of K_n . A sequence $x = (x_k)$ is said to be statistically convergent to L if for every $\varepsilon > 0$, the set $K_\varepsilon := \{k \in \mathbb{N} : |x_k - L| \geq \varepsilon\}$ has natural density zero, i.e., for each $\varepsilon > 0$,

$$\lim_n \frac{1}{n} |\{k \leq n : |x_k - L| \geq \varepsilon\}| = 0,$$

which is denoted by $st - \lim x = L$. Over the years, generalizations and applications of this notion have been investigated by various researchers [3]-[14].

Aktuglu [14] introduced $\alpha\beta$ -statistical convergence as follows. Let $\alpha(n)$ and $\beta(n)$ be two sequences of positive numbers satisfying the following conditions:

P_1 : α and β are both non-decreasing,

P_2 : $\beta(n) \geq \alpha(n)$,

P_3 : $\beta(n) - \alpha(n) \rightarrow \infty$ as $n \rightarrow \infty$.

Let Λ denote the set of pairs (α, β) satisfying P_1 , P_2 and P_3 .

For each pair $(\alpha, \beta) \in \Lambda$, $0 < \gamma \leq 1$ and $K \subset \mathbb{N}$, we define

$$\delta^{\alpha, \beta}(K, \gamma) = \lim_{n \rightarrow \infty} \frac{|K \cap P_n^{\alpha, \beta}|}{(\beta(n) - \alpha(n) + 1)^\gamma}$$

where $P_n^{\alpha, \beta}$ is the closed interval $[\alpha(n), \beta(n)]$ and $|S|$ represents the cardinality of S .

Definition 1.1. [14] A sequence $x = (x_k)$ is said to be $\alpha\beta$ -statistically convergent of order γ to L , if for every $\varepsilon > 0$

$$\delta^{\alpha,\beta}(\{k : |x_k - L| \geq \varepsilon\}, \gamma) = \lim_{n \rightarrow \infty} \frac{\left| \left\{ k \in P_n^{\alpha,\beta} : |x_k - L| \geq \varepsilon \right\} \right|}{(\beta(n) - \alpha(n) + 1)^\gamma} = 0$$

which is denoted by $st_{\alpha\beta}^\gamma - \lim x = L$. For $\gamma = 1$, we say that x is $\alpha\beta$ -statistically convergent to L , and this is denoted by $st_{\alpha\beta} - \lim x = L$.

Definition 1.2. [15] A sequence $x = (x_k)$ is said to be $[N^\gamma, \alpha\beta]_q$ -summable to a number L , $0 < q < \infty$, if

$$\lim_{n \rightarrow \infty} \frac{1}{(\beta(n) - \alpha(n) + 1)^\gamma} \sum_{k \in P_n^{\alpha,\beta}} |x_k - L|^q = 0,$$

which is denoted by $x_k \rightarrow L[N^\gamma, \alpha\beta]_q$. Similarly, for $\gamma = 1$ the sequence $x = (x_k)$ is said to be $[N, \alpha\beta]_q$ -summable to L .

By the convergence of a double sequence we mean the convergence in the Pringsheim sense, that is, a double sequence $x = (x_{jk})$ is said to be convergent to L in the Pringsheim sense, if for every $\varepsilon > 0$ there exists $N \in \mathbb{N}$ such that $|x_{jk} - L| < \varepsilon$ whenever $j, k > N$. In this case we write $P - \lim x = L$ [16].

A double sequence $x = (x_{jk})$ is bounded if there exists positive number M such that $|x_{jk}| < M$ for all $j, k \in \mathbb{N}$. We denote the set of all bounded double sequence by I_∞^2 .

Let $K \subseteq \mathbb{N} \times \mathbb{N}$ and $K(m, n) = \{(j, k) : j \leq m, k \leq n\}$. The double natural density of K is defined by

$$\delta_2(K) = P - \lim_{m,n} |K(m, n)|,$$

if the limit exists.

A double sequence $x = (x_{jk})$ is said to be statistically convergent to a number L , if for every $\varepsilon > 0$ the set $\{(j, k), j \leq m \text{ and } k \leq n : |x_{jk} - L| \geq \varepsilon\}$ has double natural density zero, i.e. for every $\varepsilon > 0$,

$$P - \lim_{m,n} \frac{1}{mn} \left| \{(j, k), j \leq m \text{ and } k \leq n : |x_{jk} - L| \geq \varepsilon\} \right| = 0,$$

which is denoted by $st_2 - \lim_{j,k} x_{jk} = L$ [17]. We denote the set of all statistically convergent double sequences by st_2 . Note that if $x = (x_{jk})$ is

P -convergent then it is statistically convergent, but not conversely. Also a statistically convergent double sequence need not be bounded. For this, consider a sequence $x = (x_{jk})$ defined by

$$x_{jk} = \begin{cases} jk, & \text{if } j \text{ and } k \text{ are square,} \\ 1, & \text{otherwise.} \end{cases}$$

Then, $st_2 - \lim x = 1$. But x is neither P -convergent nor bounded.

Our purpose is to extend the concepts of $\alpha\beta$ -statistical convergence and strong $\alpha\beta$ -summability from ordinary (i.e. single) sequences to double sequences. This paper organized as follows: In section 2, we introduce the concepts of $\alpha\beta$ -statistical convergence and strong $\alpha\beta$ -summability of double sequences, and also establish the some relations these new concepts. Moreover, statistical convergence and $\alpha\beta$ -statistical convergence of double sequences are compared under some certain assumptions. In section 3, we prove Korovkin type approximation theorem through $\alpha\beta$ -statistical convergence for functions of two variables.

2. Main results

We now begin defining the our new concepts of $\alpha\beta$ -statistical convergence and strong $\alpha\beta$ -summability for double sequences. Throughout the paper, let $(\alpha_1, \beta_1) \in \Lambda$ and $(\alpha_2, \beta_2) \in \Lambda$.

Definition 2.1. A double sequence $x = (x_{jk})$ is said to be $\alpha\beta$ -statistically convergent to a number L , if for every $\varepsilon > 0$

$$\lim_{m,n \rightarrow \infty} \frac{1}{\left| P_m^{\alpha_1, \beta_1} \right| \left| P_n^{\alpha_2, \beta_2} \right|} \left| \left\{ (j, k), j \in P_m^{\alpha_1, \beta_1} \text{ and } k \in P_n^{\alpha_2, \beta_2} : |x_{jk} - L| \geq \varepsilon \right\} \right| = 0,$$

which is denoted by $st_2(\alpha\beta) - \lim x_{jk} = L$, where $P_m^{\alpha_1, \beta_1}$ and $P_n^{\alpha_2, \beta_2}$ are the closed intervals $[\alpha_1(m), \beta_1(m)]$ and $[\alpha_2(n), \beta_2(n)]$, respectively, also $|P_m^{\alpha_1, \beta_1}| = \beta_1(m) - \alpha_1(m) + 1$ and $|P_n^{\alpha_2, \beta_2}| = \beta_2(n) - \alpha_2(n) + 1$.

This definition also includes the following special cases:

i) If we take $\alpha_1(m) = 1, \beta_1(m) = m$ for all $m \in \mathbb{N}$ and $\alpha_2(n) = 1, \beta_2(n) = n$ for all $n \in \mathbb{N}$, then $\alpha\beta$ -statistical convergence of double sequence is reduced to statistical convergence of double sequences introduced in [17].

ii) Let $\lambda = (\lambda_m)$ and $\mu = (\mu_n)$ be two non-decreasing sequences of positive numbers tending to ∞ such that

$$\lambda_{m+1} \leq \lambda_m + 1, \quad \lambda_1 = 1,$$

and

$$\mu_{n+1} \leq \mu_n + 1, \quad \mu_1 = 1.$$

Then in the case of $\alpha_1(m) = m - \lambda_m + 1, \beta_1(m) = m$ for all $m \in \mathbb{N}$ and $\alpha_2(n) = n - \mu_n + 1, \beta_2(n) = n$ for all $n \in \mathbb{N}$, $\alpha\beta$ -statistical convergence of double sequence is reduced to (λ, μ) -statistical convergence of double sequence introduced in [18].

iii) Recall that a double lacunary sequence $\theta_{r,s} = \{(k_r, l_s)\}$, which means there exist two increasing of integers such that

$$k_0 = 0, \quad h_r = k_r - k_{r-1} \rightarrow \infty \quad \text{as } r \rightarrow \infty,$$

and

$$l_0 = 0, \quad \bar{l}_s = l_s - l_{s-1} \rightarrow \infty \quad \text{as } s \rightarrow \infty.$$

If we take $\alpha_1(m) = k_{m-1} + 1, \beta_1(m) = k_m$ for all $m \in \mathbb{N}$ and $\alpha_2(n) = l_{n-1} + 1, \beta_2(n) = l_n$ for all $n \in \mathbb{N}$, then $\alpha\beta$ -statistical convergence of double sequence is reduced to lacunary statistical convergence of double sequence introduced in [19].

Definition 2.2. A double sequence $x = (x_{jk})$ is said to be strongly $\alpha\beta$ -summable or briefly $[N_2, \alpha\beta]$ -summable to a number L , if

$$\lim_{m,n \rightarrow \infty} \frac{1}{\left| P_m^{\alpha_1, \beta_1} \right| \left| P_n^{\alpha_2, \beta_2} \right|} \sum_{j \in P_m^{\alpha_1, \beta_1}} \sum_{k \in P_n^{\alpha_2, \beta_2}} |x_{jk} - L| = 0,$$

and we denote it by $x_{jk} \rightarrow L[N_2, \alpha\beta]$.

We shall denote the set of all $\alpha\beta$ -statistically convergent double sequences by $st_2(\alpha\beta)$, and the set of all $[N_2, \alpha\beta]$ -summable double sequences by $[N_2, \alpha\beta]$.

Then, we get the following results.

Theorem 2.3. If a double sequence $x = (x_{jk})$ is $[N_2, \alpha\beta]$ -summable to L , then it is $\alpha\beta$ -statistically convergent to L , that is, $[N_2, \alpha\beta] \subseteq st_2(\alpha\beta)$ and also the inclusion is strict.

Proof. Let $x_{jk} \rightarrow L[N_2, \alpha\beta]$ and given $\varepsilon > 0$. Then, we have

$$\begin{aligned} \frac{1}{\left| P_m^{\alpha_1, \beta_1} \right| \left| P_n^{\alpha_2, \beta_2} \right|} \sum_{j \in P_m^{\alpha_1, \beta_1}} \sum_{k \in P_n^{\alpha_2, \beta_2}} |x_{jk} - L| &= \frac{1}{\left| P_m^{\alpha_1, \beta_1} \right| \left| P_n^{\alpha_2, \beta_2} \right|} \sum_{\substack{j \in P_m^{\alpha_1, \beta_1} \\ |x_{jk} - L| \geq \varepsilon}} \sum_{k \in P_n^{\alpha_2, \beta_2}} |x_{jk} - L| + \frac{1}{\left| P_m^{\alpha_1, \beta_1} \right| \left| P_n^{\alpha_2, \beta_2} \right|} \sum_{\substack{j \in P_m^{\alpha_1, \beta_1} \\ |x_{jk} - L| < \varepsilon}} \sum_{k \in P_n^{\alpha_2, \beta_2}} |x_{jk} - L| \\ &\geq \varepsilon \frac{1}{\left| P_m^{\alpha_1, \beta_1} \right| \left| P_n^{\alpha_2, \beta_2} \right|} \left| \left\{ (j, k), j \in P_m^{\alpha_1, \beta_1} \text{ and } k \in P_n^{\alpha_2, \beta_2} : |x_{jk} - L| \geq \varepsilon \right\} \right|, \end{aligned}$$

which means that $st_2(\alpha\beta) - \lim x_{jk} = L$.

To show that the inclusion is strict, we consider the following example: Let $\alpha_1(m) \leq 1 \leq \beta_1(m)$ and $\alpha_2(n) \leq 1 \leq \beta_2(n)$ for all $m, n \in \mathbb{N}$, and the sequence $x = (x_{jk})$ be defined by

$$x_{jk} = \begin{cases} jk, & 1 \leq j \leq \left[\sqrt{\beta_1(m) - \alpha_1(m) + 1} \right] \text{ and } 1 \leq k \leq \left[\sqrt{\beta_2(n) - \alpha_2(n) + 1} \right], \\ 0, & \text{otherwise.} \end{cases}$$

Then, we have

$$\begin{aligned} &\frac{1}{\left| P_m^{\alpha_1, \beta_1} \right| \left| P_n^{\alpha_2, \beta_2} \right|} \left| \left\{ (j, k), j \in P_m^{\alpha_1, \beta_1} \text{ and } k \in P_n^{\alpha_2, \beta_2} : |x_{jk} - L| \geq \varepsilon \right\} \right| \\ &= \frac{\left[\sqrt{\beta_1(m) - \alpha_1(m) + 1} \right] \left[\sqrt{\beta_2(n) - \alpha_2(n) + 1} \right]}{(\beta_1(m) - \alpha_1(m) + 1)(\beta_2(n) - \alpha_2(n) + 1)} \rightarrow 0 \quad \text{as } m, n \rightarrow \infty. \end{aligned}$$

That is, $st_2(\alpha\beta) - \lim x_{jk} = 0$. But

$$\begin{aligned} &\frac{1}{\left| P_m^{\alpha_1, \beta_1} \right| \left| P_n^{\alpha_2, \beta_2} \right|} \sum_{j \in P_m^{\alpha_1, \beta_1}} \sum_{k \in P_n^{\alpha_2, \beta_2}} |x_{jk} - 0| \\ &= \frac{\left[\sqrt{\beta_1(m) - \alpha_1(m) + 1} \right] \left(\left[\sqrt{\beta_1(m) - \alpha_1(m) + 1} \right] + 1 \right) \left[\sqrt{\beta_2(n) - \alpha_2(n) + 1} \right] \left(\left[\sqrt{\beta_2(n) - \alpha_2(n) + 1} \right] + 1 \right)}{4(\beta_1(m) - \alpha_1(m) + 1)(\beta_2(n) - \alpha_2(n) + 1)} \rightarrow \frac{1}{4} \end{aligned}$$

which means $x_{jk} \not\rightarrow 0[N_2, \alpha\beta]$. □

Theorem 2.4. If a double sequence $x = (x_{jk})$ bounded and $\alpha\beta$ -statistically convergent to L , then $x_{jk} \rightarrow L[N_2, \alpha\beta]$.

Proof. Assume that $x = (x_{jk})$ is bounded and $\alpha\beta$ -statistically convergent to L . Since $x = (x_{jk})$ is bounded, there exists $M > 0$ such that $|x_{jk} - L| \leq M$ for $j, k \in \mathbb{N}$. Then we can see that

$$\begin{aligned} \frac{1}{\left| P_m^{\alpha_1, \beta_1} \right| \left| P_n^{\alpha_2, \beta_2} \right|} \sum_{j \in P_m^{\alpha_1, \beta_1}} \sum_{k \in P_n^{\alpha_2, \beta_2}} |x_{jk} - L| &= \frac{1}{\left| P_m^{\alpha_1, \beta_1} \right| \left| P_n^{\alpha_2, \beta_2} \right|} \sum_{\substack{j \in P_m^{\alpha_1, \beta_1} \\ |x_{jk} - L| \geq \varepsilon}} \sum_{k \in P_n^{\alpha_2, \beta_2}} |x_{jk} - L| + \frac{1}{\left| P_m^{\alpha_1, \beta_1} \right| \left| P_n^{\alpha_2, \beta_2} \right|} \sum_{\substack{j \in P_m^{\alpha_1, \beta_1} \\ |x_{jk} - L| < \varepsilon}} \sum_{k \in P_n^{\alpha_2, \beta_2}} |x_{jk} - L| \\ &\leq \frac{M}{\left| P_m^{\alpha_1, \beta_1} \right| \left| P_n^{\alpha_2, \beta_2} \right|} \left| \left\{ (j, k), j \in P_m^{\alpha_1, \beta_1} \text{ and } k \in P_n^{\alpha_2, \beta_2} : |x_{jk} - L| \geq \varepsilon \right\} \right| + \varepsilon. \end{aligned}$$

Taking limit as $m, n \rightarrow \infty$ on the both sides of last inequality and also using the hypothesis, we obtain that

$$\lim_{m,n} \frac{1}{\left| P_m^{\alpha_1, \beta_1} \right| \left| P_n^{\alpha_2, \beta_2} \right|} \sum_{j \in P_m^{\alpha_1, \beta_1}} \sum_{k \in P_n^{\alpha_2, \beta_2}} |x_{jk} - L| = 0,$$

which completes the proof. □

Theorem 2.5. If $\liminf_m \frac{\beta_1(m)}{\alpha_1(m)} > 1$ and $\liminf_n \frac{\beta_2(n)}{\alpha_2(n)} > 1$, then $st_2 - \lim x_{jk} = L$ implies $st_2(\alpha\beta) - \lim x_{jk} = L$.

Proof. Suppose that $\liminf_m \frac{\beta_1(m)}{\alpha_1(m)} > 1$ and $\liminf_n \frac{\beta_2(n)}{\alpha_2(n)} > 1$. Then, there exists $\delta > 0$ such that $\frac{\beta_1(m)}{\alpha_1(m)} \geq 1 + \delta$ and $\frac{\beta_2(n)}{\alpha_2(n)} \geq 1 + \delta$, hence we obtain that $\frac{\beta_1(m) - \alpha_1(m) + 1}{\beta_1(m)} \geq \frac{\delta}{1 + \delta}$ and $\frac{\beta_2(n) - \alpha_2(n) + 1}{\beta_2(n)} \geq \frac{\delta}{1 + \delta}$. Now let $st_2 - \lim x_{jk} = L$. Then, for a given $\epsilon > 0$, we may write that

$$\begin{aligned} & \frac{1}{\beta_1(m)\beta_2(n)} \left| \left\{ (j, k), j \leq \beta_1(m) \text{ and } k \leq \beta_2(n) : |x_{jk} - L| \geq \epsilon \right\} \right| \\ & \geq \frac{1}{\beta_1(m)\beta_2(n)} \left| \left\{ (j, k), j \in P_m^{\alpha_1, \beta_1} \text{ and } k \in P_n^{\alpha_2, \beta_2} : |x_{jk} - L| \geq \epsilon \right\} \right| \\ & = \frac{(\beta_1(m) - \alpha_1(m) + 1)(\beta_2(n) - \alpha_2(n) + 1)}{\beta_1(m)\beta_2(n)} \frac{\left| \left\{ (j, k), j \in P_m^{\alpha_1, \beta_1} \text{ and } k \in P_n^{\alpha_2, \beta_2} : |x_{jk} - L| \geq \epsilon \right\} \right|}{(\beta_1(m) - \alpha_1(m) + 1)(\beta_2(n) - \alpha_2(n) + 1)} \\ & \geq \left(\frac{\delta}{1 + \delta} \right)^2 \frac{\left| \left\{ (j, k), j \in P_m^{\alpha_1, \beta_1} \text{ and } k \in P_n^{\alpha_2, \beta_2} : |x_{jk} - L| \geq \epsilon \right\} \right|}{(\beta_1(m) - \alpha_1(m) + 1)(\beta_2(n) - \alpha_2(n) + 1)}. \end{aligned}$$

Since $st_2 - \lim x_{jk} = L$, the left hand side of the last inequality tends to zero as $m, n \rightarrow \infty$, which yields that

$$\lim_{m, n \rightarrow \infty} \frac{\left| \left\{ (j, k), j \in P_m^{\alpha_1, \beta_1} \text{ and } k \in P_n^{\alpha_2, \beta_2} : |x_{jk} - L| \geq \epsilon \right\} \right|}{(\beta_1(m) - \alpha_1(m) + 1)(\beta_2(n) - \alpha_2(n) + 1)} = 0.$$

This completes the proof of the theorem. □

Theorem 2.6. If $\lim_{m, n \rightarrow \infty} \frac{\alpha_1(m)\alpha_2(n)}{\beta_1(m)\beta_2(n)} = 0$, $\alpha_1(m) \geq 1$ and $\alpha_2(n) \geq 1$ for all $m, n \in \mathbb{N}$, then $st_2(\alpha\beta) - \lim x_{jk} = L$ implies $st_2 - \lim x_{jk} = L$.

Proof. Suppose that $\lim_{m, n \rightarrow \infty} \frac{\alpha_1(m)\alpha_2(n)}{\beta_1(m)\beta_2(n)} = 0$, $\alpha_1(m) \geq 1$ and $\alpha_2(n) \geq 1$ for all $m, n \in \mathbb{N}$. Then, for a given $\epsilon > 0$, we can write

$$\begin{aligned} & \frac{1}{\beta_1(m)\beta_2(n)} \left| \left\{ (j, k), j \leq \beta_1(m) \text{ and } k \leq \beta_2(n) : |x_{jk} - L| \geq \epsilon \right\} \right| \\ & = \frac{1}{\beta_1(m)\beta_2(n)} \left| \left\{ (j, k), j < \alpha_1(m) \text{ and } k < \alpha_2(n) : |x_{jk} - L| \geq \epsilon \right\} \right| \\ & \quad + \frac{1}{\beta_1(m)\beta_2(n)} \left| \left\{ (j, k), j \in P_m^{\alpha_1, \beta_1} \text{ and } k \in P_n^{\alpha_2, \beta_2} : |x_{jk} - L| \geq \epsilon \right\} \right| \\ & \leq \frac{\alpha_1(m)\alpha_2(n)}{\beta_1(m)\beta_2(n)} + \frac{1}{\left| P_m^{\alpha_1, \beta_1} \right| \left| P_n^{\alpha_2, \beta_2} \right|} \left| \left\{ (j, k), j \in P_m^{\alpha_1, \beta_1} \text{ and } k \in P_n^{\alpha_2, \beta_2} : |x_{jk} - L| \geq \epsilon \right\} \right|. \end{aligned}$$

Taking limit as $m, n \rightarrow \infty$ on the both sides of last inequality, since $st_2(\alpha\beta) - \lim x_{jk} = L$, we obtain that

$$\frac{1}{\beta_1(m)\beta_2(n)} \left| \left\{ (j, k), j \leq \beta_1(m) \text{ and } k \leq \beta_2(n) : |x_{jk} - L| \geq \epsilon \right\} \right| = 0,$$

which completes the proof. □

3. Application to Korovkin type approximation theorem

Let $C[a, b]$ be the linear space of all real valued continuous functions f on $[a, b]$. It is well known that $C[a, b]$ is a Banach space with the norm

$$\|f\|_\infty = \sup_{x \in [a, b]} |f(x)|, \quad f \in C[a, b].$$

Suppose that T be a linear operator from $C[a, b]$ into $C[a, b]$. We write $T_n(f, x)$ for $T_n(f(t), x)$ and we say that T is a positive linear operator if $T(f, x) \geq 0$ for all $f(x) \geq 0$. The classical Korovkin theorem states as follows [20]:

Suppose that (T_n) be a sequence of positive linear operators from $C[a, b]$ into $C[a, b]$. Then

$$\lim_n \|T_n(f, x) - f(x)\|_\infty = 0, \quad \text{for all } f \in C[a, b],$$

if and only if

$$\lim_n \|T_n(f_i, x) - f_i(x)\|_\infty = 0, \quad \text{for } i = 0, 1, 2,$$

where $f_0(x) = 1$, $f_1(x) = x$ and $f_2(x) = x^2$.

Recently, Korovkin type approximation theorem have been studied for functions of one or two variables by using different summability methods, see for instance [21]-[33] and etc.

By $C(K)$, we denote the space of all continuous real valued functions on any compact subset of the real two-dimensional space. This space is equipped with the supremum norm

$$\|f\|_{C(K)} = \sup_{(x, y) \in K} |f(x, y)|, \quad f \in C(K).$$

Before proceeding further, we recall here the classical Korovkin type approximation theorem for a function of two variables in Pringsheim sense given in [21].

Theorem 3.1. [21] Let (T_{jk}) be a double sequence of positive linear operators from $C(K)$ into $C(K)$. Then for all $f \in C(K)$,

$$P\text{-}\lim \|T_{jk}f - f\|_{C(K)} = 0$$

if and only if

$$P\text{-}\lim \|T_{jk}f_i - f_i\|_{C(K)} = 0, \quad (i = 0, 1, 2, 3)$$

where $f_0(x, y) = 1$, $f_1(x, y) = x$, $f_2(x, y) = y$ and $f_3(x, y) = x^2 + y^2$.

Now, we give the main result of this section.

Theorem 3.2. Let (T_{jk}) be a double sequence of positive linear operators from $C(K)$ into $C(K)$. Then for all $f \in C(K)$,

$$st_2(\alpha\beta)\text{-}\lim \|T_{jk}f - f\|_{C(K)} = 0 \tag{3.1}$$

if and only if

$$st_2(\alpha\beta)\text{-}\lim \|T_{jk}f_i - f_i\|_{C(K)} = 0, \quad (i = 0, 1, 2, 3) \tag{3.2}$$

where $f_0(x, y) = 1$, $f_1(x, y) = x$, $f_2(x, y) = y$ and $f_3(x, y) = x^2 + y^2$.

Proof. Since each $f_i \in C(K)$ for $(i = 0, 1, 2, 3)$, condition (3.2) follows immediately from (3.1). Suppose now that the condition (3.2) holds and $f \in C(K)$. By the continuity of f on compact set K , we can write $|f(x, y)| \leq M$ where $M := \|f\|_{C(K)}$. Also, since f is continuous on K , for every $\varepsilon > 0$, there exists a number $\delta > 0$ such that $|f(u, v) - f(x, y)| < \varepsilon$ for all $(u, v) \in K$ satisfying $|u - x| < \delta$ and $|v - y| < \delta$. Hence, we get

$$|f(u, v) - f(x, y)| < \varepsilon + \frac{2M}{\delta^2} \left\{ (u-x)^2 + (v-y)^2 \right\} \tag{3.3}$$

Since T_{jk} is linear and positive, from (3.3), we obtain that

$$\begin{aligned} & |T_{jk}(f; x, y) - f(x, y)| \\ &= |T_{jk}(f(u, v) - f(x, y); x, y) - f(x, y)(T_{jk}(f_0; x, y) - f_0(x, y))| \\ &\leq T_{jk}(|f(u, v) - f(x, y)|; x, y) + M|T_{jk}(f_0; x, y) - f_0(x, y)| \\ &\leq T_{jk}\left(\varepsilon + \frac{2M}{\delta^2} \left\{ (u-x)^2 + (v-y)^2 \right\}; x, y\right) + M|T_{jk}(f_0; x, y) - f_0(x, y)| \\ &\leq \left(\varepsilon + M + \frac{2M}{\delta^2}(A^2 + B^2)\right) |T_{jk}(f_0; x, y) - f_0(x, y)| \\ &\quad + \frac{4M}{\delta^2}A|T_{jk}(f_1; x, y) - f_1(x, y)| + \frac{4M}{\delta^2}B|T_{jk}(f_2; x, y) - f_2(x, y)| \\ &\quad + \frac{2M}{\delta^2}|T_{jk}(f_3; x, y) - f_3(x, y)| + \varepsilon, \end{aligned}$$

where $A := \max|x|$ and $B := \max|y|$. Taking supremum over $(x, y) \in K$, we get

$$\|T_{jk}f - f\|_{C(K)} \leq R \left\{ \|T_{jk}f_0 - f_0\|_{C(K)} + \|T_{jk}f_1 - f_1\|_{C(K)} + \|T_{jk}f_2 - f_2\|_{C(K)} + \|T_{jk}f_3 - f_3\|_{C(K)} \right\} + \varepsilon,$$

where $R = \max \left\{ \varepsilon + M + \frac{2M}{\delta^2}(A^2 + B^2), \frac{4M}{\delta^2}A, \frac{4M}{\delta^2}B, \frac{2M}{\delta^2} \right\}$.

Now, for a given $r > 0$, choose $\varepsilon' > 0$ such that $\varepsilon' < r$. Define the following sets

$$\begin{aligned} D &= \left\{ (j, k), j \in P_m^{\alpha_1, \beta_1} \text{ and } k \in P_n^{\alpha_2, \beta_2} : \|T_{jk}f - f\|_{C(K)} \geq r \right\}, \\ D_i &= \left\{ (j, k), j \in P_m^{\alpha_1, \beta_1} \text{ and } k \in P_n^{\alpha_2, \beta_2} : \|T_{jk}f_i - f_i\|_{C(K)} \geq \frac{r - \varepsilon'}{4R} \right\}, \end{aligned}$$

for $i = 0, 1, 2, 3$. Then, $D \subset \bigcup_{i=0}^3 D_i$ and so we also get

$$\begin{aligned} & \frac{1}{|P_m^{\alpha_1, \beta_1}| |P_n^{\alpha_2, \beta_2}|} \left\{ (j, k), j \in P_m^{\alpha_1, \beta_1} \text{ and } k \in P_n^{\alpha_2, \beta_2} : \|T_{jk}f - f\|_{C(K)} \geq r \right\} \\ &\leq \frac{1}{|P_m^{\alpha_1, \beta_1}| |P_n^{\alpha_2, \beta_2}|} \left\{ (j, k), j \in P_m^{\alpha_1, \beta_1} \text{ and } k \in P_n^{\alpha_2, \beta_2} : \|T_{jk}f_0 - f_0\|_{C(K)} \geq \frac{r - \varepsilon'}{4R} \right\} \\ &\quad + \frac{1}{|P_m^{\alpha_1, \beta_1}| |P_n^{\alpha_2, \beta_2}|} \left\{ (j, k), j \in P_m^{\alpha_1, \beta_1} \text{ and } k \in P_n^{\alpha_2, \beta_2} : \|T_{jk}f_1 - f_1\|_{C(K)} \geq \frac{r - \varepsilon'}{4R} \right\} \\ &\quad + \frac{1}{|P_m^{\alpha_1, \beta_1}| |P_n^{\alpha_2, \beta_2}|} \left\{ (j, k), j \in P_m^{\alpha_1, \beta_1} \text{ and } k \in P_n^{\alpha_2, \beta_2} : \|T_{jk}f_2 - f_2\|_{C(K)} \geq \frac{r - \varepsilon'}{4R} \right\} \\ &\quad + \frac{1}{|P_m^{\alpha_1, \beta_1}| |P_n^{\alpha_2, \beta_2}|} \left\{ (j, k), j \in P_m^{\alpha_1, \beta_1} \text{ and } k \in P_n^{\alpha_2, \beta_2} : \|T_{jk}f_3 - f_3\|_{C(K)} \geq \frac{r - \varepsilon'}{4R} \right\}. \end{aligned}$$

Hence, using condition (3.2), we obtain

$$st_2(\alpha\beta) - \lim \|T_{jk}f - f\|_{C(K)} = 0.$$

This completes the proof of theorem. \square

Remark 3.3. We now construct an example of sequence of positive linear operators of two variables satisfying the conditions of Theorem 3.2, but does not satisfy the conditions of the Korovkin theorem given in Theorem 3.1. For this, we consider the following Bernstein operators given by

$$B_{mn}(f; x, y) = \sum_{k=0}^m \sum_{j=0}^n f\left(\frac{k}{m}, \frac{j}{n}\right) C_m^k x^k (1-x)^{m-k} C_n^j y^j (1-y)^{n-j},$$

where $(x, y) \in K = [0, 1] \times [0, 1]$; $f \in C(K)$. Also, observe that

$$B_{mn}(f_0; x, y) = 1,$$

$$B_{mn}(f_1; x, y) = x,$$

$$B_{mn}(f_2; x, y) = y,$$

$$B_{mn}(f_3; x, y) = x^2 + y^2 + \frac{x-x^2}{m} + \frac{y-y^2}{n},$$

where $f_0(x, y) = 1$, $f_1(x, y) = x$, $f_2(x, y) = y$ and $f_3(x, y) = x^2 + y^2$. Then, by Theorem 3.1, we know that, for any $f \in C(K)$,

$$P - \lim \|B_{mn}f - f\|_{C(K)} = 0.$$

Now, we define the sequence of linear operators as $T_{mn} : C(K) \rightarrow C(K)$ with $T_{mn}(f; x, y) = (1 + x_{mn})B_{mn}(f; x, y)$, where $x = (x_{mn})$ is defined in Theorem 2.3. Note that the sequence $x = (x_{mn})$ is $\alpha\beta$ -statistically convergent to zero, but not P -convergent. Then the double sequence T_{mn} satisfies condition (3.2) for $i = 0, 1, 2, 3$, hence, by Theorem 3.2, we get

$$st_2(\alpha\beta) - \lim \|T_{mn}f - f\|_{C(K)} = 0.$$

On the other hand, we have $T_{mn}(f; 0, 0) = (1 + x_{mn})f(0, 0)$ since $B_{mn}(f; 0, 0) = f(0, 0)$, and hence we obtain

$$\|T_{mn}(f; x, y) - (f; x, y)\|_{C(K)} \geq |T_{mn}(f; 0, 0) - (f; 0, 0)| \geq x_{mn} |(f; 0, 0)|.$$

One can see that (T_{mn}) does not satisfy the Korovkin theorem for positive linear operators of two variables in the Pringsheim's sense, since $P - \lim x_{mn}$ does not exist. That is, Theorem 3.1 does not work for our operators T_{mn} . Hence, our Theorem 3.2 is stronger than Theorem 3.1. This proves our claim.

Acknowledgements

The second author would like to thank TUBITAK (The Scientific and Technological Research Council of Turkey) for their financial supports during his doctorate studies.

References

- [1] H. Fast, *Sur la convergence statistique*, Colloq. Math., **2** (1951), 241-244.
- [2] H. Steinhaus, *Sur la convergence ordinaire et la convergence asymptotique*, Colloq. Math., **2**(1) (1951), 73-74.
- [3] I. J. Schoenberg, *The integrability of certain functions and related summability methods*, Amer. Math. Monthly, **66** (1959), 361-375.
- [4] T. Šalát, *On statistically convergent sequences of real numbers*, Math. Slovaca, **30**(2) (1980), 139-150.
- [5] J. A. Fridy, *On statistical convergence*, Analysis, **5** (1985), 301-313.
- [6] J. A. Fridy, H. I. Miller, *A matrix characterization of statistical convergence*, Analysis, **11** (1991), 59-66.
- [7] J. A. Fridy, C. Orhan, *Lacunary statistical convergence*, Pacific J. Math., **160** (1993), 43-51.
- [8] F. Móricz, C. Orhan, *Tauberian conditions under which statistical convergence follows from statistical summability by weighted means*, Studia Sci. Math. Hungar., **41** (2004), 391-403.
- [9] J. S. Connor, *The statistical and strong p -Cesàro convergence of sequences*, Analysis, **8** (1988), 47-63.
- [10] P. Kostyrko, T. Šalát, W. Wilczynski, *I-convergence*, Real Anal. Exchange, **26** (2) (2000-2001), 669-685.
- [11] E. Savas, P. Das, *A generalized statistical convergence via ideals*, Appl. Math. Lett., **24** (2011), 826-830.
- [12] P. Das, E. Savas, S. Ghosal, *On generalizations of certain summability methods using ideals*, Appl. Math. Lett., **24** (2011), 1509-1514.
- [13] M. Mursaleen, *λ -statistical convergence*, Math. Slovaca, **50** (1) (2000), 111-115.
- [14] H. Aktuglu, *Korovkin type approximation theorems proved via $\alpha\beta$ -statistical convergence*, J. Comput. Appl. Math., **259** (2014), 174-181.
- [15] A. Karaisa, *Statistical $\alpha\beta$ -summability and Korovkin type approximation theorem*, Filomat, **30**(13) (2016), 3483-3491.
- [16] A. Pringsheim, *Zur Theorie der zweifach unendlichen Zahlenfolgen*, Math. Ann., **53** (1900), 289-321.
- [17] M. Mursaleen, O. H. H. Edely, *Statistical convergence of double sequences*, J. Math. Anal. Appl., **288** (2003), 223-231.
- [18] M. Mursaleen, C. Cakan, S. A. Mohiuddine, E. Savas, *Generalized statistical convergence and statistical core of double sequences*, Acta Math. Sin. (Engl. Ser.), **26** (2010), 2131-2144.
- [19] E. Savas, R. F. Patterson, *Lacunary statistical convergence of multiple sequences*, Appl. Math. Lett., **19** (2006), 527-534.
- [20] P. P. Korovkin, *Linear Operators and Approximation Theory*, Hindustan Publishing Corporation, Delhi, 1960.
- [21] V. I. Volkov, *On the convergence of sequences of linear positive operators in the space of continuous functions of two variables*, Dokl. Akad. Nauk. SSSR (N.S.), **115** (1957), 17-19.
- [22] M. Mursaleen, V. Karakaya, M. Erturk, M. Gursoy, *Weighted statistical convergence and its application to Korovkin type approximation theorem*, Appl. Math. Comput., **218** (2012), 9132-9137.
- [23] M. Mursaleen, A. Alotaibi, *Statistical summability and approximation by de la Vallée-Poussin mean*, Appl. Math. Lett., **24** (2011), 320-324.
- [24] A. D. Gadjiev, C. Orhan, *Some approximation theorems via statistical convergence*, Rocky Mountain J. Math., **32** (2002), 129-138.
- [25] E. Erkus, O. Duman, *A Korovkin type approximation theorem in statistical sense*, Studia Sci. Math. Hungar., **43** (2006), 285-294.
- [26] O. Duman, *A Korovkin type approximation theorems via I-convergence*, Czechoslovak Math. J., **57** (2007), 367-375.

- [27] F. Dirik, K. Demirci, *Korovkin type approximation theorem for functions of two variables in statistical sense*, Turkish J. Math., **34** (2010), 73-83.
- [28] S. Orhan, F. Dirik, K. Demirci, *A Korovkin-type approximation theorem for double sequences of positive linear operators of two variables in statistical A-summability sense*, Miskolc Math. Notes, **15** (2014), 625-633.
- [29] O. H. H. Edely, S. A. Mohiuddine, A. K. Noman, *Korovkin type approximation theorems obtained through generalized statistical convergence*, Appl. Math. Lett., **23** (2010), 1382-1387.
- [30] S. A. Mohiuddine, A. Alotaibi, *Statistical convergence and approximation theorems for functions of two variables*, J. Comput. Anal. Appl., **15** (2013), 218-223.
- [31] C. Belen, S. A. Mohiuddine, *Generalized weighted statistical convergence and application*, Appl. Math. Comput., **219** (2013), 9821-9826.
- [32] V. Karakaya, A. Karaisa, *Korovkin type approximation theorems for weighted $\alpha\beta$ -statistical convergence*, Bull. Math. Sci., **5** (2015), 159-169.
- [33] S. Altundag, B. Sozbir, *Weighted I-statistical convergence and its application to Korovkin type approximation theorem*, Int. J. Math. Sci. Eng. Appl., **9**(2) (2015), 63-76.